学位論文　（要約）

Magnetic study of seafloor hydrothermal systems in various tectonic settings

（多様な地質学的背景を持つ海底熱水系の磁気的研究）

平成２７年１２月博士（理学）申請

東京大学大学院理学系研究科

地球惑星科学専攻

藤井　昌和

Abstract

An understanding of the seafloor hydrothermal system is essential for discussing the cooling of the oceanic lithosphere, geochemical cycles of many elements, submarine mineral deposits, and specific chemosynthetic ecosystems. Near-seafloor magnetic anomalies can provide vital information such as the location, spatial extent, and mineralization of hydrothermal systems because magnetic minerals are oxidized, transformed, and created during the hydrothermal processes. However, previous magnetic studies are limited on basalt-hosted hydrothermal systems developed in axial areas of mid-ocean ridges (MORs), where hydrothermal fields are typically associated with reduced magnetization. Moreover, there has been limited discussion on the geological controls of hydrothermal systems in volcanic arc, back-arc, and ultramafic-hosted hydrothermal systems. Because seafloor hydrothermal circulation, fluids, and deposits are strongly controlled by tectonic processes, further study in these areas is needed to understand the geological and geophysical frameworks of seafloor hydrothermal systems.

In the present study, therefore, I analyzed near-seafloor magnetic data to discuss the magnetization structures of hydrothermal systems in various tectonic settings of three regions: (i) on- and off-axis hydrothermal fields hosted in andesite in back-arc region of the southern Mariana Trough (SMT), (ii) basalt- to rhyolite-hosted Tarama and Irabu hydrothermal fields (THF and IHF, respectively) in arc and back-arc regions of the Okinawa Trough, and (iii) an ultramafic-hosted hydrothermal field in a non-transform offset massif of the Central Indian Ridge (CIR). In addition, I measured the rock magnetic properties of host rocks from the seafloor near those subjected hydrothermal fields in order to construct an appropriate geologic interpretation of magnetic contrast.

In Chapter 2, I investigate five hydrothermal vent fields of the back-arc spreading region on the SMT. Near-seafloor magnetic data were collected using the *SHINKAI 6500*, a deep-sea human occupied vehicle (HOV). A new three-dimensional (3-D) method is applied to exploit the surrounding bathymetry and varying altitudes of the submersible for estimating the absolute crustal magnetization. The results reveal that magnetic-anomaly-derived absolute magnetizations (MADAMs) show a reasonable correlation with the natural remanent magnetizations (NRMs) of rock samples collected

from the seafloor of the same region. The distribution of MADAM suggests that all five andesite-hosted hydrothermal fields are associated with a lack of magnetization, as is generally observed at basalt-hosted hydrothermal sites of the MORs. The spatial extent of the resulting low magnetization is approximately ten times wider at off-axis sites than that at on-axis sites, possibly reflecting larger accumulations of nonmagnetic sulfides, stockwork zones, and alteration zones at the off-axis sites. Furthermore, I succeeded in distinguishing contiguous low magnetization zones (LMZs) located on the same seafloor volcano, which could not be separated in magnetic anomaly data collected at higher altitudes by an autonomous underwater vehicle (AUV).

In Chapter 3, I show the results of detailed analyses of high-resolution vector magnetic anomalies on arc and back-arc hydrothermal vent fields in the Okinawa Trough, by using the AUV *URASHIMA*. The IHF is developed on the axial area of the back-arc rift and consist of basaltic lavas. The THF is developed between a back-arc rift and arc along with dacite to rhyolite. Active hydrothermal venting was reported in both fields. The obtained magnetizations from both ship-underway and near-seafloor magnetic data are consistent with the values of NRM measured on rock samples. The distribution of crustal magnetization deduced from the magnetic anomaly revealed that both IHF and THF are associated with reduced magnetization. The spatial scale of low magnetization reflecting the extent of the discharge zone is large compared with that found at MORs. Comparisons of detailed bathymetry and magnetization distribution of the Irabu knolls reveal that the magnetization lows are located along the rim of the cauldron structure, indicating that hydrothermal fluids rise from deep areas along the caldera fault. The results show that reduced magnetization related to hydrothermal activity occurs in rhyolite-hosted systems as well as basalt-hosted systems, and that caldera faults are important pathways for forming large discharge zones of hydrothermal systems.

In Chapter 4, I investigate the Yokoniwa hydrothermal field (YHF), an inactive ultramafic-hosted hydrothermal vent field, by using high-resolution vector magnetic anomalies from the HOV *SHINKAI 6500* and the AUV *r2D4*. The YHF is developed at a non-transform offset massif of the CIR. Dead chimneys are widely observed around the YHF along with a very weak venting of low-temperature fluids. This indicates that the hydrothermal activity of the YHF is almost finished. The distribution of crustal magnetization from the magnetic anomaly revealed that the YHF is associated with

enhanced magnetization, which also occurs at the ultramafic-hosted Rainbow and Ashadze-1 hydrothermal sites of the Mid-Atlantic Ridge (MAR). The results of rock magnetic analysis on the seafloor rock samples including basalt, dolerite, gabbro, serpentinized peridotite, and hydrothermal sulfide show that only highly serpentinized peridotite carries high magnetic susceptibility and NRM intensity that can explain the high magnetization of the YHF. These observations reflect abundant and strongly magnetized magnetite grains within the highly serpentinized peridotite.

In Chapter 5, I discuss three topics on the basis of these near-seafloor magnetic anomaly surveys and rock magnetic analyses with previous studies: (i) the magnetic signature of volcanic lava-hosted hydrothermal systems, (ii) magnetic mineral formation at ultramafic-hosted hydrothermal systems, and (iii) the locations and spatial scales of seafloor hydrothermal systems. I draw the following conclusions about the general magnetic characteristics reflecting the hydrothermal alteration and evolution of hydrothermal systems.

1. Volcanic lava-hosted hydrothermal fields in various tectonic settings, including volcanic arcs and back-arc regions as well as MORs, are generally characterized by reduced magnetization, reflecting primarily the alteration of titanomagnetite within volcanic rocks, with accumulation of nonmagnetic hydrothermal deposits as a secondary source. This signature is generally common even if the type of basement rock differs from basalt to rhyolite.
2. Ultramafic-hosted hydrothermal systems developed in non-transform offset massifs of slow-spreading ridges are characterized by enhanced magnetization. I propose the following three-stage model for magnetic mineral formation in ultramafic-hosted hydrothermal fields: During the initial stage of an ultramafic-hosted hydrothermal system, magnetite forms with serpentine and H_2 through hydrothermal alteration of peridotites, and pyrrhotite mineralization occurs under reductive conditions. Once the serpentinization reaction has progressed, the amount of magnetite creation increases dramatically, strengthening the magnetization. Pyrrhotite creation continues as long as the H_2 content of the hydrothermal fluids continues to create a reducing environment in this developing stage. Hot and reduced hydrothermal fluids maintain the stability of magnetite and pyrrhotite with no low-temperature oxidation. Finally, once the reaction of the ultramafic rock ceases, H_2 is no longer formed in

the system. The conditions then become oxidative, which allows pyrrhotite to be converted into nonmagnetic iron sulfide or oxide, reducing considerably their magnetization considerably.

3. The hydrothermal process involves complex interplay between the dynamics of heat supply and the evolution of crustal permeability to allow seawater to access the source. As a result, the locations and spatial scales of hydrothermal systems are controlled by the tectonic background of each vent field. Off-axis hydrothermal vent sites in seafloor spreading regions are larger than on-axis sites, reflecting the longevity of the hydrothermal activity. On-axis sites located in neo-volcanic zones are likely controlled by dike intrusions over decadal timescales, whereas off-axis sites are controlled by off-axis magmatic activity over thousands of years. Hydrothermal fields related to volcanic arc and back-arc volcanism with summit calderas have horizontal spatial scales equal to or larger than detachment-controlled large hydrothermal fields at slow-spreading ridges. It is implied that the permeability structure and style of hydrothermal circulation may play important roles in the formation of larger demagnetized hydrothermal fluid pathways in caldera-controlled systems.

A major finding is that the presence of hydrothermal sulfides and the oxidation, transformation, and creation of magnetic minerals produce specific magnetic signatures at hydrothermal vent sites in various tectonic settings. These signatures can be used to detect and characterize both active and inactive hydrothermal sites. Near-seafloor magnetic survey using underwater vehicles such as HOVs or AUVs can therefore be an important component of deep-sea exploration of seafloor hydrothermal systems.

Contents

Chapter 1

Introduction

1-1. Significance of Understanding Seafloor Hydrothermal Systems

Hydrothermal alteration occurring in the oceanic lithosphere affects the physical, chemical, and biological processes of the Earth system. These hydrothermal systems are strongly related to the cooling of the oceanic lithosphere through vent fluids ranging from >300°C (black smokers) to <50°C, and are responsible for ~20% of the Earth's total heat loss (11 TW) [e.g., *Stein and Stein*, 1992, 1994]. Moreover, they contribute to substantial element exchange between seawater and the oceanic lithosphere with water fluxes of $\sim 3.5 \times 10^{12}$ kg/yr for black smokers, and $\sim 6.4 \times 10^{14}$ kg/yr for low-temperature venting [e.g., *Elderfield and Schultz*, 1996]. Precipitation of sulfide minerals from hydrothermal fluids at or below the seafloor is preserved as volcanogenic massive sulfide deposits in a wide range of ancient and modern geological settings [*Barrie and Hannington*, 1999]. Recycling of hydrothermally altered oceanic crust into mantle likely produces some of mantle's chemical heterogeneity [e.g., *Hofman*, 1988]. Moreover, the delivery of mantle-derived materials to seawater through hydrothermal systems has profound effects on seawater chemistry [e.g., *Wheat and Mottl*, 2000]. Chemical energy offered by hydrothermal vents creates a unique habitat for diverse biological communities [e.g., *Jannasch and Mottl*, 1985]. Further, recent studies have indicated the significance of hydrothermal systems on other planets. Active hydrothermal vents are believed to exist on Jupiter's moon Europa [e.g., *Lowell and DuBose*, 2005] and on Saturn's moon Enceladus [e.g., *Hsu et al*., 2015] and ancient hydrothermal vents have been speculated to exist on Mars [e.g., *Newsom*, 1980].

It is important to understand the geophysical and geological backgrounds of seafloor hydrothermal systems because the spatial scale, duration time, and hydrothermal fluid chemistry are controlled by differences in the host rock, heat source, and fluid pathways. The location and spatial extent of hydrothermal activity are often difficult to constrain by field observations. However, studies on near-seafloor magnetic anomalies can provide vital information on the subsurface structure because the oxidation, transformation, and production of magnetic minerals during hydrothermal processes cause distinct changes in the magnetization of the seafloor.

The extent of the hydrothermal alteration zone or the up-flow zone can be evaluated by the areal extent of the low magnetization zone in the crust, which results from the oxidation and transformation of the magnetic minerals. In the last few decades, numerous near-seafloor magnetic studies conducted on basalt-hosted hydrothermal systems of mid-ocean ridges (MORs) revealed that they are typically associated with reduced magnetization [e.g., *Tivey et al*., 1993; *Tivey and Johnson*, 2002; *Zhu et al*., 2010; *Tivey and Dyment*, 2010]. Hydrothermal vents exist in other tectonic settings such as volcanic arcs and back-arc spreading centers; however, their geophysical characteristics are presently poorly constrained, and their magnetic structures have not been effectively studied thus far. The chemical compositions of arc–back-arc hydrothermal fluids exhibit tremendous diversity relative to the basalt–rhyolite host rock with strong contributions from magmatic volatiles [*Ishibashi and Urabe*, 1995]. Further study is needed to understand the magnetic signatures of arc–back-arc hydrothermal systems hosted in more felsic, or siliceous, host rock compositions, such as andesite, dacite, and rhyolite, as well as basalt. Volcanic arc and back-arc hydrothermal systems have attracted much attention, owing mainly to the possibility of their use of submarine resources. Massive sulfides formed by hydrothermal activity in the arc–back-arc context are significantly more enriched in valuable metals such as Ag, Au, Cu, Pb, and Zn than those in other MORs [*Rona*, 2008].

Although the magnetic response of MOR hydrothermal systems hosted in volcanic rock is relatively well known, particularly in basalt, the magnetic response of ultramafic-hosted hydrothermal systems remains poorly documented. Recent studies of near-seafloor magnetics have reported high magnetization zones in the active ultramafic-hosted Rainbow and Ashadze-1 hydrothermal fields [*Nakase*, 2002; *Tivey and Dyment*, 2010; *Szitkar et al*., 2014b]. These magnetic highs are considered to reflect

the presence of mineralized stockwork, in which several chemical processes such as serpentinization and sulfide mineralization create and preserve strongly magnetized minerals. In the most often investigated ultramafic-hosted Rainbow hydrothermal field on the Mid-Atlantic Ridge (MAR), the magnetization estimated from magnetic anomaly mapping reaches ~30 A/m; however, the magnetization of sulfide-impregnated serpentinized peridotites collected in the same region is too small to explain the intensity of the magnetic anomaly [*Szitkar et al*., 2014b]. Magnetic mapping studies combined with investigation of the magnetic properties of host rocks are needed to determine the geological characteristics of the formation of high magnetization zones. Exposures of ultramafic rocks are extensively distributed within slow-spreading environments, where alteration processes significantly influence the submarine ecosystem and result in high concentrations of metals [e.g. *Fouquet et al*., 2010; *Kelley et al*., 2005; *Nakamura and Takai*, 2014]. Therefore, investigation of the magnetic signatures in these ultramafic-hosted hydrothermal systems is also important for detecting active and inactive hydrothermal sites and their mineralization states.

Diverse hydrothermal vent systems have been reported on more than 600 fields in various tectonic settings, such as MORs, volcanic arcs, back-arc spreading regions, and hot spots [e.g., *Hannington et al*., 2011]. These hydrothermal systems are generally developed at water depths of a few thousand meters, and the extent on the seafloor is usually a few hundred meters or less. To detect such relatively small geophysical and geological features, high-resolution near-seafloor surveys are required rather than those at the sea-surface. Near-seafloor surveys have become more tractable with deep-tow systems, dynamically positioned ships, and recent development of autonomous underwater vehicles, which allow detailed mapping of the seafloor on a scale relevant to the hydrothermal activity. By understanding present-day hydrothermal systems, we can explore buried deposits preserved off-axis to determine the past-history of hydrothermal activity and to assess the seafloor resources.

1-2. Previous Studies

1-2-1. Seafloor hydrothermal systems

During the early age of the development of seafloor spreading theory, *Bostrom et al*. [1969] reported that sediments from active MORs have very low Al and Ti contents and high Fe and Mn contents. They suggested that such ridges should be affected by volcanic emanations containing Fe and Mn that subsequently mix with ocean bottom waters. Moreover, the measured conductive heat flow in ocean basins younger than ~60 Ma has been reported to be less than the value predicted by the conductive plate cooling model [e.g., *Bullard et al*., 1956; *Lister*, 1970]. On the basis of these observations, *Lister* [1972] suggested that hydrothermal circulation is the dominant heat transfer process at ridge crests.

One of the first reports of an active hydrothermal field was the Trans-Atlantic Geotraverse (TAG) site on the MAR, which was based on extensive dredge samples of thick hydrothermal Mn encrustations overlying and cementing talus deposits [*Scott et al*., 1974]. However, active hydrothermal fluid venting was visually confirmed more than a decade afterward [*Rona et al*., 1986]. In 1977, the first vents, low-temperature structures <17°C hosting animal communities, were discovered near the Galápagos Rift seafloor [*Corliss et al*., 1979]. High-temperature vents at 300°C were first discovered on the East Pacific Rise (EPR) in 1979 (Fig. 1-1) [*Spiess et al*., 1980]. Such a temperature is below the boiling point of seawater at ambient pressure. These high-temperature vents are referred to as black smokers because the metal sulfide precipitation colors the hot fluids black. In 2000, a completely different type of hydrothermal system known as the Lost City was discovered on the MAR [*Kelley et al*., 2001]. Unlike black smoker vents, the chimneys at the Lost City are composed of $CaCO_3$ with maximum height of 60 m. During the past 40 years, the discovery rate of vent sites has increased dramatically in response to improved detection techniques and finding strategies. Currently, more than 600 hydrothermal vent fields have been documented in various tectonic settings such as MORs, hot spots, volcanic arcs, and back-arc basins (Fig. 1-2) [e.g., *Hannington et al*., 2011].

The newly formed oceanic lithosphere is extensively fissured and faulted, providing pathways for seawater penetration of the crust. Circulation of seawater generally occurs at depths of 1–2 km and may occur >8 km below the seafloor based on

seismicity [e.g. *Wolfe et al*., 1995; *Carbotte et al*., 2012] and axial magma chamber depth [e.g., *Sinton and Detrick*, 1992; *Singh et al*., 2006]. Water can be heated by hot rocks at depth, producing a highly chemically reactive fluid that undergoes a significant exchange of elements with the host rocks (Fig. 1-3) [*Humphris and McCollom*, 1998]. In the down-welling zone, low-temperature oxidation and alkali fractions dominate, and extensive replacement of pillow basalts and sheet flows occurs by minerals such as iron oxyhydroxides, zeolites, and clays, all of which are common at temperatures below about 100°C [e.g., *Gillis and Robinson*, 1988, 1990]. Alkalis such as K, Rb, and Cs are fixed within the replaced minerals. Uptake of these elements is balanced within the rocks by losses of Mg, Si, S, and, in some cases, Ca [e.g., *Gillis and Robinson*, 1990; *Alt*, 1995]. As fluids penetrate deeper into the crustal section, elements such as Cu, Zn, Fe, Pb, and S, as well as silica, are leached out from rocks at temperatures of 350–550°C [e.g., *Seyfried et al*., 1988; *Von Damm*, 1995], and are incorporated into the hydrothermal fluid. At temperatures higher than 150°C, uptake of Mg is accompanied by losses of alkalis such as K, Rb, and Li from the basaltic material [e.g., *Seyfried*, 1987; *Gillis and Robinson*, 1990; *Alt*, 1995]; moreover, sulfate is removed from seawater during the precipitation of anhydrite [e.g., *Barker et al*., 2010]. Elements such as Na, Mg, and Ca are added to the rock to form greenschist facies mineral assemblages that include minerals such as chlorite amphiboles, and Na-rich plagioclase at temperatures of 300–450°C. The heated fluid is sufficiently buoyant for returning to the seafloor and emerging in hydrothermal vents. Such vents may be concentrated into narrow jets or can be broadly distributed as diffuse emanations. The base of the reaction zone, where hydrothermal fluids reach their highest temperatures, is considered to be either near the sheeted dike–gabbro interface or within the underlying gabbroic rocks. The altered rock in this high-temperature zone contains amphibolite facies mineral assemblages that include amphibole and plagioclase. When fluids reach the seafloor at temperatures of 350–400°C or more, they are reduced, acidic at pH values of 2–6 and highly enriched in Li, K, Rb, Cs, Cu, Fe, and silica with respect to the seawater [e.g., *Von Damm*, 1995]. The debouching fluids actually range from just above ambient temperature (~2°C) to >400°C and have a wide range of chemical properties. They may be acidic or alkaline with salinities higher or lower than seawater, and they carry a wide and variable range of dissolved minerals that may precipitate onto the sea floor. The dissolved elements may include Ca, Fe, Mn, Zn, Ni, Cu, and Au, and the range of gases

includes H_2, He, CO_2, and CH_4. They may produce large, potentially economically important mineral deposits and can influence the chemistry of seawater. The dramatic changes in ambient temperature and chemistry near the seafloor cause precipitation of minerals such as anhydrite, barite, pyrite, chalcopyrite, and sphalerite [e.g., *Hannington et al*., 1995]. In many hydrothermal deposits, anhydrite and fine sulfide particles form the initial chimney structures. Anhydrite precipitates with sulfide from seawater at temperatures of 150°C, and during seawater mixing with hydrothermal fluid. High-temperature sulfide minerals precipitate to form the chimney structure, allowing the inner fluid to become insulated from the surrounding seawater. At temperatures above 250°C, chalcopyrite begins to form.

The most common type of hydrothermal vent in MORs is high temperature, basalt-hosted vents characterized by black smokers. This is the only type reported thus far on fast-spreading ridges, although it is also found less frequently on slow- and ultraslow-spreading ridges [e.g., *Baker and German*, 2004]. The diversity of hydrothermal vent fields among MORs can be understood by comparing three distinctly different types of deposits hosted in basalt, including those found on fast-spreading ridges such as the EPR, intermediate-spreading ridges such as the Endeavour Segment of the Juan de Fuca Ridge (JFR), and slow-spreading ridges such as the TAG active hydrothermal mound on the MAR (Fig. 1-4) [*Tivey*, 2007]. First, hydrothermal fields on the fast-spreading EPR occur in areas ranging from a few square meters to several hundreds of meters with ~2 m structures forming mounds that stand <15 m high. This type is relatively short-lived, lasting a few years or decades (Fig. 1-4a) [e.g., *Haymon and Kastner*, 1981; *Kadko et al*., 1985]. At the second type of the Main Endeavour Field on the JFR, the hydrothermal vents and the style of venting differ significantly from those on the EPR. Hydrothermal vents with chimneys rise nearly vertically from the seafloor to heights greater than 10 or 20 m (Fig. 1-4b) [*Delaney et al*., 1992]. The third type of hydrothermal field on slow-spreading ridges is considerably larger and endures for long periods, at least intermittently for 100 ka [e.g., *Lalou et al*., 1995; *Humphris and Cann*, 2000]. Basalt-hosted hydrothermal systems on slow-spreading ridges are generally associated with neo-volcanic zones within axial valleys. Examples of this type include the Snake Pit [*Karson and Brown*, 1988], the Lucky Strike [*Fouquet et al*., 1995], the 4°48′S area on the MAR [*Koschinsky et al*., 2008], the 49°39′E area of the Southwest Indian Ridge (SWIR) [*Zhu et al*., 2010], Loki's Castle on the Mohns

Ridge [*Pedersen et al*., 2010], and the Beebe vent field on the Mid Cayman Spreading Center [*Connelly et al*., 2012]. These fields are associated with neo-volcanic zones and contain high-temperature black smokers together with low-temperature diffuse venting. Conversely, the TAG site [*Rona et al*., 1986] is a good example of a hydrothermal field that is not directly associated with a neo-volcanic zone. Although its vent fluids are similar to those at neo-volcanic sites, the TAG is situated at the edge of a median valley. The hydrothermal system tends to be much larger and longer-lived than the equivalent systems at fast-spreading ridges (Fig. 1-4c).

Another type of hydrothermal vent system is that hosted in ultramafic rocks. This type has been discovered only on slow- and ultraslow-spreading ridges, where sub-seafloor peridotite outcrops are relatively common or where seawater can readily access peridotite through major faults. Several vent fields such as the Rainbow [*German et al*., 1996], Nibelungen [*Melchert et al*., 2008], and Ashadze [*Cherkashov et al*., 2008] occur in non-transform offsets where the mafic crust is thin or patchy and large-scale normal faulting or detachment faults is common [e.g., *deMartin et al*., 2007; *Escartin et al*., 2008]. The Rainbow site has high-temperature vents with black smokers that emit low-pH fluids moderately enriched in Si, Cu, and Zn [*Andreani et al*., 2014], which is consistent with reactions involving basalt or gabbro in addition to peridotite. The Rainbow site is considerably long-lived, at least intermittently for more than 20 ka [e.g., *Kuznetsov et al.,* 2006]. The Lost City appears to be hosted purely by ultramafic rocks. The vent site is located on 1.5 Ma crust 15 km from the axis of the MAR, and on top of the detachment footwall associated with the oceanic core complex of the Atlantis Massif [*Kelley et al*., 2001]. The Lost City is characterized by low-temperature fluid and carbonate precipitation and is significantly larger and longer-lived than most basalt-hosted fields [*Fruh-Green et al*., 2003; *Ludwig et al*., 2011]. An ultramafic-hosted site, Shinkai Seep Field (SSF), has also been found in a fore-arc setting in the Mariana Trench, although no evidence of active fluid venting has been noted [*Ohara et al*., 2012]. Vent fields of these ultramafic-hosted hydrothermal systems show high concentrations of H_2 and CH_4. This suggests the influence of a peridotite body because olivine and pyroxene in ultramafic rocks are hydrated to produce serpentine with the release of H_2 [e.g., *Schroeder et al*., 2002].

McCaig et al. [2007] presented a model that explains fault-controlled hydrothermal systems in terms of the development stage of detachment faults (Fig. 1-5). In their

model, hydrothermal circulation around detachment faults evolves from basalt-hosted site (TAG type), to footwall ultramafic-hosted site (Rainbow type) and then to low-temperature ultramafic-hosted site (Lost City type). Hot gabbroic plutonic rocks are intruded into the detachment footwall beneath neo-volcanic zones. Seawater penetrates into the deep crust to mine heat from gabbroic plutons and is discharged through the permeable fault zones and overlying basalts without sufficient interaction with the peridotite body. This process is similar to that of the style of the TAG site (Fig. 1-5A). If the hydrothermal fluid reaches a shallower, cooler gabbroic body that had been displaced from the neo-volcanic zone by structural movement on the detachment fault, the hydrothermal fluids can interact with both the gabbro and ultramafic body of the footwall before discharging in the axial valley wall with mixed properties. Such a process occurs at the Rainbow site (Fig. 1-5B). Off-axis, low-temperature circulation can occur completely within the ultramafic footwall, driven mainly by residual magmatic heat. This process describes that occurring at the Lost City site (Fig. 1-5C).

Seafloor hydrothermal vent fields are also widely distributed along volcanic arcs and back-arc basins. Hydrothermal vent deposits have been reported at intra-oceanic, back-arc basin spreading centers of the Mariana Trough and Lau and North Fiji Basins, in marginal back-arc basins of the Okinawa Trough, at submerged island-arc volcanoes of the Izu–Bonin, Mariana, and Tonga–Kermadec arcs, and in areas with more complex tectonic histories of the Manus Basin where arc volcanism and back-arc rifting occur in old arc crust [e.g., *Hannington et al*., 2005]. These deposits display both similarities and differences compared with that found on MORs and are as large [e.g., *Iizasa et al*., 1999; *de Ronde et al*., 2005]. The diversity observed in hydrothermal deposit compositions in back-arc basins, rifted arcs, and island-arc volcanoes can be attributed to many factors including the composition of the host rock such as basalt, andesite, dacite, and rhyolite; the contributions of magmatic volatiles; and the depth and structure of the substrate. The compositions of more felsic, or siliceous, host rock such as andesite, dacite, and rhyolite reflect the addition of H_2O and other volatiles from subducted sediments and hydrated oceanic crust in addition to partial melting in the mantle wedge [*Hannington et al*., 2005]. The chemical compositions of hydrothermal fluids exhibit tremendous diversity relative to the host rock with strong contributions from magmatic volatiles [*Ishibashi and Urabe*, 1995]. Low-pH fluids suggest the addition of magmatic volatiles such as SO_2 [*Ishibashi and Urabe*, 1995; *Hannington et*

al., 2005]. In a volcanic arc setting, hydrothermal vents are located on conical volcanoes, sometimes occurring within the summit caldera, and often emerge in water depths <1000 m. These shallow depths enable the boiling of fluids to enhance metal enrichment [*Hannington et al*., 2005]. The contents of economic metals such as Ag, Au, Ba, Cu, Pb, Sb, and Zn in massive sulfides formed by hydrothermal activity in the arc–back-arc context are generally higher than those on other MORs [*Rona*, 2008]. For example, the volcanogenic massive sulfide deposit in the Myojin Knoll of the Izu-Bonin submarine caldera, known as the Sunrise deposit, is notably rich in Au and Ag and has been interpreted as the modern analog of Kuroko-type polymetallic sulfide deposits [*Iizasa et al*., 1999]. Deposits hosted in an andesite body at the Vai Lili field on the Valu Fa Ridge of the Lau Basin are rich in barite, sphalerite, tennantite, and galena relative to the MOR deposits [*Fouquet et al*., 1993]. At the Brothers volcano in the Kermadec arc, active black smokers and massive sulfide deposits are present on the caldera wall and emit sulfur-rich very low-pH vent fluids [*de Ronde et al*., 2005]. At the PACMANUS vent area on Pual Ridge in the Manus Basin, sulfide deposits are enriched in Au, Ag, Pb, As, Sb, and Ba relative to the MOR deposits [*Moss and Scott*, 2001].

Volcanic arc and back-arc volcanisms in shallower depth can create pyroclastic rock that is very porous with much greater permeability than volcanic lavas erupted in deeper water [e.g., *Fiske et al*., 2001]. Seawater entrainment can be enhanced as the permeability increases, resulting in subsurface deposition of sulfide minerals and anhydrite, generation of more acidic fluid, and subsequent metal remobilization causing further metal enrichment. Further studies of the fluids, deposits, and geological backgrounds in volcanic arc and back-arc settings are needed to obtain better constraints for the development. In such processes, host rock composition and structure and magmatic volatile contribution play important roles, particularly in determining the composition of vent fluids and deposits.

1-2-2. Magnetic mineralogy of hydrothermal systems

Hydrothermal processes can oxidize, transform, and create magnetic minerals, which can change the crustal magnetization. The modification of three minerals generally occurs in hydrothermal systems through the (i) alteration of titanomagnetite within volcanic rock, (ii) creation of magnetite through serpentinization and

hydrothermal mineralization, and (iii) creation of pyrrhotite through sulfide mineralization under reductive conditions.

Oxides of Fe and Ti are the Earth's most important magnetic minerals and occur in three series; (i) stoichiometric titanomagnetites with spinel structures with solid solutions between end-member magnetite ($Fe^{2+}Fe_2^{3+}O_4$) and ulvöspinel ($Fe_2^{2+}Ti^{4+}O_4$); (ii) nonstoichiometric (oxidized) titanomagnetites or titanomaghemites, in which some Fe^{2+} ions migrate to the surface to be converted to Fe^{3+}, leaving ordered vacancies in the spinel lattice; and (iii) titanohematites, or hemoilmenites, with rhombohedral structures with solid solutions between hematite ($\alpha Fe_2^{3+}O_3$) and ilmenite ($Fe^{2+}Ti^{4+}O3$).

The magnetization of young oceanic crust arises primarily from the extrusive basaltic lavas that form the uppermost section of the seafloor. This magnetization is primarily a thermal remanent magnetization (TRM) carried by titanomagnetite grains. Titanomagnetites are altered into less-magnetic minerals such as titanomaghemite, titanohematite, and pyrite by contact with the pervasive circulation of hot and acidic hydrothermal fluid beneath the hydrothermal sites. Early studies of rock magnetic properties of basalt in terrestrial lava outcrops [*Ade-Hall et al*., 1971], the ocean floor [*Irving*, 1970; *Watkins and Johnson*, 1971], ocean crustal drilling sites [*Ade-Hall et al*., 1973], and laboratory experiments [*Johnson and Merrill*, 1972, 1973] have demonstrated that magnetization is significantly affected by low-temperature oxidation (maghemitization), in which the initial titanomagnetite is altered to titanomaghemite. This alteration process is considered to be relatively regional and broad in scale [e.g., *Johnson and Atwater*, 1977]. With more extreme alteration, titanomagnetite pseudomorphs change into titanohematite grains [*Ade-Hall et al*., 1971]. Clues for understanding the behavior of magnetic minerals relative to hydrothermal activity were obtained from a massive sulfide body in the Troodos Ophiolite complex in Cyprus. This investigation was based on the results of magnetic survey showing a strong low-magnetic field over a stockwork zone hosted within in a basaltic sequence [*Johnson et al*., 1982]. Rock magnetic studies have revealed that titanomagnetite in the basaltic rock had been replaced by nonmagnetic sulfide minerals and that the basalt itself had been altered to a clay, silica, and chlorite assemblage within the stockwork up-flow zone [*Johnson et al*., 1982; *Hall*, 1992].

Not all types of hydrothermal activity result in reduced magnetization and magnetic mineral destruction including oxidation and transformation. In some environments,

hydrothermal activity can result in magnetite formation. The process of serpentinization can produce significant magnetite deposition. Moreover, clear evidence has been presented that magnetite formation can occur through the normal seafloor alteration of peridotite [*Bina and Henry*, 1986; *Toft et al*., 1990; *Nazarova*, 1994; *Dyment et al*, 1997; *Oufi et al*., 2002] and in the place where vigorous hydrothermal systems that are located in serpentinized peridotite bodies [*Klein et al*., 2013b; *Szitkar et al*., 2014b]. Recent laboratory experiments designed to react the San Carlos olivine, $(Mg_{0.91}, Fe_{0.09})_2SiO_4$, with 250–350°C water at 50 MPa demonstrated a linear relationship between the magnetite production and the reaction progress of the serpentinization [*Malvoisin et al*., 2012]. Multiple studies of natural serpentinized peridotites recovered during an Ocean Drilling Program (ODP) using isotopic, magnetic, and thermodynamic constraints revealed that samples with abundant magnetite contained Fe-poor brucite and were formed through serpentinization at temperatures of 200–300°C [*Klein et al*., 2013b]. Investigations of abyssal peridotites recently exposed on the seafloor can provide important constraints for the serpentinization mechanism through comparisons with samples from xenoliths [e.g., *Ferré et al*., 2013] and onland oceanic core complexes [e.g., *Maffione et al*., 2014] because they are expected to have preserved the primary state of geological history without experiencing weathering, low-temperature oxidation, and tectonic metamorphism. Previous work by *Oufi et al*. [2002] investigated the magnetic properties of variably abyssal serpentinized peridotites obtained from seven deep-sea drilling sites, but the serpentinization degree of their samples was limited to 40%–100%. In this range, the compiled data showed that the magnetic susceptibility increased with the progression of serpentinization. In addition, some highly serpentinized peridotites having high natural remanent magnetization (NRM) showed large regional differences, which created difficulties in understanding the nonlinear changes of magnetic properties in the serpentinization reaction. Data with a wide range of serpentinization degrees from the same location are needed for further understanding of magnetite formation and magnetic susceptibility of serpentinized peridotite.

Magnetite is equally common as a primary and secondary minerals in sedimentary and metamorphic rocks and can form as part of a hydrothermally mineralization process. An example is the sediment-hosted Bent Hill hydrothermal system in the Middle Valley on the northeastern JFR, which was confirmed by drilling [e.g., *Korner*, 1994].

Pyrrhotite ($Fe_{1-x}S$) is a common magnetic mineral resulting from hydrothermal activity. The magnetic behavior of this iron sulfide mineral varies according to its crystal structure and composition. Pyrrhotite is a stable form of iron sulfide for the oxygen fugacity fO_2 < FMQ (fayalite ($FeSiO_4$) ↔ magnetite + quartz), whereas paramagnetic pyrite (FeS_2) is dominant under more oxidizing conditions [*Lorand et al*., 2005]. Monoclinic pyrrhotite (Fe_7S_8) is weakly magnetic (ferromagnetic) with a Curie temperature of 325°C; however, the magnetic properties weaken with greater S content, as the iron sulfide becomes more pyritic in composition. Hexagonal pyrrhotite (Fe_9S_{10}) is nonmagnetic (antiferromagnetic) at room temperature, although it has a restricted ferrimagnetic range due to thermally activated vacancy ordering above its λ-transition temperature of ~200°C until its Curie temperature at 265°C. Some hydrothermal vents containing pyrrhotite have been reported in the axial valley of the Endeavour Segment at 47°57′N [*Tivey and Delaney*, 1986], the Bent Hill massive sulfide (BHMS) over the Middle Valley [*Korner*, 1994] of the JFR, and the Rainbow hydrothermal field of the MAR [*Marques et al*., 2006].

1-2-3. Magnetic anomalies associated with hydrothermal systems

The location and spatial extent of hydrothermal activity are difficult to constrain by field observations; however, studies on near-seafloor magnetic anomalies can highlight these features because magnetic minerals are oxidized, transformed, and created through the hydrothermal processes. Deep-sea, high-resolution magnetic measurement techniques have been developed to detect weak and short-wavelength magnetic anomalies and to reveal the high-resolution magnetization distribution and relevant processes. Such techniques use either deep-towed magnetometers [e.g., *Sayanagi et al*., 1994; *Sager et al*., 1998; *Gee et al*., 2000; *Pouliquen et al*., 2001; *Tivey et al*., 2003; *Yamamoto et al*., 2005; *Tivey et al*., 2006; *Granot et al*., 2012; *Caratori-Tontini et al*., 2014] or deep-sea vehicles such as autonomous underwater vehicles (AUVs) [e.g., *Tivey et al*., 1998; *Zhu et al*., 2010; *Caratori-Tontini et al*., 2012a, 2012b; *Honsho et al*., 2013], remotely operated vehicles (ROVs) [e.g., *Dyment et al*., 2005; *Szitkar et al*., 2014a, 2014b], or human-occupied vehicles (HOVs) [e.g., *Tivey et al*., 1993; *Fujiwara and Fujimoto,* 1998; *Honsho et al*., 2009; *Sato et al*., 2009]. The results of previous near-seafloor magnetic surveys on seafloor hydrothermal fields

in various tectonic settings are summarized in Table 1-1.

High-resolution magnetic field mapping has revealed discrete zones of demagnetized crust associated with hydrothermal vent deposits hosted in basaltic seafloor, which represents patterns of subsurface up-flow of the hydrothermal fluid. The first observation showing the reduction of magnetization at a hydrothermal site was acquired over the TAG basalt-hosted hydrothermal site of the MAR by using a three-component fluxgate magnetometer fixed to the frame of the HOV *Alvin* (Fig. 1-6) [*Tivey et al*., 1993]. The authors of that study continued the observed magnetic anomaly upward to a datum plane at a depth of 3600 m (~20 m above the highest point of the mound), and they inverted the data to equivalent magnetization. The relative magnetization low was located directly beneath a sulfide mound area ~200 m in diameter with an abrupt contrast to higher magnetization at the edge of the mound, indicating a tightly constrained source. The amplitude of the magnetization low was approximately 12 A/m relative to the mean magnetization of the surrounding area. In addition, similar reduced magnetization associated with hydrothermal deposits has been observed in other hydrothermal fields of MORs including the 4°48′S fields [*Tivey and Dyment*, 2010] and the inactive site Krasnov [*Szitkar et al*., 2014a] of the MAR, the Main Endeavour Field of the JFR [*Tivey and Johnson*, 2002; *Tivey et al*., 2014], and a site on the SWIR [*Zhu et al*., 2010]. The near-bottom *Autonomous Benthic Explorer* (*ABE*) collected magnetic data over the 4°48′S area, where several active black smoker fields including the Comfortless Cove, Turtle Pits, and Red Lion are located within the axial rift on very fresh volcanic lava, and the zones of discrete reduced magnetization associated with the Red Lion and Comfortless Cove vent areas were clarified (Fig. 1-7) [*Tivey and Dyment*, 2010; *German et al*., 2008]. Because the Turtle Pits hydrothermal site also lies on the edge of a large zone of reduced magnetization ~200 m diameter, a wider area of alteration was believed to be buried under recently erupted lava flows. In the Main Endeavour Field of the JFR, *Tivey and Johnson* [2002] found discrete magnetization lows associated with each cluster of vents separated from each other by only 200 m, implying highly focused zones of hydrothermal alteration or hydrothermal deposits (Fig. 1-8). Relatively intense magnetization lows at <3 A/m compared with that in the surrounding area with diameters of ~100 m were centered directly beneath the vent clusters, which implies a near-vertical, narrow, pipe-like source region was located directly beneath the surface expression of the vent edifices. Magnetization lows were

also associated with both inactive and extinct vent zones, suggesting that the alteration of magnetic minerals rather than temporary thermal demagnetization is the primary process responsible for the reduced magnetization. In the ultraslow-spreading SWIR, *Zhu et al*. [2010] reported near-seafloor magnetic data collected during the AUV *ABE* survey at multiple elevations, and revealed a well-defined low crustal magnetization zone near a local topographic high (Fig. 1-9). This active hydrothermal vent field is the first to be observed on the SWIR and was located within and adjacent to the reduced magnetization zone at the local topographic high. This implies that the magnetic low may be the result of hydrothermal alteration of magnetic minerals. The maximum reduction in the crustal magnetization was 3 A/m.

Reduced magnetization associated with hydrothermal vent fields have also been found in hydrothermal systems along volcanic arcs and back-arc basins. Although the chemical compositions of arc–back-arc hydrothermal fluids exhibited tremendous diversity relative to the basalt–rhyolite host rock species with strong contributions from magmatic volatiles [*Ishibashi and Urabe*, 1995], the magnetic signature of the arc–back-arc hydrothermal fields was similar to that of MORs. The few studies performed on the magnetic signatures of specific arc–back-arc vent fields include the Hakurei Field within a caldera of the Izu–Ogasawara arc–back-arc volcano (Bayonnaise knoll) [*Honsho et al*., 2013], the Brothers Field within a caldera of the Kermadec intraoceanic arc volcano (Brothers volcano) [*Caratori-Tontini* et al, 2012], and the hydrothermal site on the Aeolian Palinuro arc [*Caratori-Tontini* et al., 2014]. The near-seafloor magnetic study for the Bayonnaise knoll was conducted by using the AUV *URASHIMA* at a general altitude of 80 m (Fig. 1-10) [*Honsho et al*., 2013]. That study reported the distribution of a low magnetization zone extending across an area of ~500 m × ~300 m associated with the Hakurei hydrothermal deposit, which contains active and inactive sulfide chimneys over an area of ~500 m × ~700 m within the summit caldera ~3 km in diameter. The amplitude of the magnetization low was approximately 0.5 A/m relative to the surrounding area. The correlation between the elongated direction of the magnetization low and the caldera wall strike strongly suggests that the up-flow zone was restricted by the caldera fault structure. At the Brothers volcano of the Tonga–Kermadec arc, a near-seafloor magnetic study using the AUVs *ABE* and *Sentry* at an altitude of ~50 m revealed two hydrothermal fields marked by reduced magnetization (Fig. 1-11) [*Caratori-Tontini et al*., 2012]. The amplitude of that magnetization low was

approximately 3–4 A/m relative to the surrounding area. In the hydrothermal field of the NW caldera wall, the very low magnetization extending across an area of 1 km × 0.5 km is consistent with the area of focused venting that includes black smoker chimneys and numerous dead spires. The hydrothermal site on the dacitic volcanic cone with lower temperature venting and apparent magmatic degassing is also consistent with the reduced magnetization zone, although its amplitude and spatial scale were less than those at the NW caldera wall site.

Weakened magnetic anomalies are interpreted as locally altered up-flow zones formed through hydrothermal activity because hydrothermal alteration processes oxidize and transform Fe–Ti oxide minerals such as titanomagnetite, which preserves magnetic remanence in oceanic extrusive rocks [*Irving*, 1970; *Ade-Hall et al*., 1971; *Watkins and Johnson*, 1971; *Rona*, 1978; *Johnson et al*., 1982; *Wooldridge et al*., 1990; *Pariso and Johnson*, 1991; *Hall*, 1992]. Similar magnetic lows have been confirmed in the ancient analogs of seafloor hydrothermal systems found in ophiolites, where zones of demagnetized crust are associated with the mineralized stockwork of ore bodies [*Hall*, 1992; *Richards et al*., 1989; *Walls and Hall*, 1998]. Furthermore, studies on volcanic geothermal areas in New Zealand have shown that hydrothermal alteration of magnetic minerals rather than thermal demagnetization is the most important mechanism for reduced magnetic anomalies [*Hochstein and Soengkono*, 1997]. In the seafloor realm, reduced magnetization zones have been observed in both active and extinct vent areas, suggesting that differences in the thermal environment do not significantly affect magnetic anomalies [*Tivey and Johnson*, 2002; *Szitkar et al*., 2014a]. Another explanation for reduced magnetic anomalies is the progressive accumulation of thick nonmagnetic hydrothermal deposits that cover the underlying magnetized layer and result in an apparent magnetic low owing to the increased distance between the measurement point and the underlying magnetized basalt [*Szitkar et al*., 2014a; *Szitkar and Dyment*, 2015].

In addition to the magnetic low at the basalt-hosted systems, it has been shown that hydrothermal activity led to enhanced crustal magnetization in the BHMS deposits, which are located on a sediment-covered axial valley of the JFR [*Tivey*, 1994; *Gee et al*., 2001]. In a deep-tow magnetic survey conducted at altitudes of 50–100 m, and a strong magnetization of 5 A/m assuming a uniformly magnetized body was reported (Fig. 1-12) [*Gee et al*., 2001]. This magnetic high was interpreted as the upper portion of a

sulfide mound with significantly higher induced magnetization of 10% magnetite + pyrrhotite. *Korner* [1994] showed that the ratio of saturation remanence to saturation magnetization of a drilled hydrothermal deposit was 0.01–0.15, suggesting that the magnetite within the sulfide mound occurred primarily as coarse, multi-domain grains.

Magnetization highs associated with hydrothermal vent fields have also been found in ultramafic-hosted active hydrothermal fields of the MAR [*Tivey and Dyment*, 2010; *Szitkar et al*., 2014b]. Previous studies on near-seafloor magnetics have reported high magnetization zones in the active ultramafic-hosted hydrothermal fields where high-temperature venting occurs; these include the Rainbow site with relatively higher magnetization intensity of ~30 A/m (Fig. 1-13) and the Ashadze-1 site with relatively higher magnetization intensity of ~4 A/m (Fig. 1-14) [*Tivey and Dyment*, 2010; *Szitkar et al*., 2014b]. These magnetic highs are considered to reflect the presence of mineralized stockwork, in which several chemical processes such as serpentinization and sulfide mineralization create and preserve strongly magnetized magnetite [*Szitkar et al*., 2014b]. At the Rainbow hydrothermal site, the estimated magnetization determined by magnetic anomaly mapping reached to ~30 A/m; however, the magnetization of sulfide-impregnated serpentinized peridotites collected in the same region was too small to explain the intensity of the magnetic anomaly [*Szitkar et al*., 2014b].

Enhanced magnetic anomalies in ultramafic-hosted hydrothermal sites are interpreted as magnetized bodies with large quantities of magnetic minerals, mostly magnetite and pyrrhotite, created by high-temperature hydrothermal alteration [*Tivey*, 1994; *Gee et al*., 2001; *Tivey and Dyment*, 2010; *Szitkar et al*., 2014b]. However, despite some high-resolution studies on magnetization around hydrothermal fields as previously mentioned, magnetic mapping studies combined with rock magnetic studies are limited. Therefore, the origin of magnetic anomalies such as the type of magnetic mineral, its amount, and whether magnetization was induced or remanent remain unclear. Exposures of ultramafic rocks are extensively distributed within slow-spreading environments [e.g., *Dick*, 1989; *Cannat*, 1993; *Cannat et al*., 1995; *Michael et al*., 2003], where alteration processes significantly influence the submarine ecosystem and result in high concentrations of metals [e.g. *Fouquet et al*., 2010; *Kelley et al*., 2005; *Takai et al*., 2006; *Nakamura and Takai*, 2014]. Therefore, detailed investigation of these ultramafic-hosted hydrothermal systems is important for understanding active and inactive hydrothermal sites and their mineralization states.

1-3. Goal of This Study

In this study, I determine the magnetic signatures of seafloor hydrothermal systems in various tectonic settings by utilizing both mapping of magnetic anomalies and rock magnetic properties.

On the basis of near-seafloor magnetic anomaly surveys and rock magnetic analyses presented in chapters 2, 3, and 4 and the results of previous research, I discuss the overall magnetic response of hydrothermal systems in various tectonic settings to reveal following parameters: (i) the magnetic signature of volcanic lava-hosted hydrothermal systems, (ii) the magnetic mineral formation at ultramafic-hosted hydrothermal systems, and (iii) the locations and spatial scales of seafloor hydrothermal systems. In terms of (i), I newly reveal magnetic signatures of hydrothermal systems in a back-arc spreading region, back-arc rift, and a rhyolite-hosted volcanic arc, which are described in Chapter 2 for the southern Mariana Trough (SMT) and Chapter 3 for the Okinawa Trough. To clarify (ii), particularly the origin of magnetization highs, I provide new field data of an inactive ultramafic-hosted hydrothermal site of the Central Indian Ridge (CIR), based on comprehensive magnetic data including both magnetic anomalies and rock magnetic properties described in Chapter 4. In addition, I investigate the relationship between the magnetic properties and serpentinization process. For (iii), I newly discuss the relationship between the spatial scale and duration time of hydrothermal fields based on my original results in a back-arc spreading region (Chapter 2), back-arc rift calderas (Chapter 3), and an ultramafic exposure (Chapter 4) and previous research of fast-spreading ridges, slow-spreading ridges controlled by detachment faults, volcanic arc and back-arc rift calderas, and ultramafic exposures.

In Chapter 2, I present detailed analyses of the near-seafloor, high-resolution vector magnetic data acquired by the HOV *SHINKAI 6500* both on and off the SMT back-arc spreading region, where five hydrothermal vent fields are located. I use the vector magnetic anomaly along the HOV tracks to estimate the absolute magnetization intensity of the shallow sub-seafloor by applying an improved 3-D version of the analysis method based on forward modeling proposed by *Honsho et al*. [2009] for 2-D structures. To evaluate estimated magnetic-anomaly-derived absolute magnetization (MADAM), I compare values of MADAM with both the equivalent magnetization computed by using AUV data and the NRM measured on rock samples. I clarify the

spatial extent and magnetic signature associated with the hydrothermal vent fields by using detailed seafloor geological features, which are analyzed by using video and photographs acquired during the *SHINKAI 6500* dives. Moreover, I discuss the relationship between the obtained magnetization distribution and the tectonic background of on- and off-axis hydrothermal systems.

In Chapter 3, I present multiple analyses of ship-underway and near-seafloor magnetic data and rock magnetic properties of collected samples from the Tarama and Irabu knolls in the Okinawa Trough. I perform near-seafloor vector magnetic measurements at an altitude of ~100 m by using the AUV *URASHIMA* during the R/V *Yokosuka* cruise YK14-16 in 2014. The Irabu knolls are located on the axial area of a back-arc rift and consist of basaltic lavas. The Tarama Knoll is located between a back-arc and an arc along with rhyolite. I use magnetic anomalies along the AUV tracks to estimate the equivalent magnetization intensity by applying the inversion technique using the Akaike Bayesian information criterion (ABIC) [*Honsho et al*., 2012]. I inspect the effects of host rock variation by comparing the estimated magnetizations from both ship-underway and near-seafloor magnetic anomalies with the NRM measured on rock samples. In addition, I clarify the relationship between the magnetization distribution and confirmed hydrothermal vent fields. Finally, I discuss the spatial extent of the hydrothermal vent fields in addition to the magnetic contrast of these fields compared with that of surrounding fresh lava flows. This information is determined from detailed seafloor topographic features derived from high-resolution multibeam bathymetry data acquired by using the AUV *URASHIMA*.

In Chapter 4, I explore the ultramafic-hosted Yokoniwa Hydrothermal Field (YHF), located on the CIR. The YHF is primarily an extinct hydrothermal system; therefore, it represents a unique target for investigating the differences in magnetic signatures between active and inactive hydrothermal systems hosted within ultramafic rocks. I investigate the magnetization distribution from magnetic anomalies obtained by the AUV *r2D4* and the HOV *SHINKAI 6500*, and I analyze the magnetic properties of rock samples collected near the YHF including basalt, dolerite, gabbro, serpentinized peridotite, and hydrothermal sulfide. On the basis of these multiple analyses, I discuss the magnetic signature of the inactive ultramafic-hosted YHF, the evolution of magnetite grains during serpentinization, and the process causing the strong magnetization at the YHF.

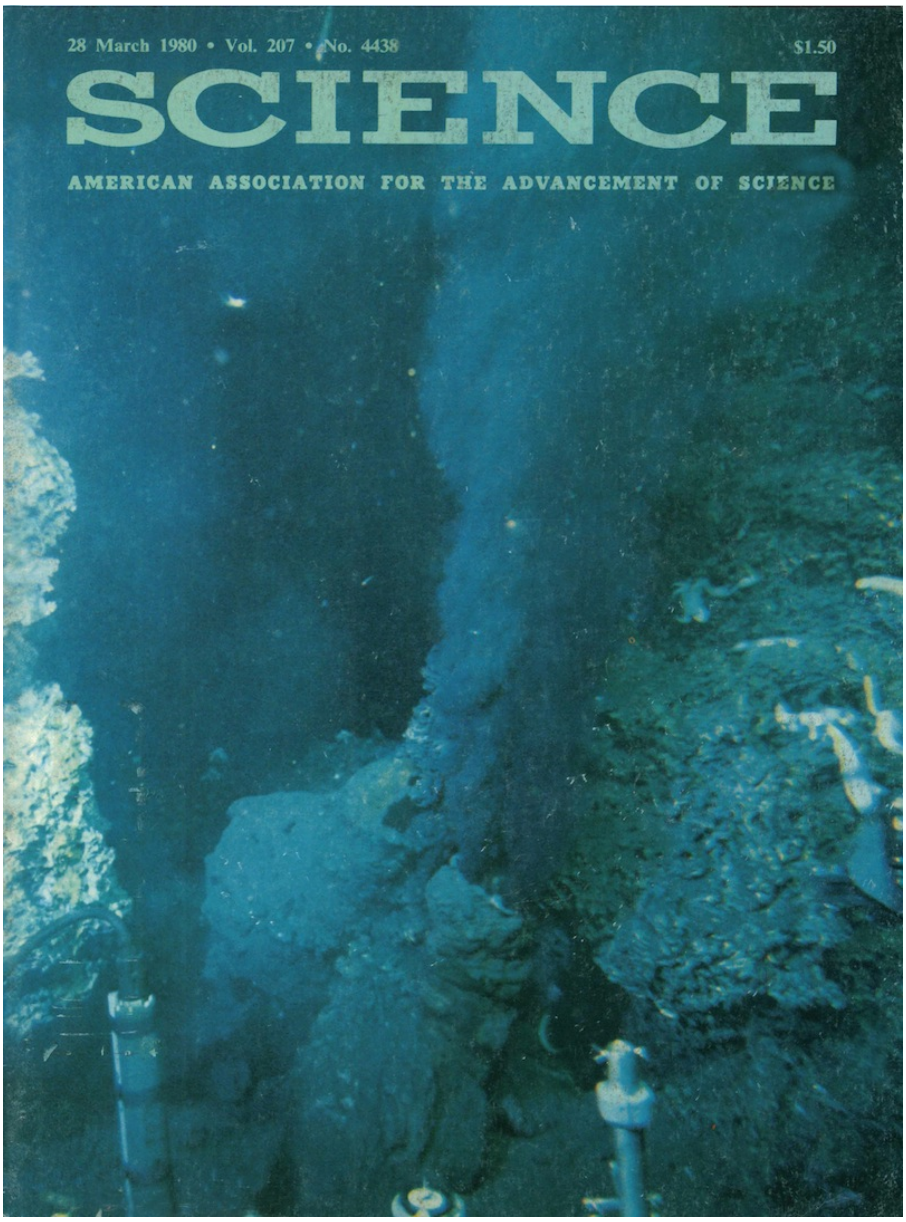

Figure 1-1. First published image of black smoker venting [*Spiess et al*., 1980].

First published image of black smoker venting captured by the submersible *Alvin* during the RISE cruise on the East Pacific Rise in 1979.

Image courtesy of *Spiess et al*. [1980].

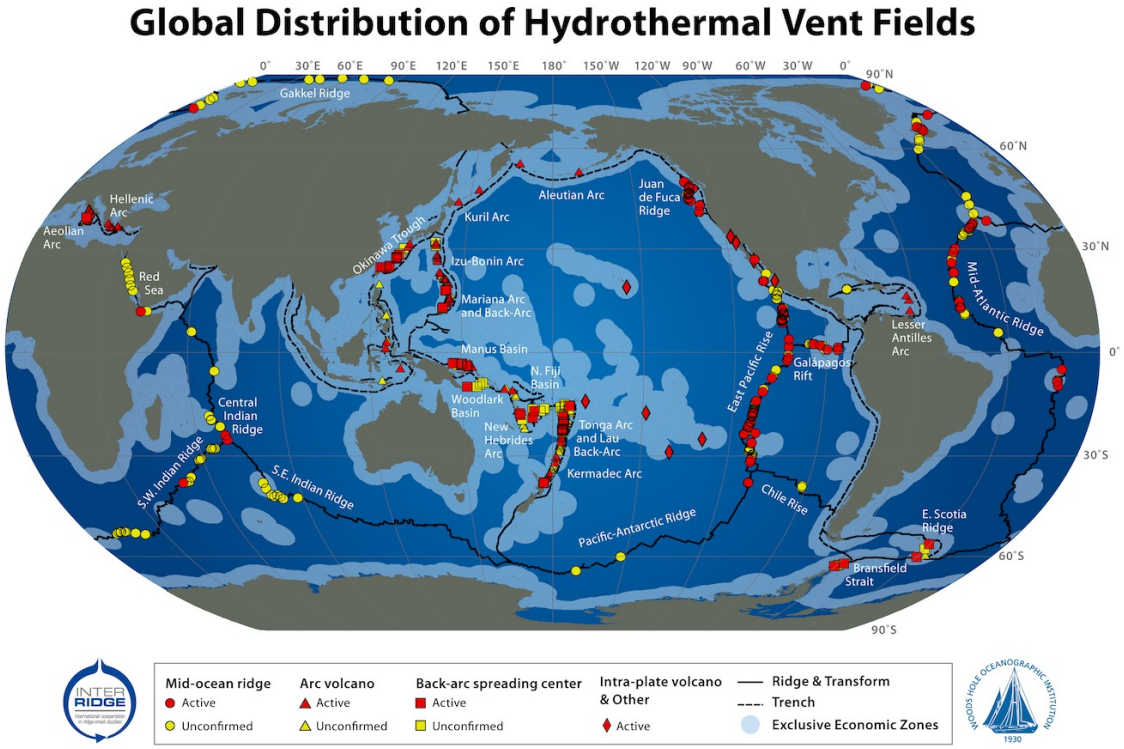

Figure 1-2. Global distribution of hydrothermal vent fields.

The data are from InterRidge Vents Database, Version 2.0, released on March 5, 2010. The static map is credited to S. Beaulieu, K. Joyce, and S.A. Soule, Woods Hole Oceanographic Institution (*WHOI*) [2010]. The plate boundary shape was determined by data sources of the University of Texas PLATES Project.
(http://vents-data.interridge.org/maps)

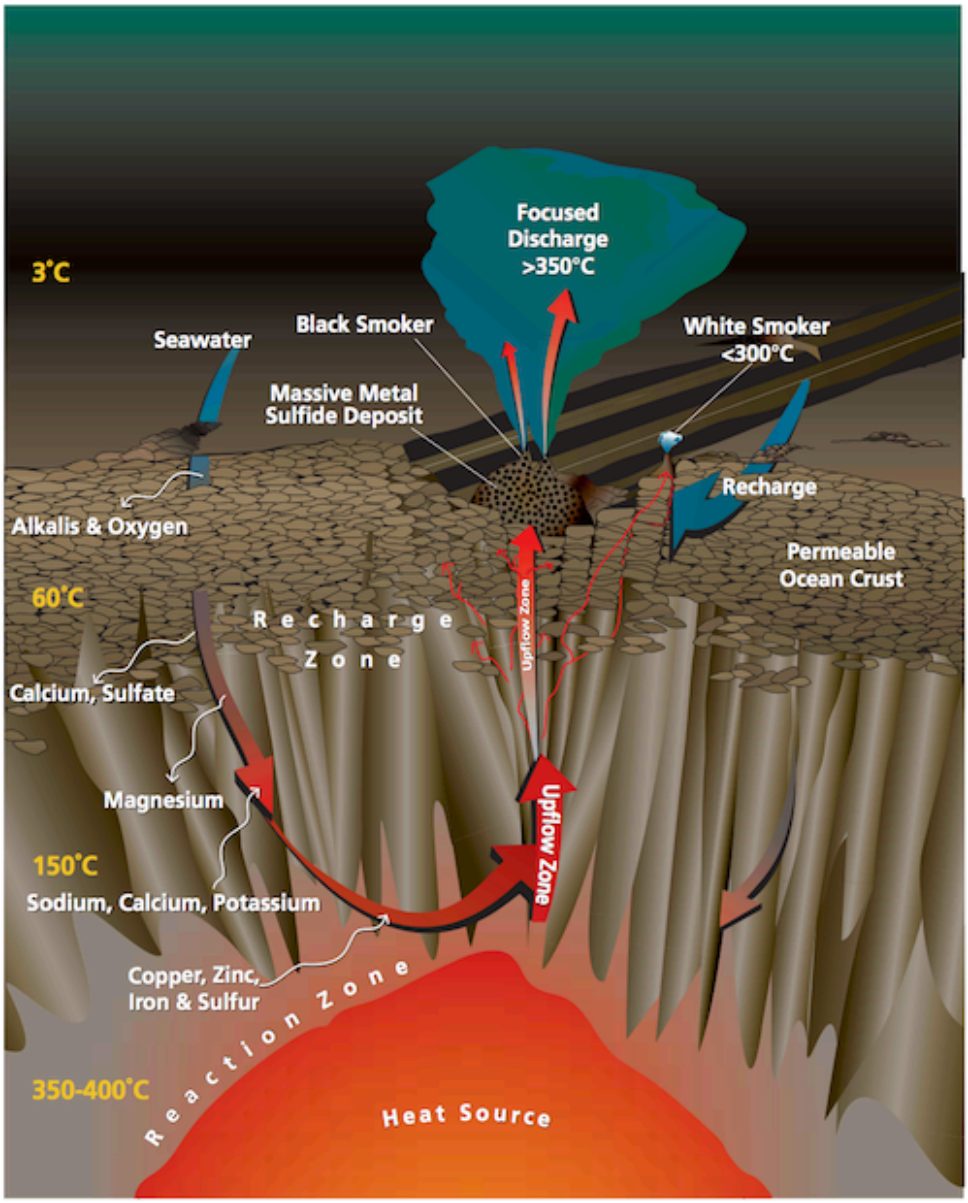

Figure 1-3. Schematic diagram showing downwelling of seawater and progressive heating with changes in the resultant hydrothermal fluid compositions, properties, and temperature [*Humphris and McCollom*, 1998].

The interaction with basaltic host rocks causes fluids to lose all Mg, O_2, and sulfate. At their deepest penetration, the resultant fluids are enriched in metals and magmatic gases, and become extremely hot at temperatures >400°C. The fluids are also buoyant, causing them to rise toward the seafloor through narrow, pipe-like conduits. The mixing of hydrothermal fluids with seawater causes metal precipitation, forming black smoker edifices. Figure courtesy of *Humphris and McCollom* [1998]

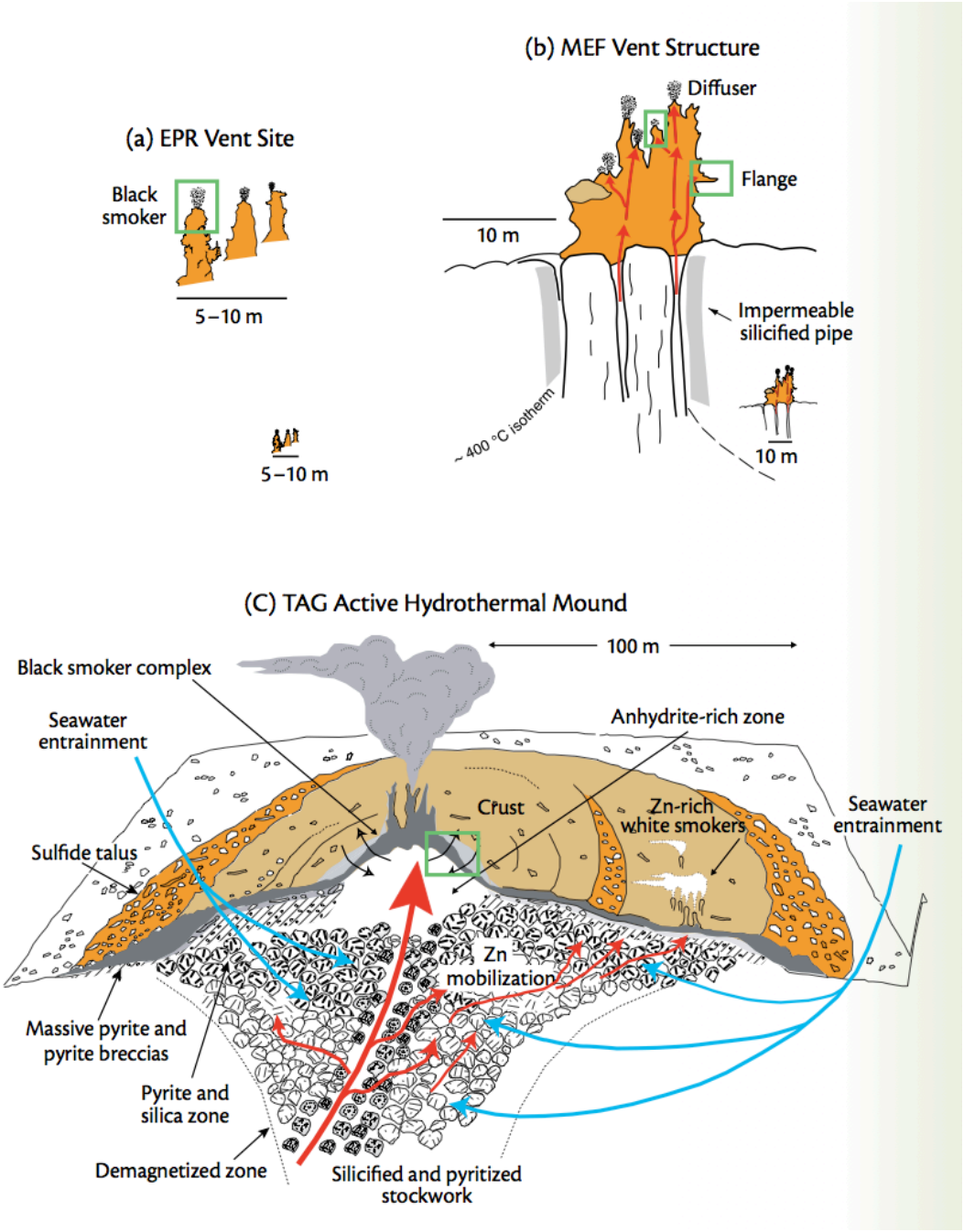

Figure 1-4. Schematic diagram showing differences in vent structure size, morphology, and influencing processes in different tectonic and geologic settings [*Tivey*, 2007].

(a) East Pacific Rise (EPR) hydrothermal vent fields showing tall spires topped by black smoker chimneys. The total accumulation at each vent site is low likely owing to the passage of hot fluids through the structure into the plume above coupled with frequent eruptions, which can bury the deposits.

(continued)

(b) The Main Endeavour Field (MEF) of the Juan de Fuca Ridge (JFR). The MEF includes ~15 structures and covers an area of ~400 m × 200 m. It has been proposed that the steep-sided structures are underlain by pipe-like stockworks sealed by intense silicification of the alteration pipes, preventing entrainment of seawater. The presence of higher-pH fluids provides an explanation for the silicification. (c) The Trans-Atlantic Geotraverse (TAG) active hydrothermal mound. Vigorous venting through the black smoker combined with significant entrainment of seawater into and beneath the mound triggers the deposition of pyrite, chalcopyrite and anhydrite; the generation of fluid with lower pH; and the remobilization of Zn and other trace metals, which are then deposited at the outer edges and on the upper surface of the mound. The very large size compared with structures from the EPR and MEF is the result of efficient mineral deposition owing to seawater entrainment combined with the recurrence of hydrothermal activity at this same location over a period of several tens of thousands of years. Figure courtesy of *Tivey* [2007].

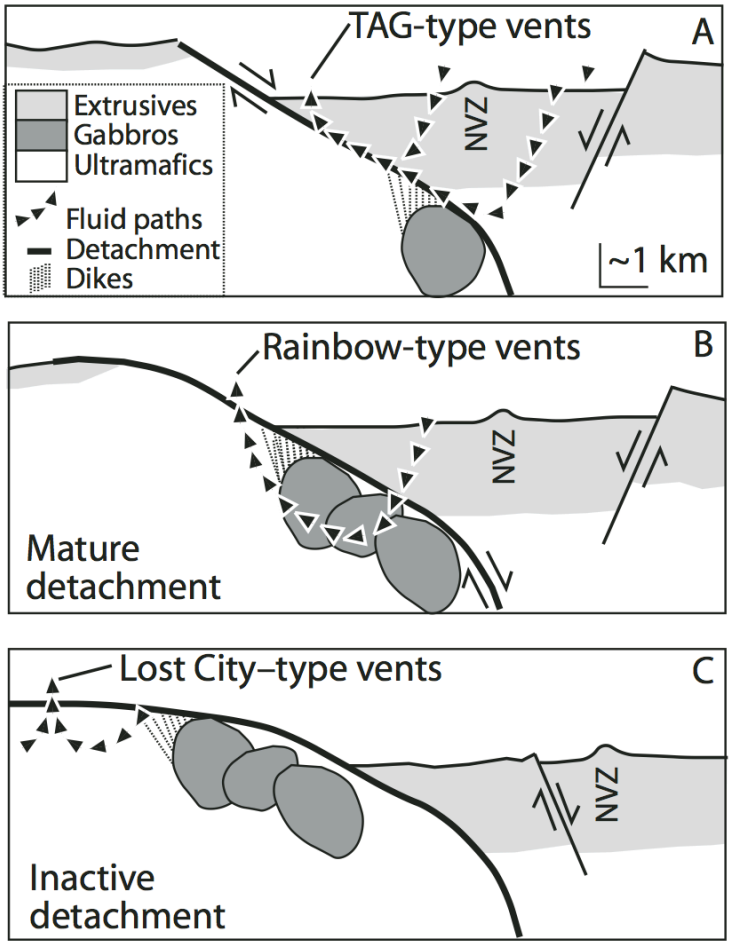

Figure 1-5. Model for fluid circulation and types of hydrothermal venting in and around detachment faults [*McCaig et al*., 2007].

(A) Early intense circulation at high temperatures is driven by gabbroic intrusions into the variably serpentinized ultramafic footwall. The flow follows detachment owing to deformation-enhanced permeability. Trans-Atlantic Geotraverse (TAG)-type vents arise if final discharge passes through highly permeable basaltic lavas at shallow depths in the hanging wall. (B) As early-formed gabbros move away from neo-volcanic zone, the flow moves down into the cooling foot-wall, resulting in the observed isotopic alteration in gabbro and intense talc–tremolite alteration in serpentinized peridotite. Discharge through the exposed ultramafic-rich footwall gives rise to vent fluids similar in composition to those of the Rainbow-type vents. (C) Far from the ridge axis, low-temperature circulation in the serpentinite leads to Lost City–type venting once the footwall peridotite has cooled by exposure on the seafloor. Figure courtesy of *McCaig et al*. [2007].

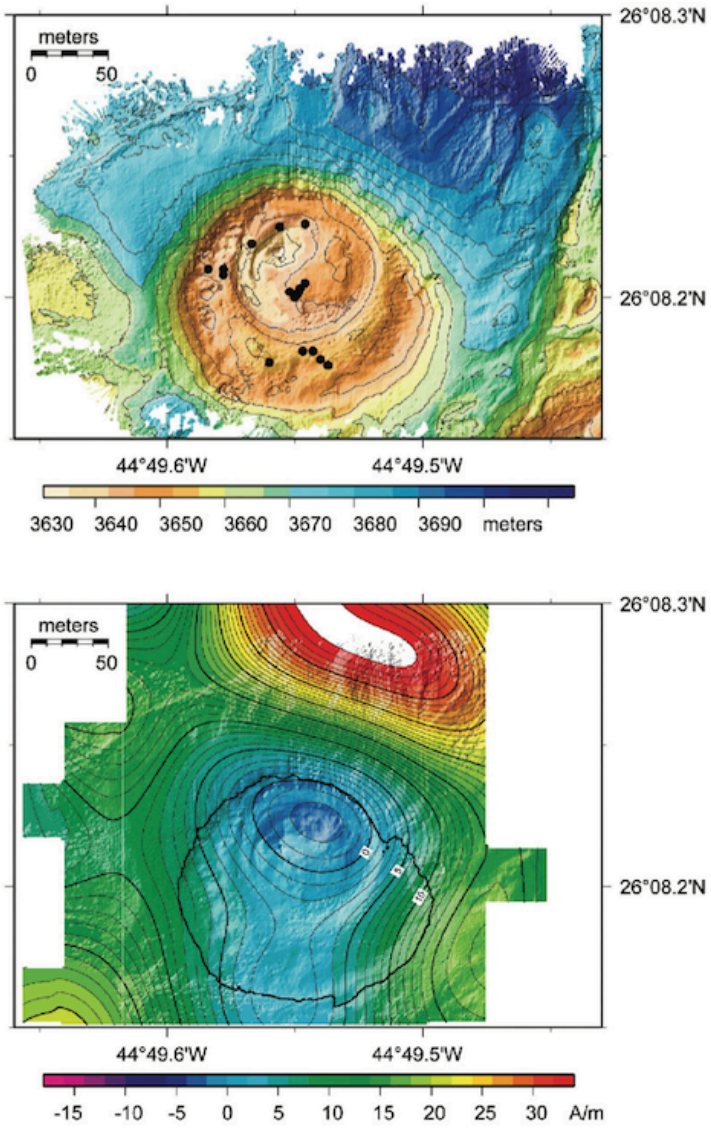

Figure 1-6. Detailed bathymetry and magnetization distribution over the Trans-Atlantic Geotraverse (TAG) hydrothermal mound on the Mid-Atlantic Ridge (MAR) [*Tivey and Dyment*, 2010].

(Top) High-resolution multibeam bathymetry of the TAG mound obtained by ROV *Jason* [*Roman and Singh*, 2007]. The contour interval is 5 m. (Bottom) High-resolution crustal magnetization from near-seafloor magnetic data collected by submersible *Alvin* over the TAG mound at an altitude of ~20 m showing reduced magnetization directly over the mound [*Tivey et al.*, 1993]. The contour interval is 1 A/m. The bold line is the 3645 m isobath delineating the mound extent. Figure courtesy of *Tivey and Dyment* [2010].

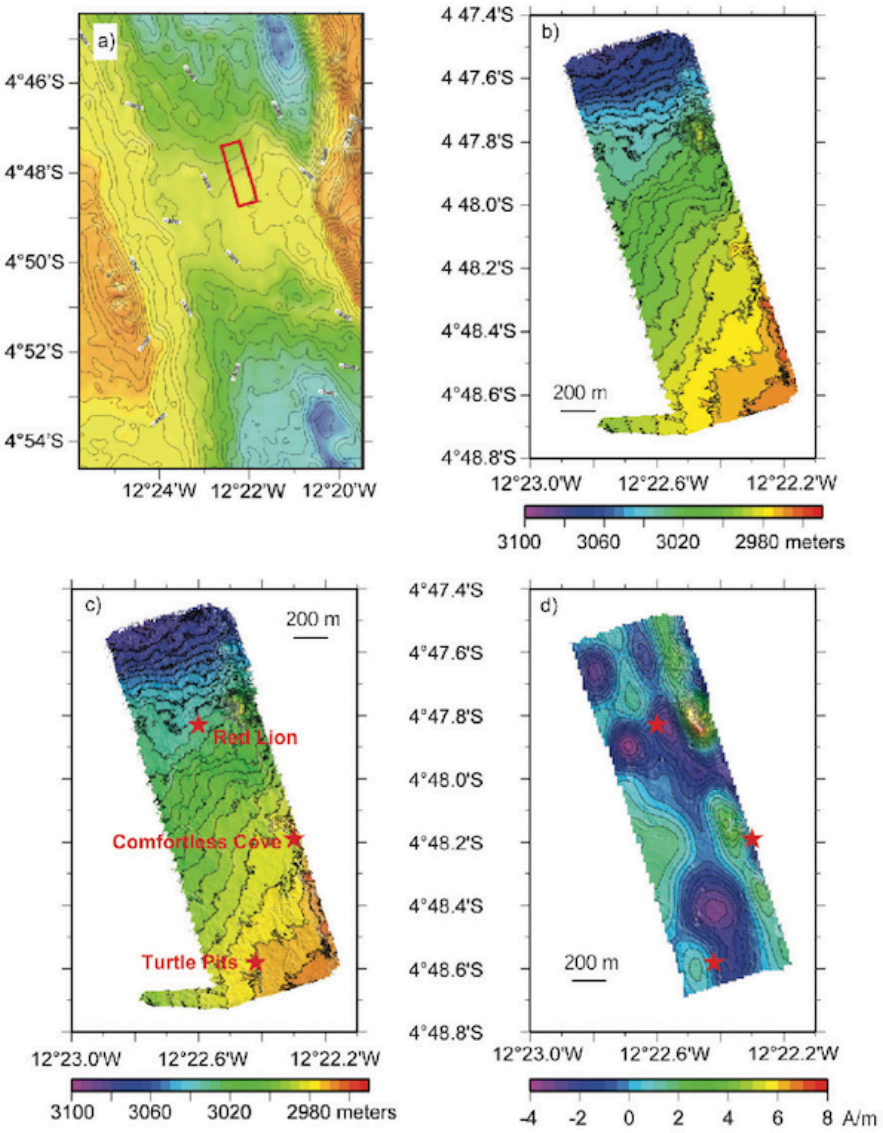

Figure 1-7. Detailed bathymetry and magnetization distribution over the hydrothermal sites of the 4°48′S region on the Mid-Atlantic Ridge (MAR) [*Tivey and Dyment*, 2010].

(a) Regional ship-based multibeam echo sounder bathymetry [*German et al.*, 2008]. (b) High-resolution near-bottom multibeam bathymetry data from the *Autonomous Benthic Explorer* (*ABE*) multibeam. (c) High-resolution bathymetry with the locations and names of active vent sites represented by red stars. (d) Relative crustal magnetization showing zones of reduced magnetization associated with the active vent sites shown by red stars in (c). The data were collected along track lines spaced ~50 m apart at an altitude of ~50 m. Figure courtesy of *Tivey and Dyment* [2010].

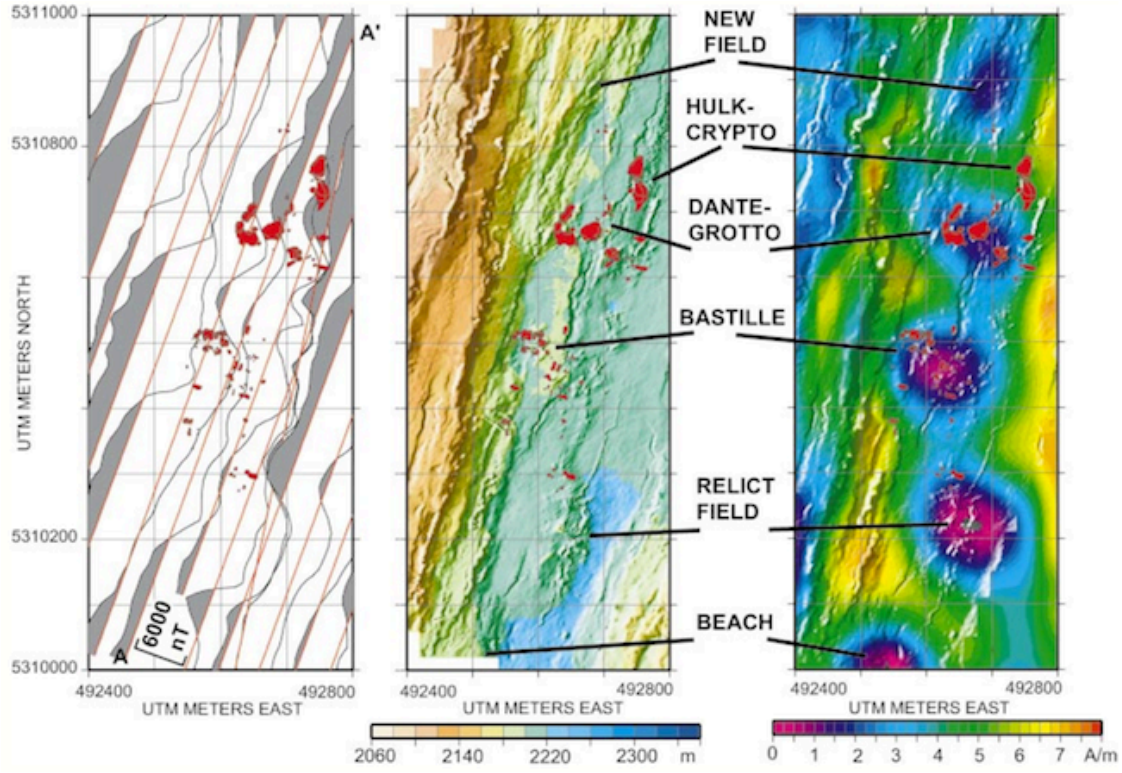

Figure 1-8. Detailed bathymetry and magnetization distribution over the hydrothermal sites of the 4°48′S region on the Mid-Atlantic Ridge (MAR) [*Tivey and Johnson*, 2002].

(Left) Observed magnetic anomalies along the ROV *Jason* track lines shown in red lines. Red areas are published locations of the Main Endeavour Field sulfide chimney edifices. (Middle) High-resolution near-bottom multibeam bathymetry. (Right) Crustal magnetizations showing correlation of circular magnetization lows with active and inactive vent areas. Data were collected along track lines spaced ~40 m apart at altitude of ~20 m. Figure courtesy of *Tivey and Johnson* [2002].

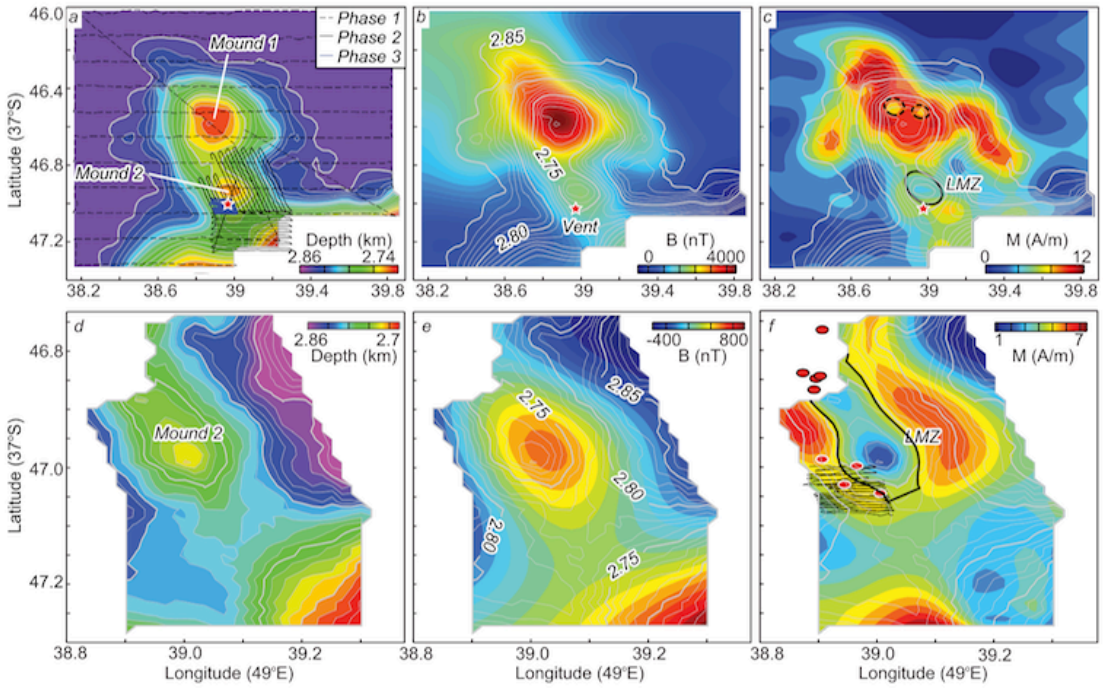

Figure 1-9. Detailed bathymetry and magnetization distribution over the hydrothermal sites of Southwestern Indian Ridge (SWIR) [*Zhu et al.*, 2010].

(a) Bathymetry collected during the *Autonomous Benthic Explorer* (*ABE*) Phase-1 survey. Gray contours delineate the seafloor depth with 10 m intervals. The track lines of *ABE* surveys Phase-1 (flying at a constant depth of 2625 m), Phase-2 (50 m above the seafloor with a track spacing of 30 m), and Phase-3 (5 m above the seafloor with a track spacing of 10 m) are shown by black dashed, black solid, and blue dashed lines, respectively. (b) Near-seafloor magnetic anomalies collected during the *ABE* Phase-1 survey. (c) Crustal magnetization from data collected during the *ABE* Phase-1 survey. The two sub-circular local topographic highs are labeled as Mound 1 and Mound 2. The red star indicates the location of the high-temperature hydrothermal vent field. The ellipses indicate three low magnetization zones (LMZs). (d) Bathymetry collected during the *ABE* Phase-2 and Phase-3 surveys. (e) Near-seafloor magnetic anomalies collected during the *ABE* Phase-2 and Phase-3 surveys. (f) Crustal magnetization from data collected during the *ABE* Phase-2 and Phase-3 surveys. The black ellipse indicates the area of the LMZ. Black solid lines show the track lines of the *ABE* Phase-3 survey, during which time the bottom photographs were obtained. Red dots represent the locations of active hydrothermal vents. Figure courtesy of *Zhu et al.* [2010].

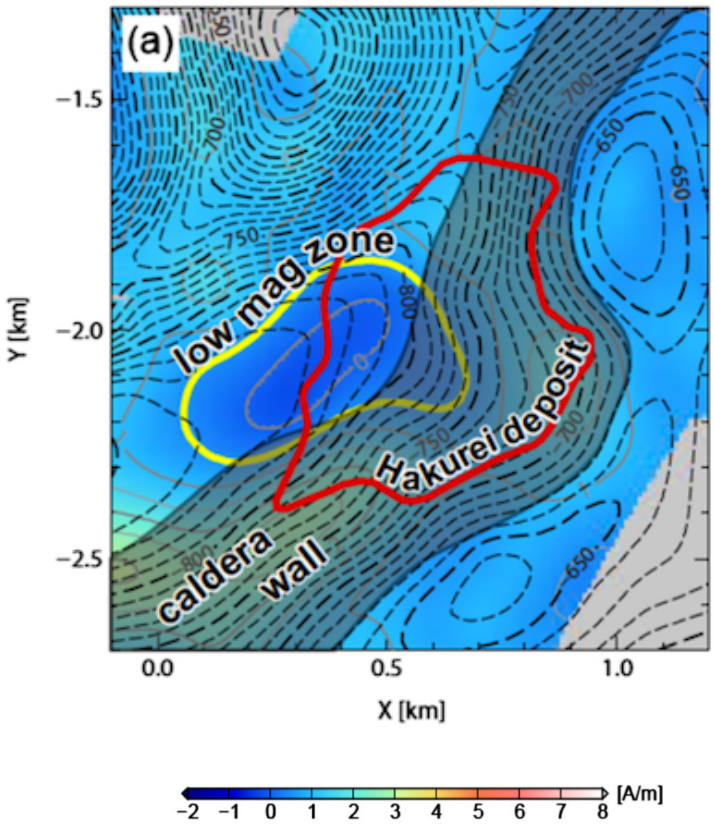

Figure 1-10. Detailed bathymetry and magnetization distribution over the Hakurei hydrothermal sites of Izu–Ogasawara arc–back-arc volcano [*Honsho et al*., 2013]. The magnetization map is shown by the color scale. The low magnetization zone (LMZ) is represented by an area of magnetization intensity lower than 0.5 A/m. The topographic contours (dashed lines) have an interval of 10 m. The data were collected along track lines at an altitude of ~80 m. The configuration of the Hakurei deposit is outlined by the red line [*Iizasa et al*., 2004]. The LMZ and the caldera wall fault are represented by a yellow line and by the shading, respectively. Figure courtesy of *Honsho et al.* [2013].

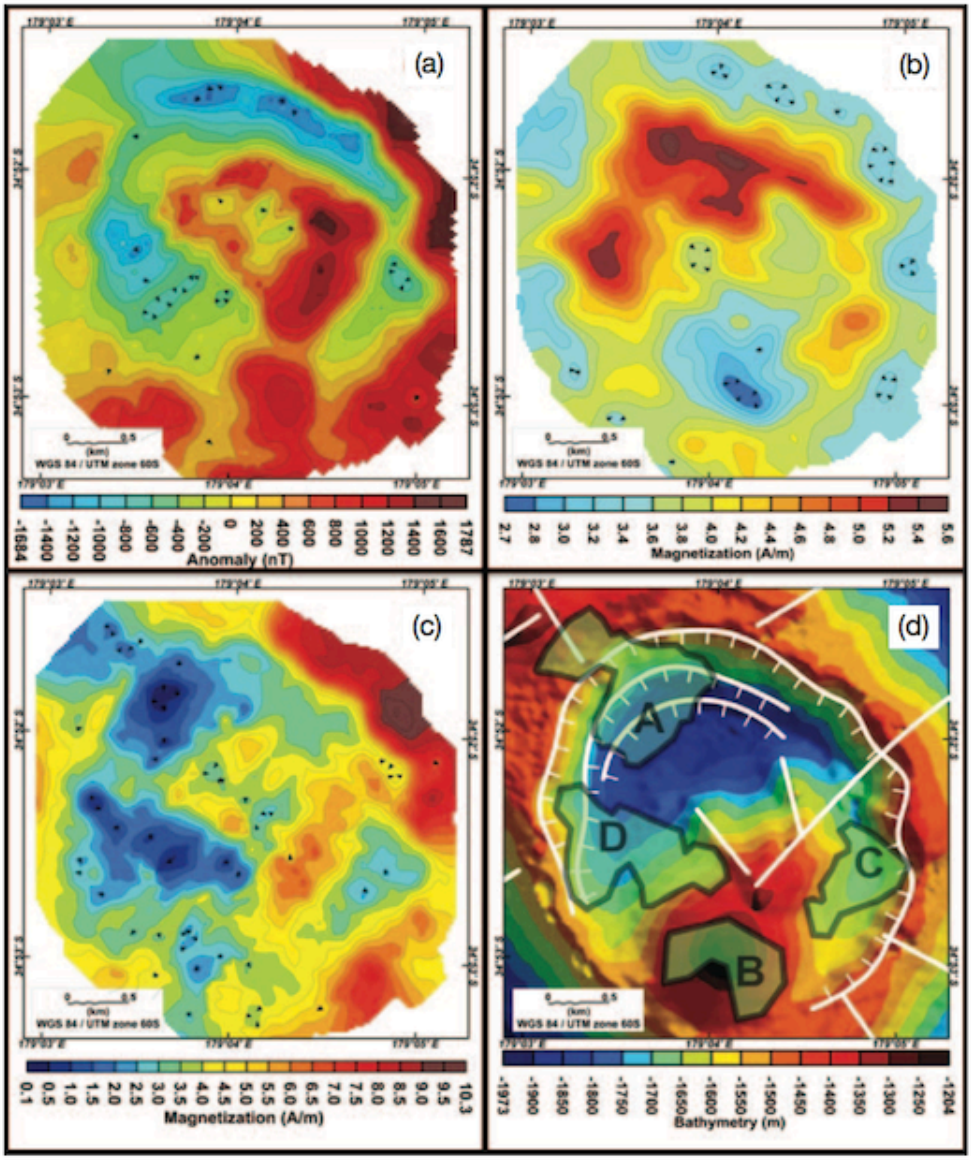

Figure 1-11. Detailed bathymetry and magnetization distribution over the hydrothermal sites of the Brothers volcano on the Tonga–Kermadec arc [*Caratori-Tontini et al*., 2012].

(a) Nears-seafloor magnetic anomaly map from data collected by the AUVs *Autonomous Benthic Explorer* (*ABE)* and *Sentry* at an altitude of ~50 m. (b) Annihilator map. (c) Crustal magnetization distribution from inversion of magnetic data determined after adding the annihilator. (d) Bathymetric map with the main faults, lineaments, and hydrothermal fields of the NW caldera wall site (A) and Brothers caldera at the cone site (B). Figure courtesy of *Caratori-Tontini et al*. [2012].

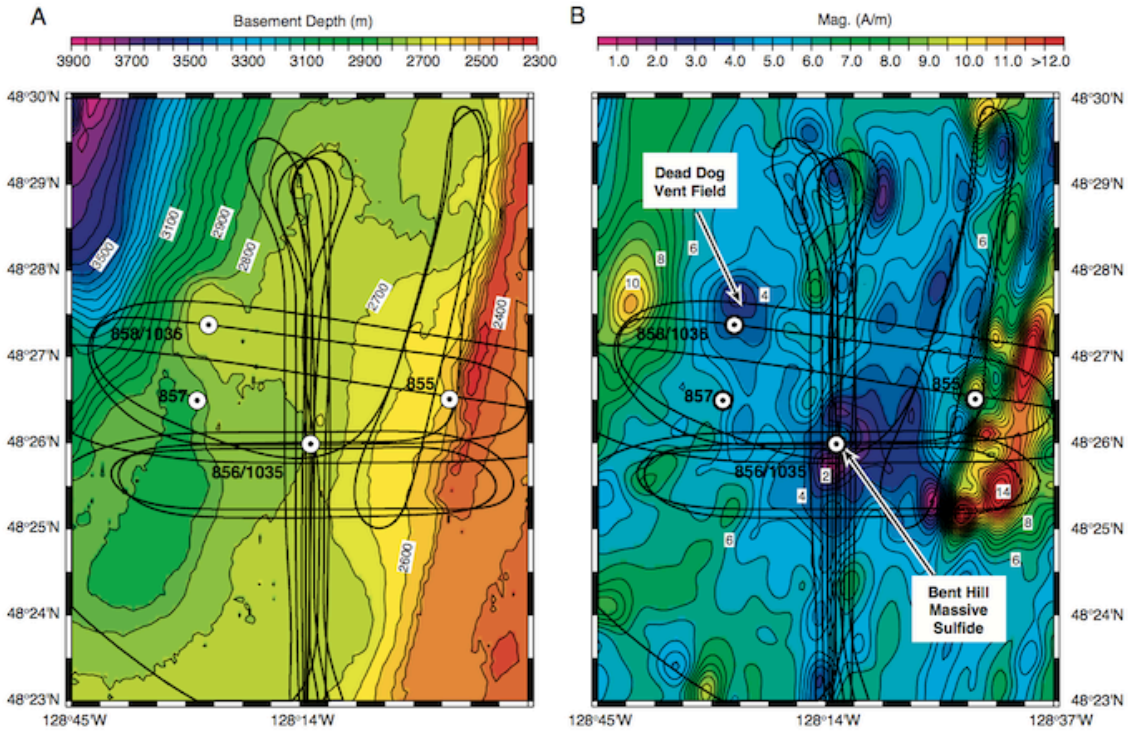

Figure 1-12. Detailed bathymetry and magnetization distribution over the Bent Hill Massive Sulfide of the Middle Valley on the Juan de Fuca Ridge (JFR) [*Gee et al*., 2001].

(a) Contour map of sediment-basement interface used for magnetic inversion. (b) Crustal magnetization distribution. Sufficient magnetic annihilator has been added to the solution to make the magnetizations positive. Locations of Ocean Drilling Program (ODP) drill sites (circles) and near bottom survey tracks are shown for reference. Figure courtesy of *Gee et al*. [2001].

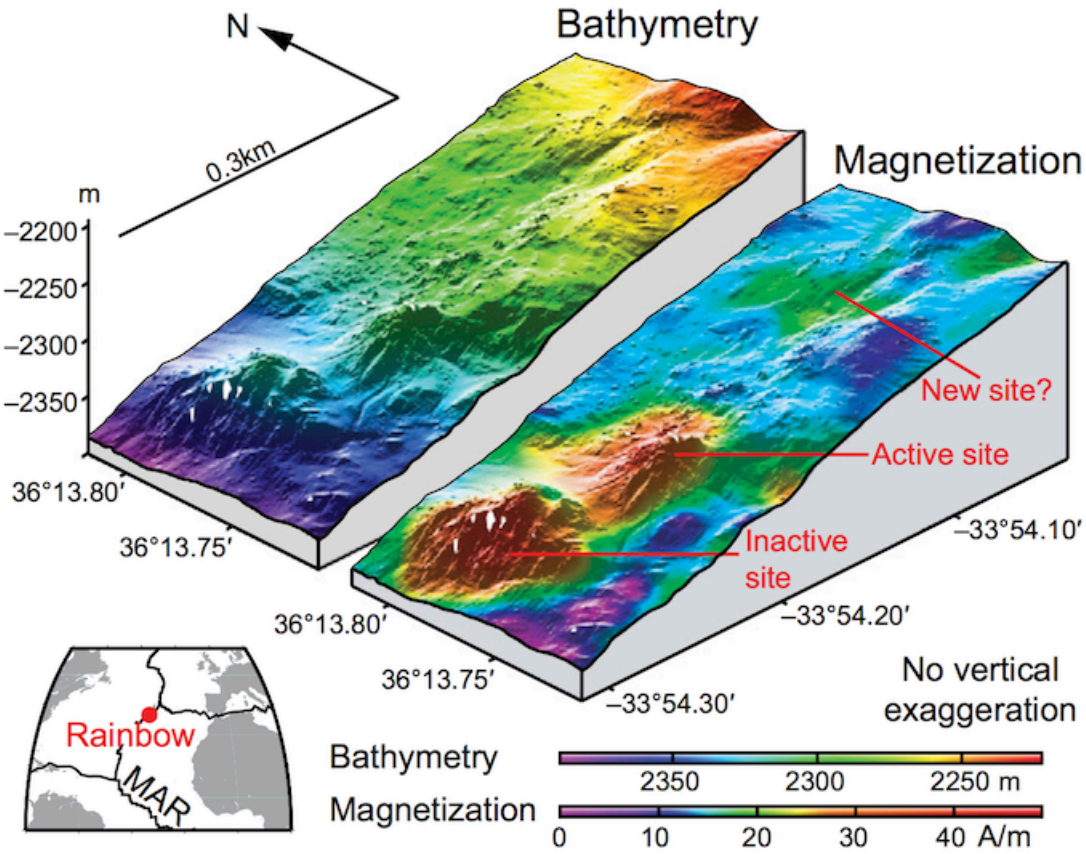

Figure 1-13. Detailed bathymetry and magnetization distribution over the ultramafic-hosted hydrothermal site Rainbow of the Mid-Atlantic Ridge (MAR) [*Szitkar et al*., 2014b].

(Left) High-resolution near-seafloor multibeam bathymetry in three-dimensional (3-D) view. The westernmost hydrothermal mound is cut by a fault on its western flank, resulting in stockwork mineralization outcrops and hydrothermal debris in the talus. (Right) Crustal magnetization draped on bathymetry in 3-D view. The strong positive magnetization contrast is associated with the two active hydrothermal mounds. The data were collected by the ROV *Victor* along track lines spaced ~10 m apart at an altitude of ~10 m. Figure courtesy of *Szitkar et al*. [2014b].

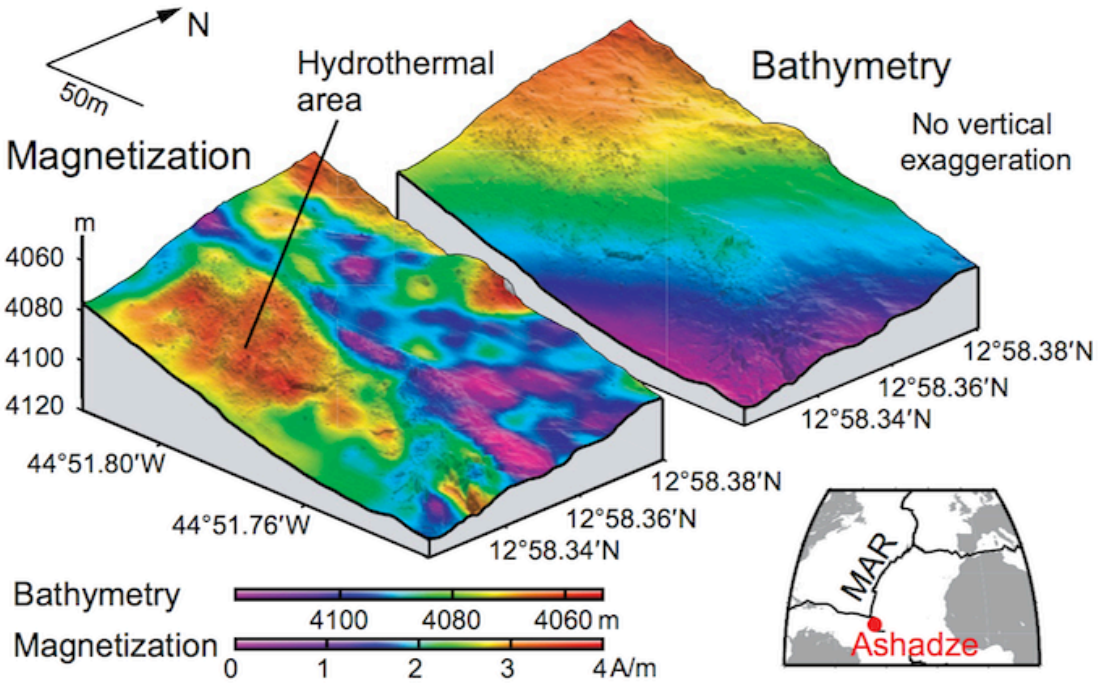

Figure 1-14. Detailed bathymetry and magnetization distribution over the ultramafic-hosted hydrothermal site Ashadze-1 of the Mid-Atlantic Ridge (MAR) [*Szitkar et al.*, 2014b].

(Right) High-resolution near-seafloor multibeam bathymetry in three-dimensional (3-D) view. (Left) Crustal magnetization draped on bathymetry in 3-D view. The strong positive magnetization contrast is associated with the active hydrothermal site. The data were collected by the ROV *Victor* along track lines spaced ~10 m apart at an altitude of ~10 m. Figure courtesy of *Szitkar et al*. [2014b].

Table 1-1. Summary of previous near-seafloor magnetic surveys in various tectonic setting.

Vent field	Active (A) Inactive (I)	Region	Tectonic setting	Terrain	Magnetization contrast	Reference
TAG	A	Mid-Atlantic Ride	Mid-ocean ridge	Basaltic	- 12 A/m	1, 2, 3
Krasnov	I	Mid-Atlantic Ride	Mid-ocean ridge	Basaltic	- 12 A/m	4
4°48′S area	A	Mid-Atlantic Ride	Mid-ocean ridge	Basaltic	- 3–4 A/m	2
Rainbow	A	Mid-Atlantic Ride	Mid-ocean ridge	Ultramafic	+ >30 A/m	2, 5, 6
Ashadze	A	Mid-Atlantic Ride	Mid-ocean ridge	Ultramafic	+ 4A/m	6
Main Endeavour	A	Juan de Fuca Ridge	Mid-ocean ridge	Basaltic	- 3 A/m	7, 8
Bent Hill Massive Sulfide	I	Juan de Fuca Ridge	Mid-ocean ridge	Sedimeted-basaltic	+ 5 A/m	9
Nameless	A	Southwest Indian Ridge	Mid-ocean ridge	Basaltic	- 3 A/m	10
Hakurei	A	Izu-Ogasawara arc	Back-arc rift	Andesitic to dacitic	- <1 A/m	11
Brothers	A	Kemdec arc	Arc volcano	Dacitic	- 3–4 A/m	12
Palinuro	A	Aeolian arc	Arc volcano	Basaltic	- <2 A/m	13, 14

1: *Tivey et al*., 1993, 2: *Tivey and Dyment*, 2010, 3: *Szitkar and Dyment*, 2014, 4: *Szitkar et al*., 2014a, 5: *Nakase*, 2002, 6: *Sztikar et al*., 2014b, 7: *Tivey and Johnson*, 2002, 8: *Tivey et al*., 2014, 9: *Gee et al*., 2001, 10: *Zhu et al*., 2010, 11: *Honsho et al*., 2013, 12: *Caratori-Tontini et al*., 2012, 13; *Caratori-Tontini et al*., 2014, 14; *Szitkar et al*., 2015.

Chapter 2

On- and Off-axis Hydrothermal Fields in Back-arc Region of Southern Mariana Trough

In this chapter, I present a detailed analysis of the high-resolution vector magnetic data acquired by the HOV *SHINKAI 6500* on five hydrothermal vent fields in the back-arc spreading axis (Snail and Yamanaka sites), off-axis foot (Archean site), and off-axis volcano (Pika and Urashima sites) areas of the southern Mariana Trough (SMT). A new 3-D forward scheme was applied to exploit the surrounding bathymetry and varying altitudes of the submersible for estimating the absolute crustal magnetization. The results reveal that magnetic-anomaly-derived absolute magnetizations (MADAMs) show reasonable correlation with the natural remanent magnetizations (NRMs) of the rock samples collected from the seafloor of same region. The distribution of MADAM suggests that all five andesite-hosted hydrothermal fields are associated with reduction of magnetization, as is generally observed at basalt-hosted hydrothermal sites. Furthermore, both the Pika and Urashima sites were found to have their own distinct low magnetization zones, which could not be distinguished in the magnetic anomaly data collected at higher altitudes by the AUV. The spatial extent of the resulting low magnetization is approximately ten times wider at off-axis sites than that at on-axis sites, possibly reflecting larger accumulations of nonmagnetic sulfides, stockwork zones, and alteration zones at the off-axis sites.

2-1. Geological Background

The southern Mariana Trough (SMT) is located along the convergent margin between the Pacific and Philippine Sea plates [e.g., *Stern et al*., 2003] (Fig. 2-1a). The subduction of the Pacific plate beneath the Philippine Sea plate began in early Eocene (~50 Ma) [e.g., *Seno and Maruyama*, 1984]. From ~30 Ma to ~20 Ma, the proto-Mariana arc rifted, forming the Parece Vela back-arc basin [*Okino et al*., 1999]. Seafloor extension has focused on the eastern side of the Philippine Sea plate for the last 6 Ma, resulting in the development of the Mariana Trough [*Hussong and Uyeda*, 1982]. Seafloor spreading started in the central part of the trough, which was followed by propagation to both the northern and southern areas [*Martinez et al*., 2000; *Yamazaki et al*., 2003], forming a crescent-shaped basin ~200-km wide at its central point. The spreading axis is now located on the eastern side of the basin, indicating highly asymmetric spreading [*Deschamps and Fujiwara*, 2003; *Asada et al*., 2007].

In the southernmost part of the SMT, the general trend of the arc-trench system changes from N–S to E–W. South of 14°N, seafloor spreading began 3 Ma, with a half rate of 33 km/Myr for the west side and 13 km/Myr for the east side [*Seama et al*., 2015]. The seafloor morphology of axial high features is characteristic of fast and/or strongly magmatic spreading context. The distance between the spreading axis and the active Mariana arc volcanic front is ~20 km, suggesting a complex magmatic environment influenced by back-arc and arc-type magmas [*Martinez et al*., 2000]. Analyses of sea-surface gravity data have revealed a thick crust (5800–6800 m on average) in the SMT, which is in agreement with vigorous magmatic activity with sheet-like mantle upwelling under the spreading axis [*Kitada et al*., 2006].

Five active hydrothermal vent fields have been discovered in the SMT between 12°55’N and 12°57’N (Fig. 2-1b) [*Wheat et al*., 2003; *Ishibashi et al*., 2004; *Urabe et al*., 2004; *Kakegawa et al*., 2008; *Nakamura et al*., 2013]. These fields are aligned perpendicularly to, and within ~5 km from, the spreading axis. The Snail and Yamanaka sites are located on the axial area, where undeformed volcanic structures have been reported based on high-resolution bathymetric surveys, which have been interpreted as the current neo-volcanic zone (NVZ) [*Yoshikawa et al*., 2012]. At the Snail site that displays both active and dead chimneys, and is surrounded by fresh pillow basalt, the maximum temperature of venting fluid was 248°C at the time of discovery in May 2003

[*Wheat et al*., 2003]. The Yamanaka site is located on a volcanic edifice 1.2 km southwest of the Snail site. It consists of white smokers, dead sulfide chimneys, and altered pillow lavas [*Kakegawa et al*., 2008].

The Archean site is located at the eastern foot of the axial high, where active black smokers have been observed on the top of a 50-m-high mound made of pyrite, chalcopyrite, and sphalerite [*Urabe et al*., 2004]. The highest recorded fluid temperatures were 213°C in 2004 and 341°C in 2005 [*Ishibashi et al*., 2004, YK05-09 cruise report].

The Pika and Urashima sites lie on a 400-m-high off-axis seamount ~5 km from the spreading axis. The Pika site is located on the top of a seamount and consists of black smokers, white smokers, dead chimneys, and sulfide mounds. The Urashima site was discovered in 2010 at the northern foot of the seamount 500 m from the Pika site and it comprises large black smokers (>10 m) and dead chimneys [*Nakamura et al*., 2013]. The highest recorded fluid temperatures at the Pika and Urashima sites are 330°C and 280°C, respectively [*Urabe et al*., 2004, *Nakamura et al*., 2013].

2-2. Data and Methods

2-2-1. Data acquisition

Near-seafloor exploration surveys were conducted around the five hydrothermal vent fields of the SMT using the HOV *SHINKAI 6500* of the Japan Agency for Marine-Earth Science and Technology (JAMSTEC) during two scientific cruises of the *R/V Yokosuka*. Five dives were conducted during the YK10-10 cruise in August 2010 and other nine dives during the YK10-11 cruise in September 2010. Four dives (#1218, #1220, #1227, and #1228) were devoted to the axial area, including the Snail and Yamanaka sites, five dives (#1216, #1217, #1221, #1223, and #1224) to the off-axis area around the Archean site, and five dives (#1214, #1219, #1222, #1225, and #1226) to the off-axis seamount on which the Pika and Urashima sites are located. All fourteen dives were navigated by acoustic ranging using the super-short baseline positioning system. Magnetic data were generally collected at altitude lower than 15 m, but occasionally, at altitudes of several tens of meters.

A three-component fluxgate magnetometer, developed by the Atmosphere and Ocean Research Institute of the University of Tokyo, was rigidly fixed to the front side

of *SHINKAI 6500*. Both vector magnetic data and the attitude of the submersible (heading, pitch, and roll) from a gyrocompass and a motion sensor (OCTANS, IXBLUE Inc.) were collected at a 10-Hz sampling rate. The accuracy of the magnetometer is 0.4 nT.

The surface geology along the dive tracks was constrained by examining video and still camera records for each dive. In some limited areas, no visual observation of the surface geology was obtained because of the higher altitude of the submersible. I classified the geological features into five categories: (i) fresh lava, (ii) fractured lava, (iii) sediment-covered lava, (iv) debris and breccia, (v) and hydrothermal material. The hydrothermal areas were characterized by sulfide deposits, chimneys, pluming hot water, white bacteria mats, and biological habitats.

2-2-2. Initial processing

Because the magnetometer was mounted on the submersible, magnetic data were strongly affected by the magnetization of the vehicle. The observed magnetic field vector ($\vec{H}_{obs}$) is expressed as the sum of induced ($\mathbf{AR}\vec{F}$) and permanent ($\vec{H}$) magnetic fields of the vehicle and the ambient geomagnetic field ($\vec{F}$) as following [*Isezaki*, 1986];

$$\begin{aligned}\vec{H}_{obs} &= \mathbf{R}\vec{F} + \mathbf{AR}\vec{F} + \vec{H}_p \\ &= (\mathbf{A} + \mathbf{E})\mathbf{R}\vec{F} + \vec{H}_p\end{aligned}$$

where,

$$\begin{aligned}\mathbf{R} &\equiv \mathbf{r}(\theta_2)\mathbf{p}(\theta_3)\mathbf{h}(\theta_1) \\ &\equiv \begin{pmatrix}1 & 0 & 0\\ 0 & \cos(\theta_2) & \sin(\theta_2)\\ 0 & -\sin(\theta_2) & \cos(\theta_2)\end{pmatrix}\begin{pmatrix}\cos(\theta_3) & 0 & -\sin(\theta_3)\\ 0 & 1 & 0\\ \sin(\theta_3) & 0 & \cos(\theta_3)\end{pmatrix} \\ &\quad \begin{pmatrix}\cos(\theta_1) & \sin(\theta_1) & 0\\ -\sin(\theta_1) & \cos(\theta_1) & 0\\ 0 & 0 & 1\end{pmatrix}.\end{aligned}$$

I used data collected during 360° rotations performed spontaneously by the submersible during its descent to estimate both the induced magnetization vector of the vehicle, expressed by the magnetic susceptibility tensor **A** (nine coefficients) and remanent magnetization vector $\vec{H}_p$ (three coefficients) of the vehicle using a dumped least square method developed by *Honsho et al*. [2009]. Parts of the data obtained at depths

shallower than 500 m below sea surface or deeper than 500 m above the seafloor were not used in order to avoid the magnetic effects of the ship and the seafloor. The coefficients were estimated individually for each dive. For example, I obtained the following coefficients of dive#1223 using a dumping factor of 7,

$$\mathbf{A} = \begin{pmatrix} 0.03618 & 0.03499 & 0.00155 \\ -0.03769 & 0.01583 & 0.00051 \\ -0.06182 & 0.00616 & 0.00021 \end{pmatrix},\ \vec{\mathrm{H}}_{\mathrm{p}} = \begin{pmatrix} -274 \\ -1928 \\ 441 \end{pmatrix} \text{ and } \sigma = \begin{pmatrix} 47 \\ 47 \\ 34 \end{pmatrix}.$$

The quantity σ is model error of observation equation. Based on these coefficients, the attitude of the submersible, and the regional geomagnetic field (approximated by the International Geomagnetic Reference Field, IGRF [*IAGA Working Group V-MOD*, 2010]), I computed the magnetic effects of the submersible during the survey and removed them from the data. The correction was performed for each dive and the resulting vector magnetic field was rotated to the geographical coordinates, giving the model error σ in the ranges 47–200, 47–175, and 29–68 nT in the northern, eastern, and downward components, respectively.

The subsequent three-dimensional analysis required both the position of the magnetometer and the seafloor topography. The super-short baseline position was smoothed and resampled at intervals of 1 sec using a Gaussian function filter after removing outliers. The altitude data were collected every 1 sec with 1-m resolution and the distance between the altimeter and magnetic sensor was taken into account to obtain the geometry of the experiment. The seafloor topography was extracted from the 2-m-interval grid built from data collected by the AUV *Urashima* using a 400-kHz multibeam echo sounder (SeaBat 7125 AUV, Reson Inc., Denmark) during the YK09-09 cruise [*Yoshikawa et al*., 2012]. Additional sea-surface bathymetric data (50-m-interval grid) were compiled for areas not surveyed by the AUV *Urashima*.

2-2-3. Forward modeling

The three components of the synthetic magnetic anomaly along the dive tracks, at the same locations as the observed data, were simulated assuming uniform magnetization of the seafloor, with direction parallel to the geocentric axial dipole field (inclination: 24°, declination: 0°) and intensity of 1 A/m (Fig. 2-2). There was not much difference between the results based on assumption of magnetization direction parallel to the geocentric axial dipole and the IGRF (inclination: 11°, declination: 1°). A

half-infinite magnetic source was considered, the upper boundary of which was constrained by the bathymetry. The magnetic source was modeled by a collection of half-infinite rectangular prisms with lateral dimensions of 2 m. Magnetic anomalies at each calculation point were obtained by applying the algorithm of *Bhattacharyya* [1964], which provides the magnetic anomaly produced by uniformly magnetized prisms, via the summing up of the contributions of all prisms located within 100 m from the point. Each prism is oriented parallel to the northern, eastern, and downward axes, and has magnetization **M** (M_N, M_E, M_Z). Dimensions are given by $n2 \leqq n' \leqq n1$, $e1 \leqq e' \leqq e2$, and $z_1 \leqq z \leqq \infty$. If the anomaly due to the prism is observed in a regional field directed parallel to **F** (F_N, F_E, F_Z), the three components of anomalous field (northern: ΔN, eastern: ΔE, downward: ΔZ) at the origin is given by

$$\Delta N = C_m F_N \left[-M_N \arctan\left(\frac{n'e'}{n'^2 + rz_1 + {z_1}^2}\right) - M_E \log(r + z_1) + \frac{M_Z}{2} \log\left(\frac{r - e'}{r + e'}\right) \right] \Bigg|_{n1}^{n2} \Bigg|_{e1}^{e2}$$

$$\Delta E = C_m F_E \left[-M_N \log(r + z_1) - M_E \arctan\left(\frac{n'e'}{r^2 + rz_1 - x'^2}\right) + \frac{M_Z}{2} \log\left(\frac{r - n'}{r + n'}\right) \right] \Bigg|_{n1}^{n2} \Bigg|_{e1}^{e2}$$

$$\Delta Z = C_m F_Z \left[-\frac{M_N}{2} \log\left(\frac{r - e'}{r + e'}\right) + \frac{M_E}{2} \log\left(\frac{r - n'}{r + n'}\right) + M_Z \arctan\left(\frac{n'e'}{rz_1}\right) \right] \Bigg|_{n1}^{n2} \Bigg|_{e1}^{e2}$$

where

$$r = n'^2 + e'^2 + {z_1}^2,$$

and C_m is magnetic permeability of free space in SI unit. This equation provide magnetic anomaly of a prism with top at z_1 and bottom at infinity [*Bhattacharyya,* 1964]. If magnetic anomaly is calculated twice, once for $z_1 = z_t$ and $M = M_0$, and once for $z_1 = z_b$ and $M = -M_0$, then according to superposition principle, the sum of the two

calculations provide the magnetic field of a prism with magnetization M_0, top at z_t and bottom at z_b.

Figure 2-3 shows synthetic total magnetic anomaly profiles computed for magnetic source layers of various thicknesses. Although I adopted a half-infinite source, these models show that the synthetic magnetic anomalies at altitudes lower than 40 m are not significantly affected by magnetic sources deeper than 200 m.

Figure 2-4 shows a comparison between observed and synthetic magnetic anomalies along dive #1227. The three components of the synthetic anomaly show similarities with those of the observed anomaly, except for the scale that reflects the low (1 A/m) intensity of magnetization assumed for the modeling.

2-2-4. Estimation of absolute magnetization

The ratio of the observed magnetic anomaly to the synthetic anomaly, computed with unit magnetization intensity, represents an estimate of the absolute magnetization intensity of the shallow sub-seafloor. In order to estimate this ratio quantitatively, I used the linear transfer function technique in the frequency domain [*Honsho et al*., 2009]. This approach has been originally used in gravity studies to estimate a ratio of gravity to elevation as a function of wave number [*McKenzie and Bowin*, 1976; *Watts*, 1978].

Both observed and synthetic anomalies were resampled at every 1-m interval along the dive tracks. The magnetization was estimated for each 128-m-wide sliding window shifted by steps of 16 m along the tracks. The coherency, ratio of the observed to synthetic anomalies together with its error, and polarity (given by the phase difference between the two signals) were obtained over wavelengths between 16 and 128 m. This procedure was applied to each component of the anomaly. I retained estimations with a coherency greater than 0.3 on at least two components for further interpretation. The ratios of observed to synthetic northern and downward components were finally averaged and adopted as best estimate of absolute magnetization intensity of the shallow sub-seafloor. This was done for two reasons: (ii) the eastern component is nearly perpendicular to the IGRF direction in the survey area, i.e. it is more susceptible to correction errors mainly affected by heading error, resulting in a lower S/N ratio; and (ii) the absolute magnetization computed from this component tends to be extremely large, because the synthetic magnetic anomaly is small due to the assumption that the

magnetization direction is parallel to the axial dipole field. The magnetization polarity was regarded as normal for phases between -90° and 90° and reversed for phases between 90° and 270°.

2-3. Results

2-3-1. MADAM and seafloor geology

The four dives in the axial area including the Snail and Yamanaka sites provided 312 reliable estimates of magnetic-anomaly-derived absolute magnetization (MADAM) ranging from 1–116 A/m (Fig. 2-5a). The 55 estimates among them shows coherency higher than 0.5 in both northern and downward components. Thirty-two percent of the data indicate high magnetization stronger than 30 A/m, whereas 19% are associated with magnetizations weaker than 10 A/m. Extremely high intensities (>70 A/m) are observed in the NVZ, north of the Snail site, south of the Yamanaka site, and in the central volcanic mound (12°56’52”N, 143°36’57”E). Relatively low intensities (<10 A/m) are observed around the Snail site and in an area ~200–500 m from the NVZ, where many faults trending NNE–SSW to NE–SW extend parallel to the NVZ.

The video records in this area show fresh lavas, fractured lavas, and hydrothermal material. Sulfide deposits, biological communities, and chimneys were observed near the Snail site (Figs. 2-5b and 2-5c), and fresh pillow lavas seen around the Snail hydrothermal area (Figs. 2-5b and 2-5d). At the Yamanaka site, sea anemones are growing within the weak fluid venting (Figs. 2-5b and 2-5e) on top of fresh pillow lavas (Figs. 2-5b and 2-5e): lavas on the western slope of the axial high are fractured and appear to be older (Figs. 2-5b and 2-5g).

The five dives in the off-axis area including the Archean site provided 204 reliable estimates of MADAM ranging from 0.4–29 A/m (Fig. 2-6a). The 22 estimates among them shows coherency higher than 0.5 in both northern and downward components. More than 85% show intensities weaker than 10 A/m. At the top of the mound, the magnetization is generally weaker than 3 A/m, whereas stronger magnetizations (>10 A/m) are found outside the mound.

In this off-axis area, video records show debris and breccia, sediment-covered lavas, and hydrothermal material. Active and dead chimneys and sulfide deposits were observed at the top of the mound (Figs. 2-6b and 2-6c), and debris and breccia

distributed widely on the slopes of the mound (Figs. 2-6b and 2-6d). The relatively flat seafloor around the mound was covered mostly by pillow lavas with sediment (Figs. 2-6b and 2-6e).

The five dives in the area of the off-axis seamount including the Pika and Urashima sites provided 250 estimates of MADAM ranging from 0.6–61 A/m (Fig. 2-7a). The 28 estimates among them shows coherency higher than 0.5 in both northern and downward components. Sixty-six percent indicate magnetization weaker than 10 A/m, and 12% stronger than 20 A/m. The magnetization is weak (<5 A/m) on the top of the seamount where the Pika site is situated. Relatively high magnetization (<17 A/m) is indicated on the northern slope of the seamount between the Pika and Urashima sites. At the northern foot of the seamount, low magnetization values (<5 A/m) are concentrated around the Urashima site. This low magnetization concentration is surrounded by an area of high magnetization larger than 10 A/m, including several very high magnetization points (~60 A/m) near the northeastern edge of the survey area. The magnetization is also very high (~54 A/m) on the southwestern side of the seamount where small conical mounds are observed.

The video records show fresh lavas, sediment-covered lavas, debris and breccia, and hydrothermal material in the area of the off-axis seamounts. Sulfide sediments and both active and dead chimneys were seen near the Pika site (Figs. 2-7b and 2-7c). Dead chimneys were scattered within a few 100 m of the top of the seamount. Sediment-covered lavas were distributed just south of the Pika site (Figs. 2-7b and 2-7d), and Active chimneys, many dead chimneys, and sulfide deposits were observed at the Urashima site (Figs. 2-7b and 2-7e). Sediment-covered lavas were distributed widely outside the hydrothermal areas (Figs. 2-7b and 2-7f), and debris and breccia observed on the slope between the Pika and Urashima sites (Figs. 2-7b, 2-7g, and 2-7h). An extensive area of fresh pillow lavas was discovered on the southwestern side of the seamount (Figs. 2-7b, 2-7i, and 2-7j).

The five investigated hydrothermal fields in the SMT (Fig. 2-1b) are clearly associated with a low MADAM: essentially, the three off-axis sites appear almost non magnetic. Only the Yamanaka site is not associated with a clear zone of weak magnetization, but the estimated MADAM values are relatively lower (27–46 A/m) than those of the nearby volcanic mound (~116 A/m) (Figs. 2-5a and 2-5b).

While the hydrothermal areas are characterized by weak magnetization, the areas

covered by lavas often display strong magnetization (with one exception, discussed below). Extremely high magnetizations are associated with fresh pillow lavas along the NVZ, outside the Snail and Yamanaka sites (Figs. 2-5a and 2-5b) and on the southwestern part of the off-axis seamount (Figs. 2-7a and 2-7b). The areas of fractured lavas in the axial zone also exhibit relatively strong magnetization (>10 A/m) (Figs. 2-5a and 2-5b). In addition, the MADAM values in the area of sediment-covered lavas near the Archean mound and Urashima are relatively high (>10 A/m) (Figs. 2-6a and 2-6b, and 2-7a and 2-7b). A notable exception is the western topographic high in the spreading center (12°56'52"N, 143°36'57"E), which is surrounded by an area of low magnetization (Figs. 2-5a and 2-5b). In this area, fractured lavas are widespread (Fig. 2-5b) and numerous regional normal faults resulting from tectonic deformation are observed [*Yoshikawa et al*., 2012]. Thus, it would be expected that many fissures enable seawater to permeate the lavas and sub-seafloor crust, promoting low-temperature alteration of the volcanic layer, and therefore reducing crustal magnetization.

2-3-2. Evaluation of MADAM by comparison with rock NRM

Several methods have been developed to invert magnetic anomalies into equivalent magnetization [e.g., *Parker and Huestis*, 1974]. Because of the intrinsic non-uniqueness of the potential field problem, an infinite number of solutions exist: an annihilator, i.e. a distribution of magnetization that produces no anomaly in the geometry of the experiment, can be determined and added in any amount to a given solution to produce an infinity of other solutions. On the other hand, my forward scheme provides estimates of absolute magnetization of the shallow sub-seafloor (MADAM), which can be directly compared with the magnetization borne by rock samples, i.e., the natural remanent magnetization (NRM) of lavas. The thickness of effective source is generally up to 30 m for my experiment design, in which data were mostly acquired at an altitude of ~10 m (Fig. 2-3). NRM measurements were reported by *Mochizuki et al*. [2012] on samples from the study area: 19 volcanic rocks collected during nine *SHINKAI* 6500 dives in various places and seven seafloor cores obtained using benthic multi-cores. One-inch specimens were drilled from the rock and core samples in the laboratory. NRMs of the specimens were measured using a spinner magnetometer (Natsuhara Giken) at Kumamoto University. NRM measurements were performed on specimens of 11

samples from the axial area, 7 samples from the off-axis area, and 8 samples from the off-axis seamount area. For the sake of comparison, we averaged 2 to 39 MADAM values around each rock sampling location within a 50-m radius (100-m radius for five sampling locations), and the averages were compared with the NRM values (Fig. 2-8). It can be seen that the MADAM determinations are generally consistent with the NRM values.

It is observed that NRM of rock samples tend to be larger for higher values (>10 A/m) than MADAM and smaller for lower values. The former signature is explained by the grain-size distribution of lava flows. The NRM measured on rock samples reflects the magnetization of lava flows, whereas MADAM characterizes the sources located within the shallow sub-seafloor. Due to the quick cooling, magnetic grain size is smaller in lava outcrops than in the sub-seafloor, and its NRM is stronger [e.g. *Marshal and Cox* 1971; *Kent and Gee*, 1996], suggesting high values of NRM on samples collected from the lava surface. The latter signature might be affected by the degree of low-temperature oxidation of titanomagnetite. A wide range of magnetization intensity is observed for the results of both MADAM and NRM of the rocks samples, from just a few to several tens of A/m. This is primarily due to low-temperature oxidation, which causes an exponential reduction of NRM of lava flows with age [e.g. *Irving*, 1970; *Johnson and Atwater*, 1977; *Gee and Kent*, 1994; *Zhou et al*., 2001]. This process must be faster on the surface than in the interior of the lavas, resulting in weaker NRM than MADAM of the rock samples when both values are low (<10 A/m).

The maximum value of MADAM in the axial area is extremely high compared to the values from previous study of magnetic anomaly [*Honsho et al*., 2009] and rock samples [e.g. *Gee and Kent*, 1994; *Zhou et al*., 2001]. However, I adopted all MADAM estimations, up to 116 A/m for interpretation, based on following two reasons, (i) the reliability of MADAM estimations is confirmed by comparison with rock NRM values collected at very close places as mentioned above (Fig. 2-8), and (ii) rock NRM values in the axial area are also extremely high (>100 A/m in 1 site and 70–90 A/m in 4 sites). Moreover, 12 specimens of rock samples show NRM values higher than 100 A/m.

2-3-3. Comparison of MADAM with AUV equivalent magnetization

A distribution of equivalent magnetization (EM) was computed using magnetic

anomaly data collected by the AUV Urashima in 2009 during YK09-08 [*Nogi et al*., 2011]. The EM was estimated by a spectral inversion method [*Parker and Huestis*, 1974; *Macdonald et al*., 1980] using the vertical component of the anomaly, assuming a thickness of 250 m for the magnetized layer and a magnetization direction parallel to the axial dipole field [*Nogi et al*., 2011; *Nakamura et al*., 2013]. Because the AUV survey was conducted at an altitude of ~100 m above the seafloor, the EM from the AUV data likely reflects the wider and deeper crustal structures than the MADAM estimates from my HOV study. The MADAM distribution is generally consistent with the large-scale structures depicted by the EM in all the surveyed areas (Fig. 2-9).

In the axial area, both the EM and MADAM values are highest along the NVZ, especially in the central volcanic mound (12°56’52”N, 143°36’57”E), and on the southern volcanic edifice where fresh lavas are observed (Fig. 2-9a). A zone of high EM is aligned NE–SW, consistent with the distribution of high MADAM on crossing dive tracks, suggesting recent lava flows. Far from the NVZ, both MADAM and EM are lower, especially near the western topographic high in the fault zone (Fig. 2-9a). Next to the Snail site, relatively low values of both EM and MADAM align along a NNE–SSW trend.

While the lowest values of both EM and MADAM are recognized on the top of the Archean mound, higher values are consistently distributed around the mound (Fig. 2-9b). In particular, the highest values of both EM and MADAM are located on the western and southwestern sides of the mound, suggesting that younger lava flows erupted on the surrounding older and rugged seafloor [*Yoshikawa et al*., 2012].

In the off-axis seamount area, high values of EM are located on its northeastern and western flanks, consistent with the MADAM distribution (Fig. 2-9c). In contrast, low values of both MADAM and EM are located on the Pika and Urashima sites. Moreover, according to the EM map, these sites appear located within a continuous low-magnetization zone, whereas they can be distinguished as two separate lows on the MADAM results. This observation confirms that near-seafloor magnetic measurements using HOVs help to characterize small-scale features that would remain undetected with AUV surveys.

2-4. Discussion

2-4-1. Processes causing the weak magnetization zones

All five back-arc hydrothermal sites investigated in the SMT are clearly associated with low crustal magnetization (Figs. 2-5, 2-6, and 2-7). The followings could be a cause for magnetization reduction: (i) thermal demagnetization, where hot fluid heats the surrounding lava above the Curie temperature of its magnetic minerals [*Wooldridge et al*., 1992]; (ii) hydrothermal alteration, in which volcanogenic magnetic minerals, such as titanomagnetite, are replaced by non-magnetic minerals within the up-flow zone [*Johnson et al*., 1982; Hall, 1992]; and/or (iii) the presence of non-magnetic hydrothermal deposits [*Szitkar et al*., 2014a]. In the off-axis area, inactive hydrothermal areas also exhibit reduced magnetizations (Figs. 2-6 and 2-7), confirming that the alteration of the magnetic minerals and/or the presence of non-magnetic hydrothermal deposits rather than thermal demagnetization are the major processes leading to the reduced magnetization. The narrow zones of low magnetization are centered on vent areas, moreover low magnetization zones are confirmed in both HOV (~10 m altitude) and AUV (~100 m altitude) results, indicating the presence of low magnetization source at depths from near-seafloor to hundreds of meters. The modeling study of the magnetization zone in the TAG hydrothermal site proposed a pipe-like source body with a radius of 100 m [*Tivey et al*., 1993; *Tivey and Dyment*, 2010; *Szitkar and Dyment*, 2015]. The horizontal extent of this narrow pipe-like body is comparable to my investigated sites and also to the stockwork zones found in volcanogenic massive sulfide deposits such as the Cyprus ophiolite [e.g. *Johnson et al*., 1982]. These observations potentially suggest that the zones of reduced or null magnetization of hydrothermal sites in SMT are either up-flow zones of hydrothermal fluid beneath separate vent systems in the uppermost crust, or accumulations of sulfide deposits associated with each vent system.

2-4-2. Duration of hydrothermal activity and size of magnetic low

In the SMT, I observe that the spatial extent of the low magnetization zone differs depending on the on- or off-axis location of the sites (Fig. 2-10). Low magnetization zones at the on-axis sites of Snail and Yamanaka are ~30 m in diameter, whereas they are ~120 m at the off-axis sites of Archean, Pika, and Urashima. This difference is

probably a consequence of a longer duration of hydrothermal activity.

Both the Snail and Yamanaka sites are located in the NVZ. Gravity data suggest a relatively thick crust (~6.8 km) in the 12.7–13.5°N segment, i.e., a stronger magmatic activity with sheet-like mantle upwelling [*Kitada et al*., 2006]. Moreover, a seismic refraction study reveals that the upwelling zone is characterized by low seismic velocity 1.5 km below the seafloor, beneath the axial area in this region [*Sato et al*., 2015b]. A magma chamber was detected 15 km northeast along the spreading axis at ~3-km depth during a reflection seismic study [*Becker et al*., 2010]. Therefore, the heat source for the Snail and Yamanaka hydrothermal activity is probably episodic dike intrusion at the spreading axis, similar to the fast-spreading East Pacific Rise hydrothermal systems, where vent site activity might be controlled by dike intrusion over decadal timescales [e.g., *German and Lin*, 2004]. This type of heat supply sustains hydrothermal circulations in an episodic manner, and the hydrothermal areas tend to be small in the axial area.

On the other hand, the Archean site is located 2 km from the NVZ, and although there is no direct information regarding the heat source for this site, the existence of a large hydrothermal mound indicates a stronger hydrothermal flux or a longer duration of hydrothermal circulation. Radiometric dating showed that the maximum age of the sulfide deposits from the Archean site is at least ~3500 years [*Takamasa et al*., 2013; *Ishibashi et al*., 2015], substantiating the presence of long-lived hydrothermal activity.

Both the Pika and Urashima sites find their heat source in the off-axis volcanism forming the seamount on which they are located. The off-axis eruption is confirmed by the observation of fresh lavas with high magnetization in this study (Figs. 2-7a, 2-7b, 2-7i, and 2-7j), and the high seismic velocity structure [*Sato et al*., 2015b]. The off-axis volcano covers an area of more than several tens of square kilometers with a maximum height of ~400 m. This off-axis volcanism is probably a long-lived heat source during the formation and cooling of the seamount. *Sato et al*. [2015b] showed that the seismicity around the off-axis volcano was very low during the observation period of three months, suggesting that volcanism might have ceased. Sulfide chimneys and debris/breccia collected from these sites also indicates an age of up to ~9000 years [*Ishibashi et al*., 2015]. The growth of the Pika and Urashima hydrothermal sites might therefore be in their late stage.

The hydrothermal alteration zones and hydrothermal deposit zones grow with age

and hydrothermal activity, which in turn is controlled by the heat source, i.e., the magmatic activity. Long-lived and giant hydrothermal sites have been reported in slow and ultraslow-spreading environments, e.g., the TAG field, controlled by tectonic faults associated with a low-angle detachment fault [e.g., *Tivey and Dyment*, 2010], or the large field discovered at 49°39'E on the Southwest Indian Ridge [*Zhu et al*., 2010]. In contrast, the hydrothermal systems in the SMT are not associated with large fault systems cutting across the deeper crust and uppermost mantle, as suggested by the bathymetry and the very low seismicity [*Sato et al*., 2015b]. The five studied hydrothermal fields investigated are primarily controlled by magmatic activity.

2-5. Chapter Conclusions

I applied a method based on the comparison of near-seafloor three-component magnetic anomaly data with the 3-D forward modeling approach in the spectral domain to estimate the absolute crustal magnetization of the shallow sub-seafloor near five hydrothermal sites of the SMT. The analysis of these MADAMs led to the following conclusions:

1. The five hydrothermal vent fields of the back-arc spreading region in the SMT are characterized by low-intensity magnetization generally lower than 5 A/m in the off-axis area. The hydrothermal alteration of magnetic minerals present in the extrusive lavas and/or the deposits of non-magnetic hydrothermal material are responsible for the reduced magnetization in these zones.
2. The MADAM estimates are generally consistent with the NRM values of rock samples from the seafloor of the same region, although the NRM values tend to be larger than the MADAM estimates for higher values and smaller for lower values. The former difference might reflect variations in magnetic grain size, in which fast cooling results in a smaller grain size; therefore, stronger NRM is observed for the outcropping rock samples with respect to the bulk MADAM estimates. The latter difference might reflect the difference in degree of low-temperature oxidation. Indeed, the low-temperature oxidation of the outcropping rock is higher than that of the sub-seafloor; therefore, the NRM values could be weaker than the MADAM values.
3. The distribution of MADAM estimates is generally consistent with equivalent magnetizations deduced from AUV surveys, although the resolution of the former is higher than the latter. For example, the individual magnetic signatures of the Pika and Urashima sites could be detected only by using high-resolution near-seafloor measurements undertaken by the HOV.
4. The off-axis hydrothermal vent sites are larger than the on-axis sites, reflecting the longevity of the hydrothermal activity. The Snail and Yamanaka sites, both located in the axial area, are likely controlled by dike intrusions over decadal timescales, whereas the Archean, Pika, and Urashima sites are likely controlled by off-axis magmatic activity over thousands of years.

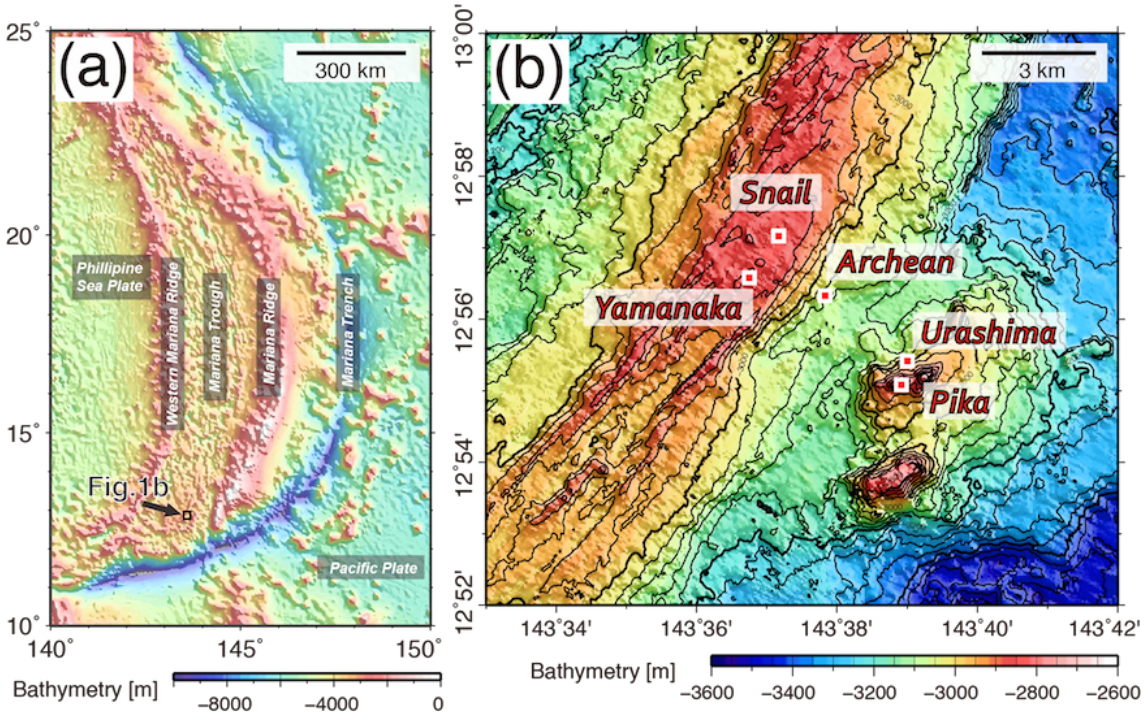

Figure 2-1. Seafloor bathymetry and locations of studied hydrothermal fields.

(a) Seafloor bathymetry of the Mariana Trough. Contour interval is 1 km. Bathymetry map is based on grid data from ETOPO1 [*Amante and Eakins*, 2009]. (b) Detailed seafloor bathymetry of the southern Mariana Trough. Red squares indicate locations of hydrothermal vents fields. Contour interval is 40 m. Bathymetry is made using 0.025-nmi-interval grid data from *Seama et al*. [2015].

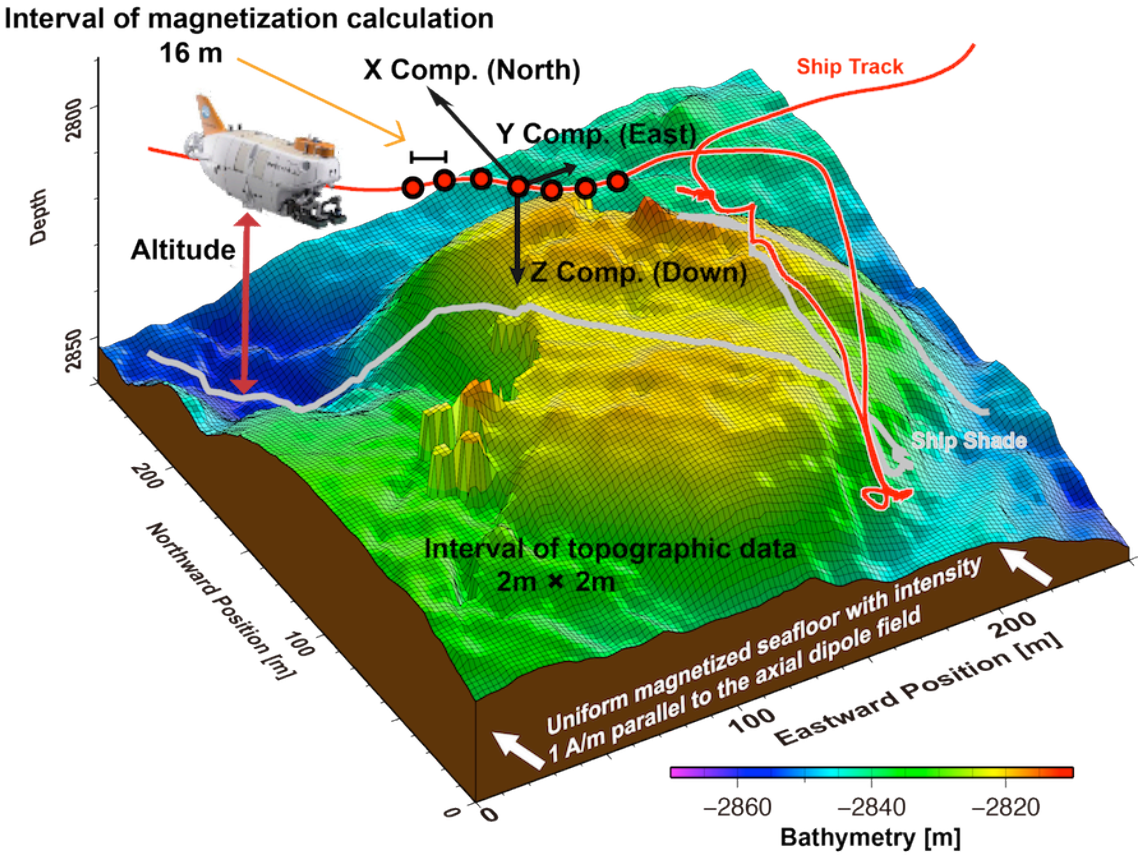

Figure 2-2. Schematic diagram of the method deriving the absolute magnetization. Colored grid: bathymetry collected by AUV; red line: submersible track; white line: submersible path projected on the seafloor. See text for details.

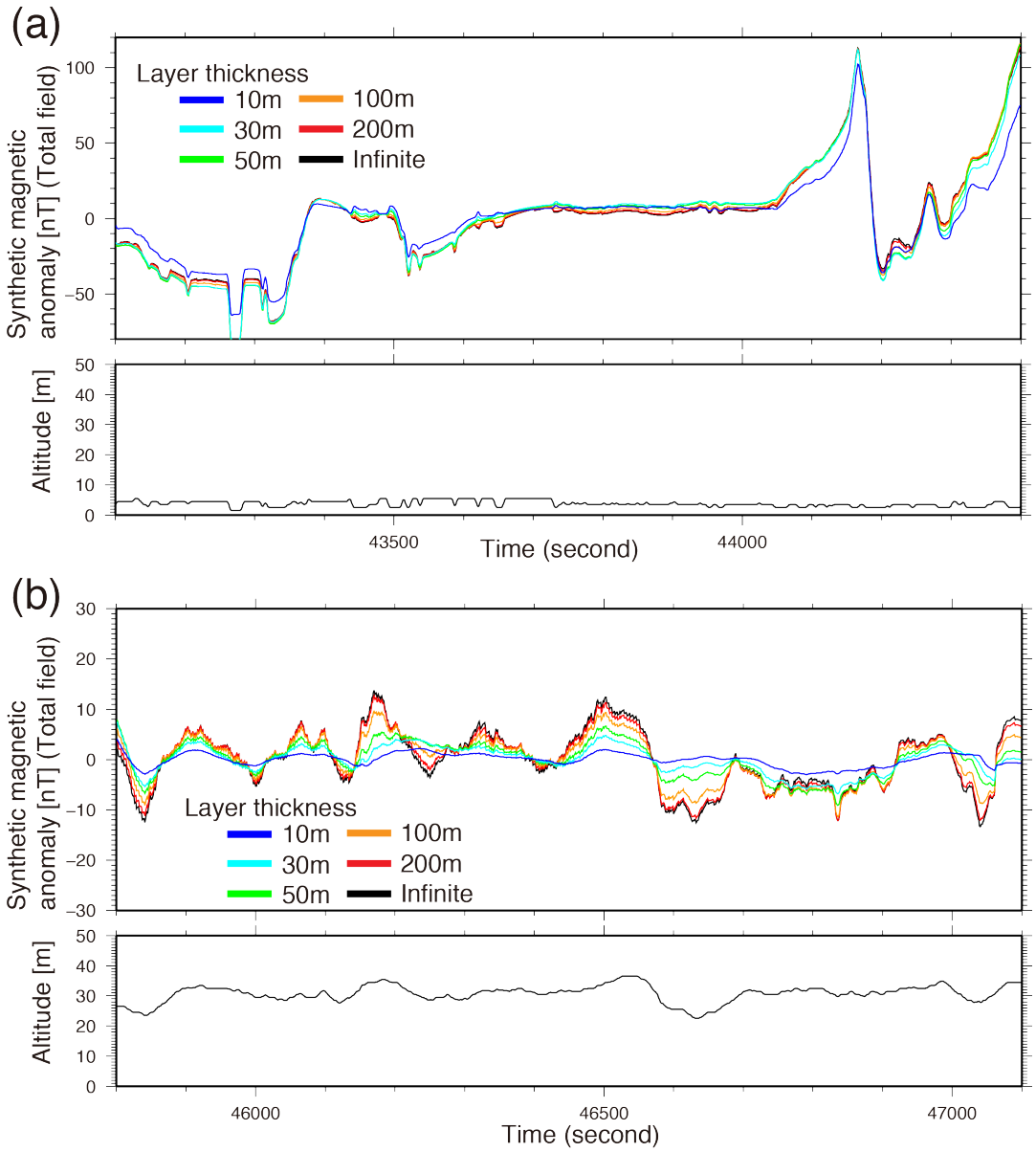

Figure 2-3. Synthetic magnetic anomalies assuming various thickness of layer source.

Synthetic total magnetic anomaly calculated by 3D forward modeling along the track of dive 6K#1227 using bathymetric data collected by AUV, for dive altitudes of (a) <10 m and (b) 20–40 m, assuming different magnetic source layer thicknesses: 10 m (blue line), 30 m (light blue line), 50 m (green line), 100 m (orange line), 200 m (red line), and infinite (black line).

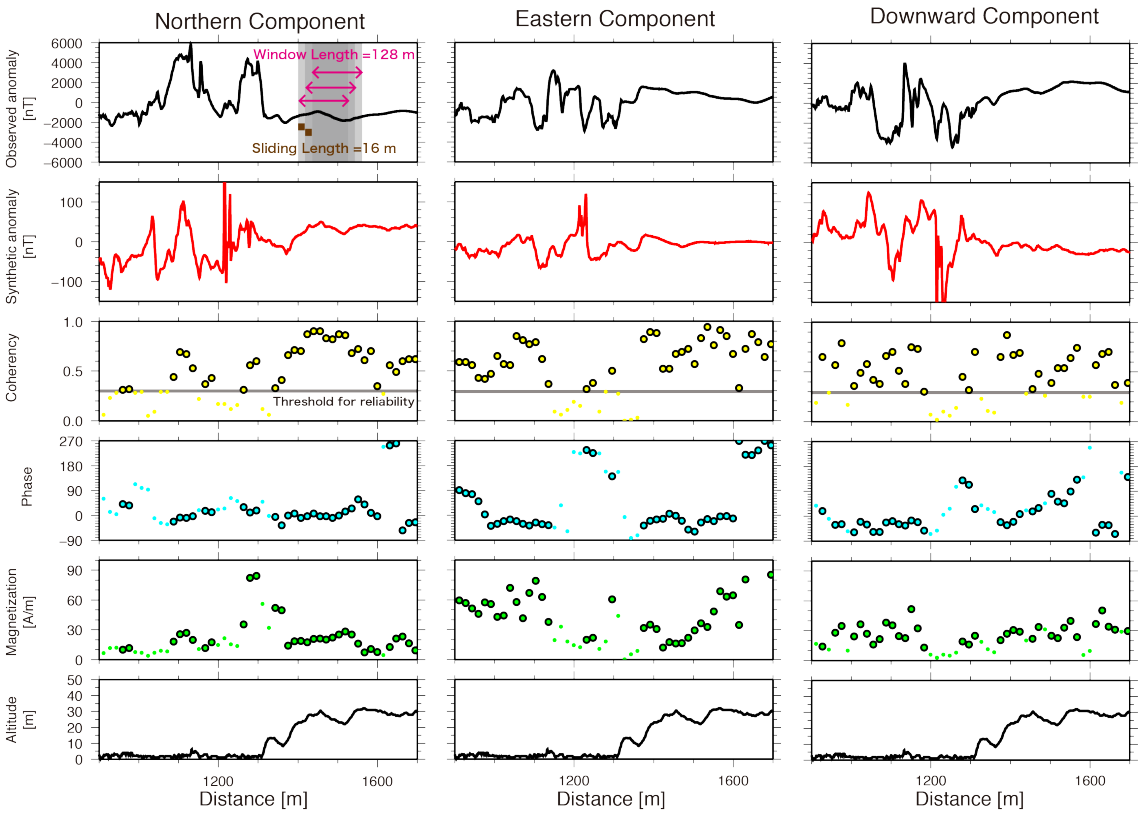

Figure 2-4. Example of absolute magnetization estimations.

Analysis of the northern (left), eastern (center), and downward (right) components of the magnetic anomaly. From top to bottom, observed (black line) and synthetic (red line) magnetic anomaly intensity, coherency (yellow circles), phase (blue circles), magnetization (green circles), and vehicle altitude (black line). Circles with black solid rims are those considered reliable (coherency >0.3 on at least two components).

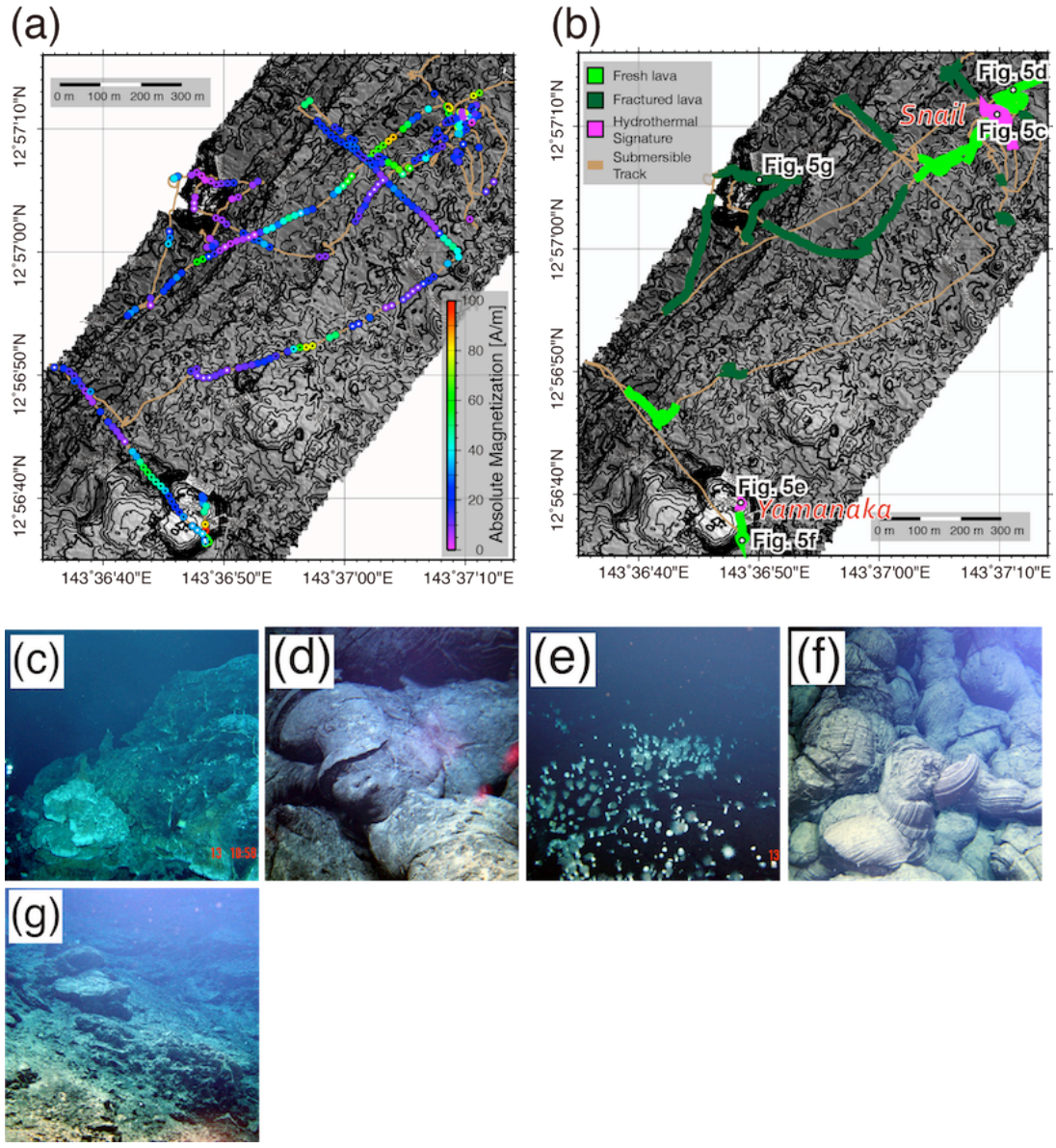

Figure 2-5. Results from the axial area including the Snail and Yamanaka sites.

(a) Distribution of magnetic-anomaly-derived absolute magnetization (MADAM). Magnetization intensity is shown by the rainbow colors of the outer circles and polarity shown by the black and white colors of the inner circles. Black and white circles mean normal and reverse polarity, respectively. Background: contoured and shaded bathymetry. (b) Geological observation along dive tracks. Photographs of (c) hydrothermal site Snail, (d) fresh pillow lava around the Snail site, (e) hydrothermal site Yamanaka, (f) fresh pillow lava near the Yamanaka site, (g) fractured lavas west of the neo-volcanic zones.

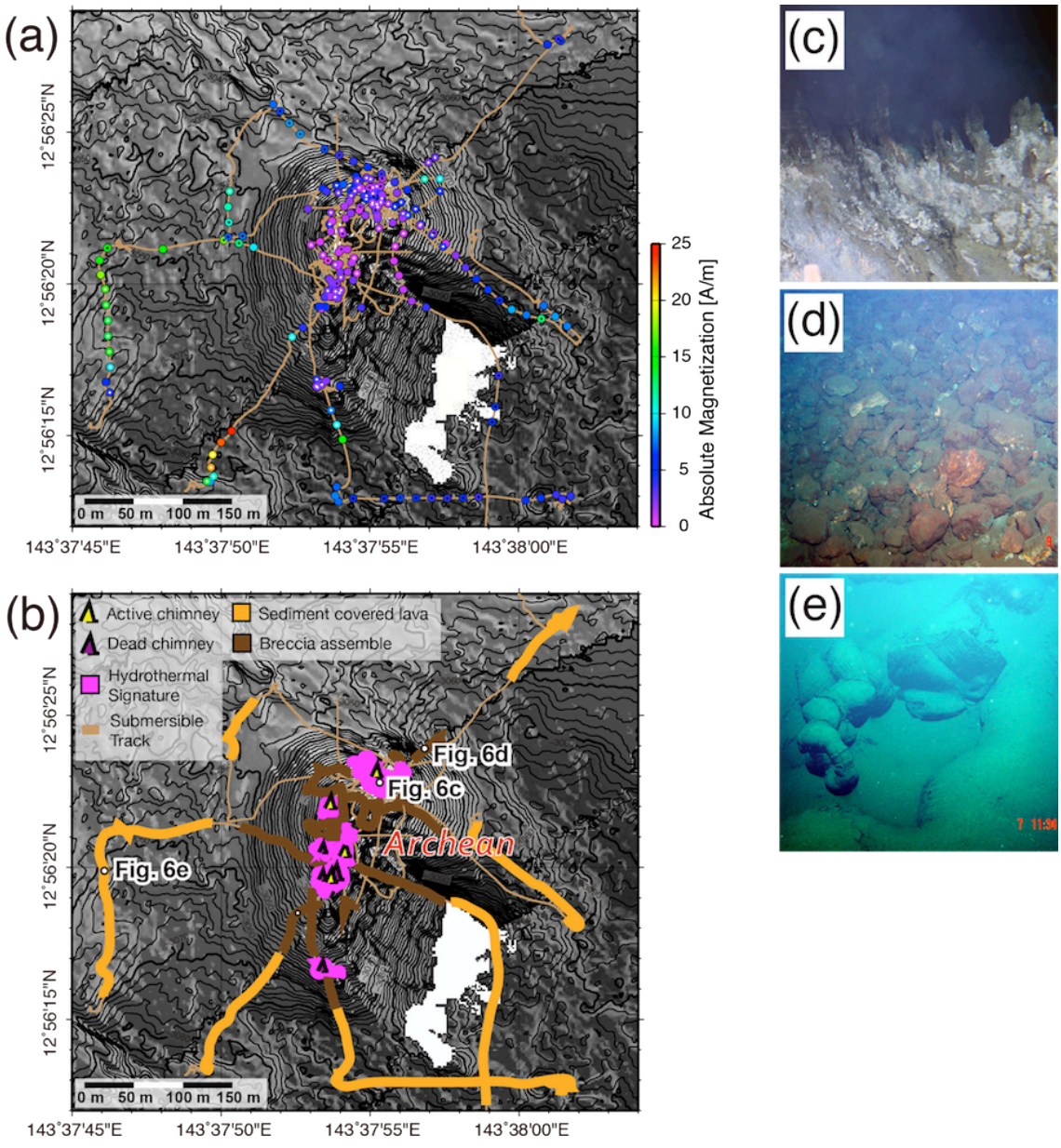

Figure 2-6. Results from the off-axis area including the Archean sites.

(a) Distribution of magnetic-anomaly-derived absolute magnetization (MADAM). Intensity is shown by the rainbow colors of the outer circles and polarity shown by the black and white colors of the inner circles. Black and white circles mean normal and reverse polarity, respectively. Background: contoured and shaded bathymetry. (b) Geological observations along dive tracks. Photographs of (c) hydrothermal site Archean, (d) debris and breccia around the Archean site, (e) sediment-covered lavas around the Archean site.

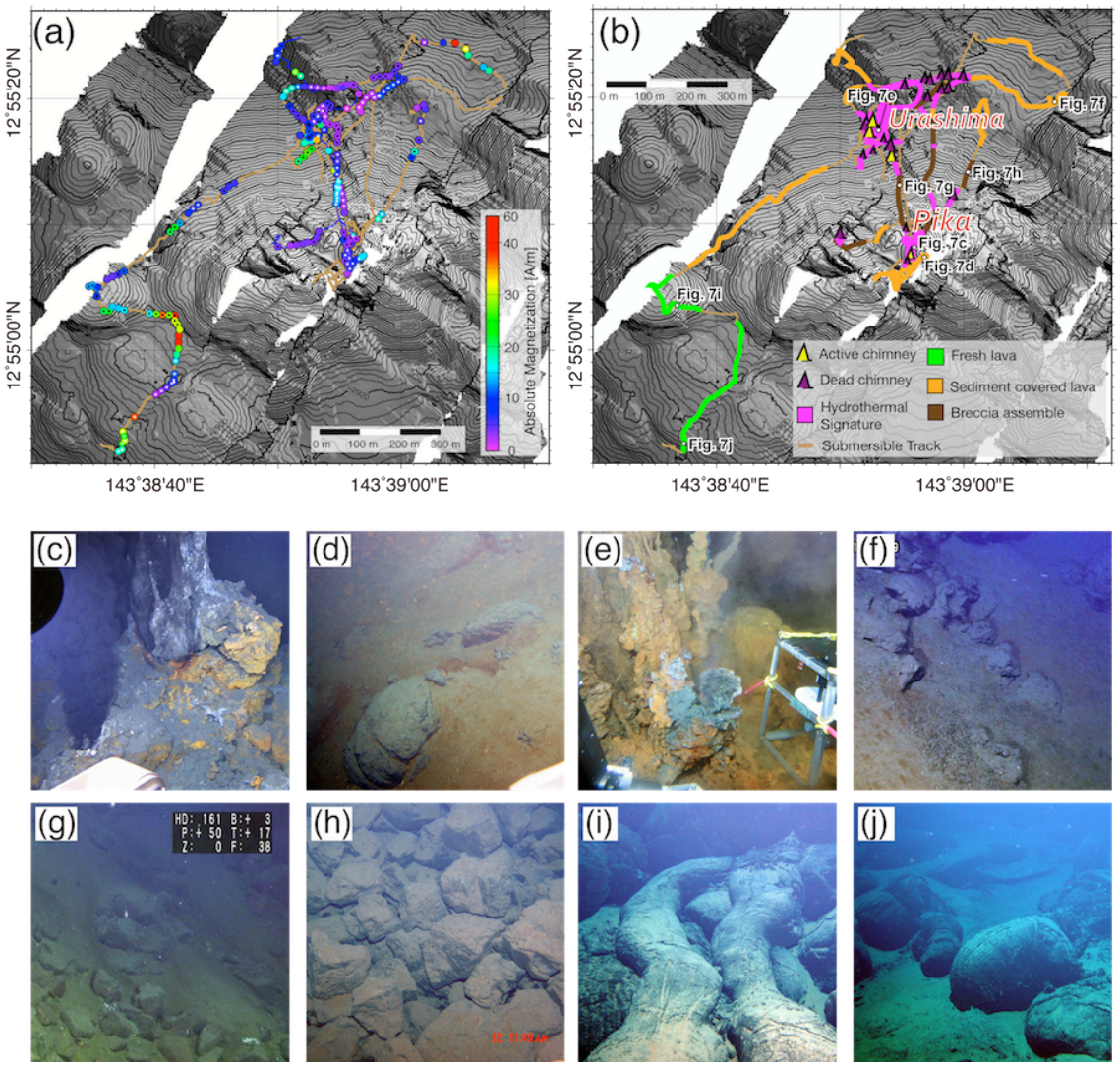

Figure 2-7. Results from the axial area including the Pika and Urashima sites.

(a) Distribution of magnetic-anomaly-derived absolute magnetization (MADAM). Intensity is shown by the rainbow colors of the outer circles and polarity shown by the black and white colors of the inner circles. Black and white circles mean normal and reverse polarity, respectively. Background: contoured and shaded bathymetry. (b) Geological observations along dive tracks. Photographs of (c) hydrothermal site Pika, (d) sediment-covered lavas near the Pika site, (e) hydrothermal site Urashima, (f) sediment-covered lavas around the Urashima site, (g) and (h) debris and breccia between the Pika and Urashima sites, (i) and (j) fresh pillow lava on the southwestern slope of the off-axis seamount.

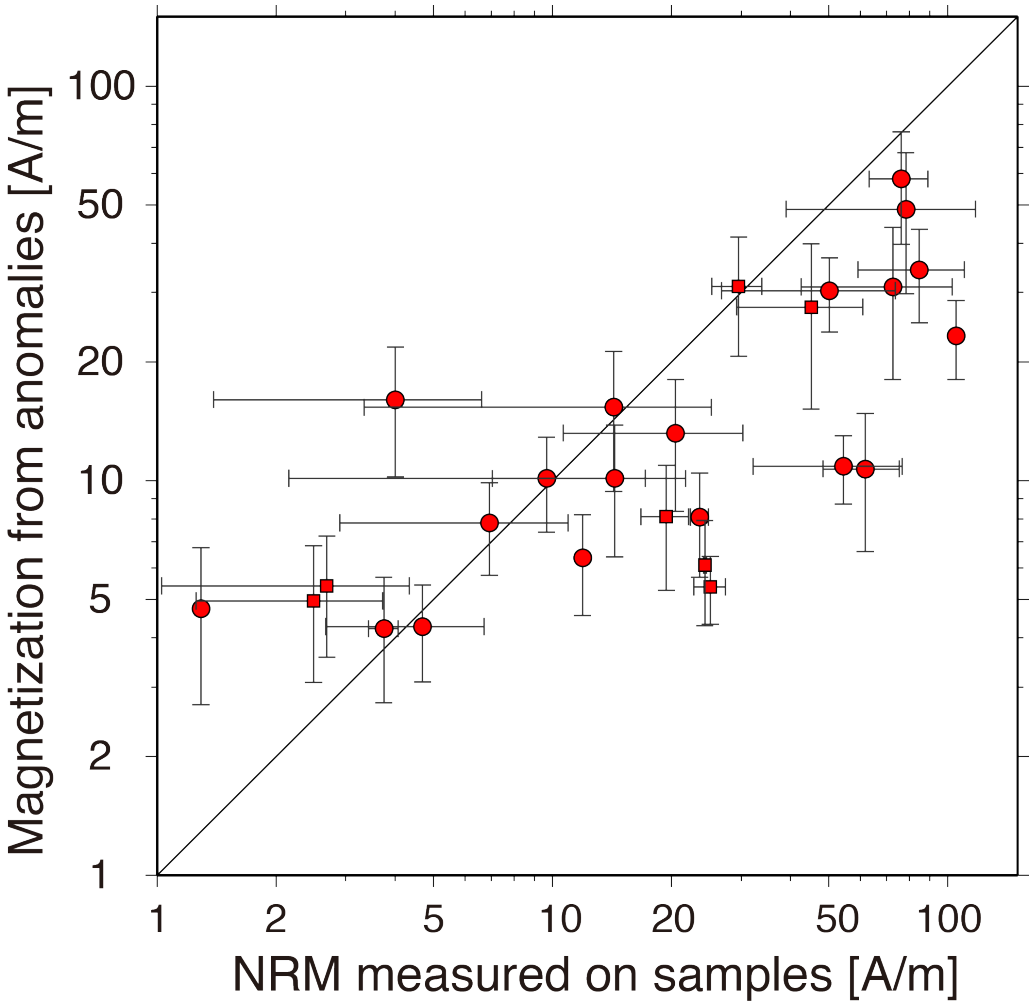

Figure 2-8. Comparison between MADAM and NRM measured on rock samples. Magnetic-anomaly-derived absolute magnetization, MADAM. NRM, natural remanent magnetization. Circles and squares show NRM dataset from samples collected by submersible and seafloor coring [*Mochizuki et al*., 2012], respectively. Error bars of x- and y-axes show standard deviations of NRM values and MADAM estimates for each point, respectively.

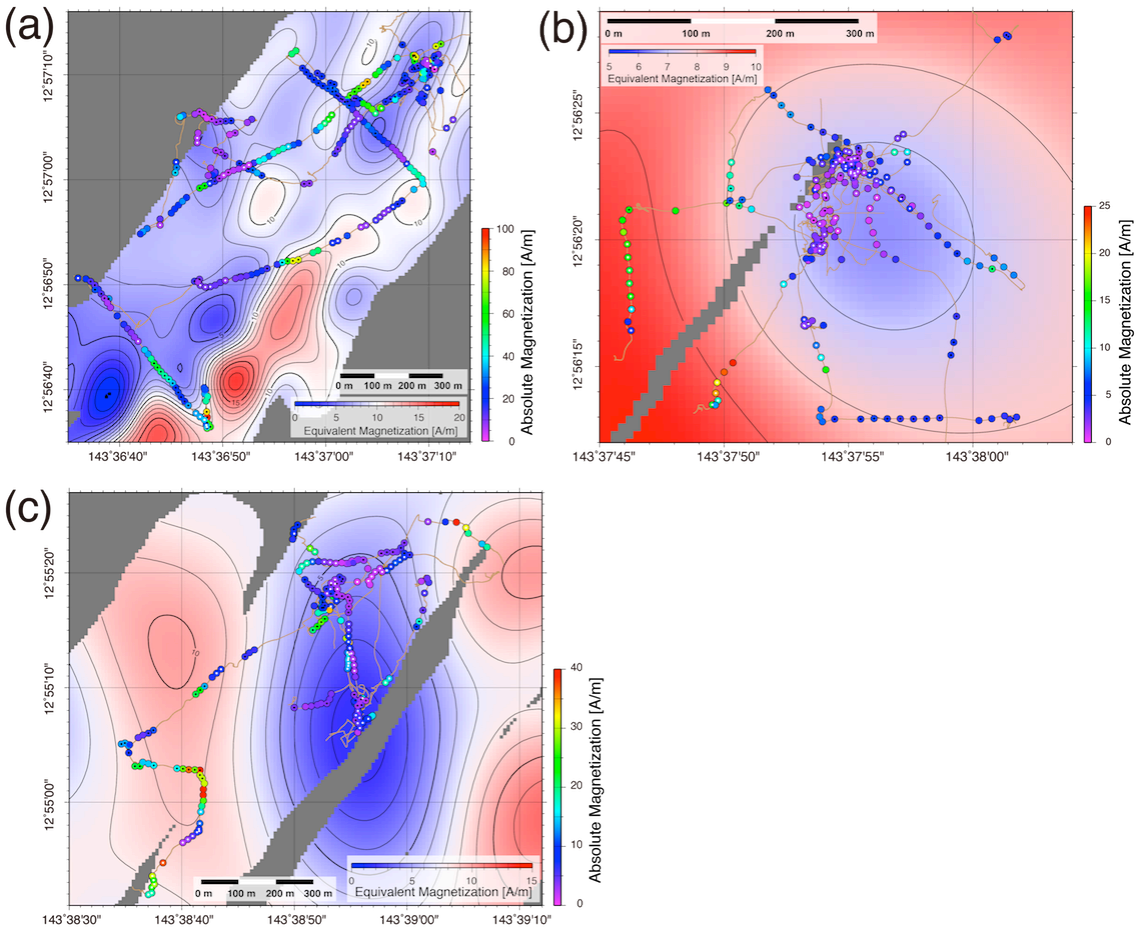

Figure 2-9. Comparison between MADAM from HOV and EM from AUV. Magnetic-anomaly-derived absolute magnetization, MADAM. Human occupied vehicle, HOV. Equivalent magnetization, EM. Autonomous underwater vehicle, AUV. The EM data is based on *Nogi et al*. [2011]. MADAM plots are those shown in Figs. 5–7. (a) On-axis area, including the Snail and Yamanaka sites; (b) off-axis area at the foot of the axial high, including the Archean site; (c) off-axis seamount area, including the Pika and Urashima sites.

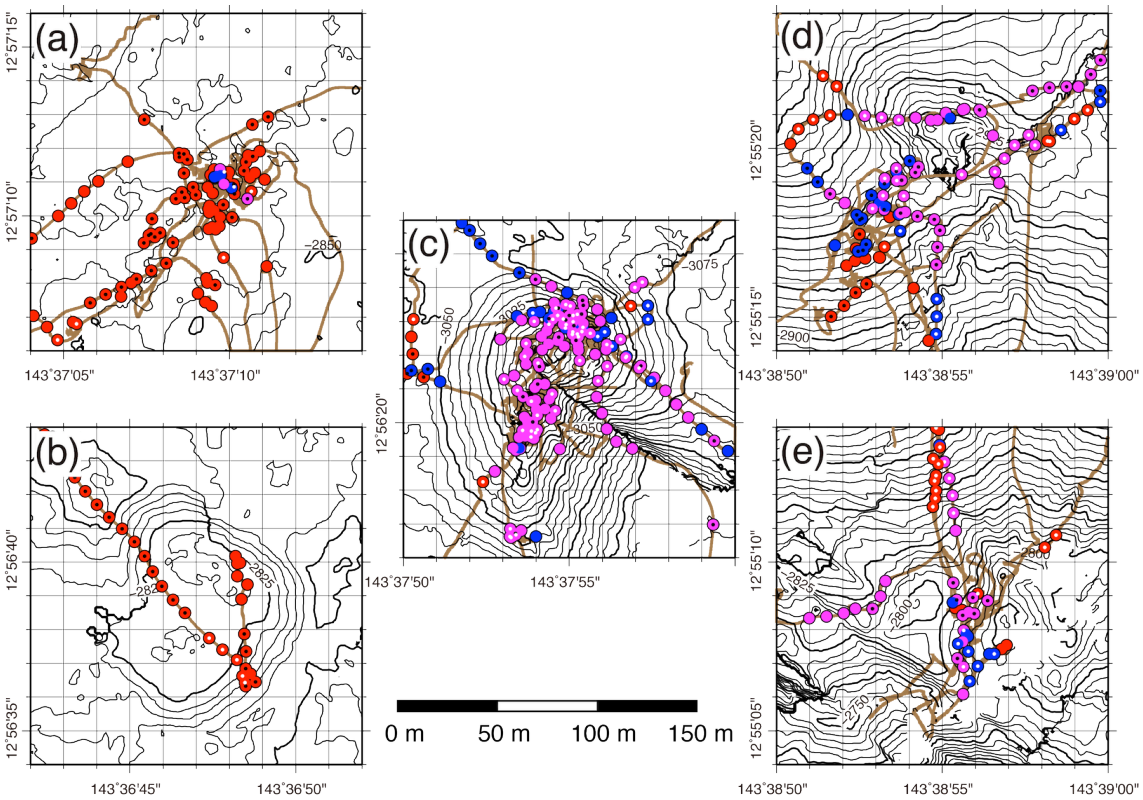

Figure 2-10. Spatial scale of low magnetization zones.

Distribution of magnetic-anomaly-derived absolute magnetization around five hydrothermal fields of the Southern Mariana Trough, represented at the same scale: Sites Snail (a), Yamanaka (b), Archean (c), Urashima (d), and Pika (e). Red circles denote magnetization intensity >10 A/m, blue circles 5–10 A/m, and purple circles <5 A/m. Brown lines show submersible dive tracks. Isobaths of the background are plotted for every 10 m (thin lines) and 50 m (thick lines).

Chapter 3

Basalt- to Rhyolite-hosted Tarama and Irabu Hydrothermal Fields in Arc and Back-arc Regions of Okinawa Trough

本章については、5 年以内に雑誌等で刊行予定のため、非公開。

3-1. Geological Background

3-2. Data and Methods

3-2-1. Data acquisition

3-2-2. Imaging the magnetic anomaly: ship-underway

3-2-3. Imaging the magnetic anomaly: AUV

3-2-4. Rock magnetic properties and petrological observation

3-3. Results

3-3-1. Magnetization from ship-underway mapping

3-3-2. Magnetization from AUV mapping

3-3-3. Rock magnetic properties and petrography

3-4. Discussion

3-4-1. Magnetization intensity reflecting host rock difference

3-4-2. Strongly magnetized Irabu knolls

3-4-3. Processes causing weak magnetization zones

3-5. Chapter Conclusions

Chapter 4

Ultramafic-hosted Yokoniwa Hydrothermal Field in Non-transform Offset Massif of Central Indian Ridge

本章については、5 年以内に雑誌等で刊行予定のため、非公開。

4-1. Geological Background

4-2. Data and Methods

4-2-1. Imaging the magnetic anomaly: AUV

4-2-2. Imaging the magnetic anomaly: HOV

4-2-3. Rock magnetic properties measurements

4-2-4. Grain density and petrology on serpentinized peridotites

4-3. Results

4-3-1. Magnetization from AUV data

4-3-2. Magnetization from HOV data

4-3-3. Magnetic properties of rock samples

4-3-4. Serpentinization degree and petrography

4-4. Discussion

4-4-1. Basaltic volcanism on western slope of Yokoniwa Rise

4-4-2. Evolution of magnetite during serpentinization

4-4-3. Processes causing strong magnetization zones

4-5. Chapter Conclusions

Chapter 5

Discussion

本章については、5 年以内に雑誌等で刊行予定のため、非公開。

5-1. Magnetic Signature of Volcanic Lava-hosted Hydrothermal Systems

5-2. Magnetic Evolution at Ultramafic-hosted Hydrothermal Systems

5-3. Location and Spatial Scale of Seafloor Hydrothermal Systems

Chapter 6

Conclusions

本章については、5 年以内に雑誌等で刊行予定のため、非公開。

Acknowledgements

I first would like to express my sincere gratitude to my supervisor, *Kyoko Okino* for providing this precious study opportunity to me as a PhD student at the University of Tokyo. She also provided many opportunities for me to meet many domestic and foreign researchers, which helped my research to have a wide scope.

I also express my deepest appreciation to my advisor *Chie Honsho* for invaluable discussion and comments, particularly concerning the methodology of this research. She encouraged and helped my work from the initial processing of data to the publication of articles. The various discussions about the magnetic anomalies are essentially for this work and will be the basis of my future studies.

I am very grateful to my advisor *Toshitsugu Yamazaki* for his elaborated guidance, considerable encouragement, and discussion that enable the great achievement of my research and made my research unforgettable. He provided many comments related to rock magnetic research.

I spent five years in the Department of the Ocean Floor Geoscience (OFGS), Atmosphere and Ocean Research Institute (AORI), University of Tokyo. I would like to thank all people in the OFGS as well as my advisors for offering advice throughout my studies, including *Juichiro Ashi*, *Hidekazu Tokuyama*, *Shuro Yoshikawa, Jin-Oh Park*, *Asuka Yamaguchi*, *Hironori Otsuka*, *Arata Kioka*, *Hodaka Kawahata*, *Yusuke Yokoyama*, *Toshihiro Yoshimura*, *Akiko Omura*, *Kazuya Naito*, *Kanehara Tomiko*, *Chieko Komatsu*, and *Akiko Mochizuki*. In particular, I am deeply grateful to *Chiori Tamura* for her technical support of magnetometer handling.

I would like to thank *Jerome Dyment* at the Institut de Physique du Globe de Paris for his advice and discussion during my two-month visit there. I also thank many researchers and friends I met during my visit, particularly *Florent Szitkar* for his kind support in developing the new analytical technique.

My heartfelt appreciation goes to *Masako Tominaga* at Michigan State University, whose encouragement and suggestions regarding my English ability are of inestimable

value. She provided the opportunity for me to stay in Michigan for three months and to hone my English skills by participating in graduate student classes and daily discussions.

I am grateful to many researchers for their offering sound advice in the meetings, workshops, research cruises, and geological field trips, including *Nobukazu Seama*, *Yoshifumi Nogi*, *Taichi Sato*, *Hiroshi Sato*, *Yasuhiko Ohara*, *Naoto Ishikawa*, *Miho Asada*, *Kentaro Nakamura, Tatsuo Nozaki, Hidenori Kumagai, Tetsuo Matsuno, Takuroh Noguchi, Toshiya Fujiwara, Keiichi Tadokoro, Koukichi Iizasa*, *Osamu Ishizuka*, *Tamaki Ura*, *Michinari Sunamura*, *Kazuo Nakahigashi*, *Shiki Machida, Sumio Miyashita*, *Yoshiko Adachi*, *Shusaku Yamazaki*, *Satoru Haraguchi*, *Susumu Umino*, *Katsuyoshi Michibayashi*, *Takafumi Kasaya*, *Junichiro Ishibashi*, *Hidetoshi Shibuya*, *Hirokuni Oda*, *Masao Ohno*, *Kazuto Kodama*, *Tomoaki Morishita*, *Natsue Abe*, and all others that cannot be mentioned here owing to space concerns. In particular, I learned measurement techniques for rock magnetism from *Yuhji Yamamoto* and *Nobutatsu Mochizuki* during my visit to the Center for Advance Marine Core Research, Kochi University, and to Kumamoto University.

I am greatly indebted to the crew of R/Vs *Yokosuka*, *Hakuho-maru*, *Oshoro-maru*, and *Shinsei-maru* and to the support teams of the HOV *SHINKAI 6500* and AUV *URASHIMA* for their professional support during cruises.

I have been financially supported by the Japan Society for the Promotion of Science (JSPS). The Department of Earth and Planetary Science, University of Tokyo, provided the opportunity for me to stay at the Institut de Physique du Globe de Paris with the financial support of the Institutional Program for Young Researcher Overseas Visits of the JSPS.

Finally I would like to extend my indebtedness to my family and friends for their support, understanding, and warm encouragement throughout my study.

Bibliography

Ade-Hall, J., F. Aumento, P. J. C. Ryall, R. E. Gerstein, J. Brooke, and D. L. McKeown (1973), The Mid-Atlantic Ridge Near 45 °N. XXI. Magnetic Results from Basalt Drill Cores from the Median Valley, *Can. J. Earth Sci.*, *10*(5), 679–696, doi:10.1139/e73-068.

Ade-Hall, J. M., H. C. Palmer, and T. P. Hubbard (1971), The Magnetic and Opaque Petrological Response of Basalts to Regional Hydrothermal Alteration, *Geophys. J. R. Astron. Soc.*, *24*(2), 137–174, doi:10.1111/j.1365-246X.1971.tb02171.x.

Alt, J. C. (1995), Subseafloor processes in mid-ocean ridge hydrothennal systems, in *Seafloor Hydrothermal Systems: Physical, Chemical, Biological, and Geological Interactions*, vol. 91, pp. 85–114, AGU, Washington, DC.

Amante, C., and B. W. Eakins (2009), ETOPO1 1 Arc-Minute Global Relief Model: Procedures, Data Sources and Analysis., *NOAA Tech. Memo. NESDIS NGDC-24*, 19 pp.

Andreani, M., J. Escartin, A. Delacour, B. Ildefonse, M. Godard, J. Dyment, A. E. Fallick, and Y. Fouquet (2014), Tectonic structure, lithology, and hydrothermal signature of the Rainbow massif (Mid-Atlantic Ridge 36°14′N), *Geochemistry, Geophys. Geosystems*, *15*(9), 3543–3571, doi:10.1002/2014GC005269.

Asada, M., A. Deschamps, T. Fujiwara, and Y. Nakamura (2007), Submarine lava flow emplacement and faulting in the axial valley of two morphologically distinct spreading segments of the Mariana back-arc basin from Wadatsumi side-scan sonar images, *Geochemistry, Geophys. Geosystems*, *8*(4), Q04001, doi:10.1029/2006GC001418.

Bach, W., C. J. Garrido, H. Paulick, J. Harvey, and M. Rosner (2004), Seawater-peridotite interactions: First insights from ODP Leg 209, MAR 15°N, *Geochemistry, Geophys. Geosystems*, *5*(9), Q09F26, doi:10.1029/2004GC000744.

Bach, W., H. Paulick, C. J. Garrido, B. Ildefonse, W. P. Meurer, and S. E. Humphris (2006), Unraveling the sequence of serpentinization reactions: petrography, mineral chemistry, and petrophysics of serpentinites from MAR 15°N (ODP Leg 209, Site 1274), *Geophys. Res. Lett.*, *33*(13), L13306, doi:10.1029/2006GL025681.

Baker, E. T., and C. R. German (2004), On the Global Distribution of Hydrothermal Vent Fields, in *Mid-Ocean Ridges*, pp. 245–266, American Geophysical Union.

Barker, A. K., L. A. Coogan, and K. M. Gillis (2010), Insights into the behaviour of sulphur in mid-ocean ridge axial hydrothermal systems from the composition of the sheeted dyke complex at Pito Deep, *Chem. Geol.*, *275*(1–2), 105–115, doi:http://dx.doi.org/10.1016/j.chemgeo.2010.05.003.

Barrie, C. T., and M. D. Hannington (1999), Classification of Volcanic-Associated Massive Sulfide Deposits Based on Host-Rock Composition, *Rev. Econ. Geol.*, *8*, 1–11.

Beard, J. S., B. R. Frost, P. Fryer, A. McCaig, R. Searle, B. Ildefonse, P. Zinin, and S. K. Sharma (2009), Onset and Progression of Serpentinization and Magnetite Formation in Olivine-rich Troctolite from IODP Hole U1309D, *J. Petrol.* , *50* (3), 387–403, doi:10.1093/petrology/egp004.

Becker, N. C., P. Fryer, and G. F. Moore (2010), Malaguana-Gadao Ridge: Identification and implications of a magma chamber reflector in the southern Mariana Trough, *Geochemistry, Geophys. Geosystems*, *11*(4), Q04X13, doi:10.1029/2009GC002719.

Bhattacharyya, B. (1964), Magnetic anomalies due to prism-shaped bodies with arbitrary polarization, *GEOPHYSICS*, *29*(4), 517–531, doi:10.1190/1.1439386.

Bina, M. M., and B. Henry (1990), Magnetic properties, opaque mineralogy and magnetic anisotropies of serpentinized peridotites from ODP Hole 670A near the Mid-Atlantic Ridge, *Phys. Earth Planet. Inter.*, *65*(1–2), 88–103, doi:10.1016/0031-9201(90)90078-C.

Boström, K., M. N. A. Peterson, O. Joensuu, and D. E. Fisher (1969), Aluminum-poor ferromanganoan sediments on active oceanic ridges, *J. Geophys. Res.*, *74*(12), 3261–3270, doi:10.1029/JB074i012p03261.

Briais, A. (1995), Structural analysis of the segmentation of the Central Indian Ridge between 20°30′S and 25°30′S (Rodriguez Triple Junction), *Mar. Geophys. Res.*, *17*(5), 431–467, doi:10.1007/BF01371787.

Bullard, E. C., A. E. Maxwell, and R. Revelle (1956), *Advances in Geophysics Volume 3*, Advances in Geophysics, Elsevier.

Cannat, M. (1993), Emplacement of mantle rocks in the seafloor at mid-ocean ridges, *J. Geophys. Res. Solid Earth*, *98*(B3), 4163–4172, doi:10.1029/92JB02221.

Cannat, M. et al. (1995), Thin crust, ultramafic exposures, and rugged faulting patterns at the Mid-Atlantic Ridge (22°–24°N), *Geol.* , *23* (1), 49–52, doi:10.1130/0091-7613(1995)023<0049:TCUEAR>2.3.CO;2.

Caratori-Tontini, F., B. Davy, C. E. J. De Ronde, R. W. Embley, M. Leybourne, and M. A. Tivey (2012), Crustal Magnetization of Brothers Volcano, New Zealand, Measured by Autonomous Underwater Vehicles: Geophysical Expression of a Submarine Hydrothermal System, *Econ. Geol.*, *107*(8), 1571–1581, doi:10.2113/econgeo.107.8.1571.

Caratori-Tontini, F., G. Bortoluzzi, C. Carmisciano, L. Cocchi, C. E. J. de Ronde, M. Ligi, and F. Muccini (2014), Near-Bottom Magnetic Signatures of Submarine Hydrothermal Systems at Marsili and Palinuro Volcanoes, Southern Tyrrhenian Sea, Italy, *Econ. Geol.*, *109*(8), 2119–2128, doi:10.2113/econgeo.109.8.2119.

Caratori-Tontini, F., C. E. J. de Ronde, D. Yoerger, J. Kinsey, and M. Tivey (2012), 3-D focused inversion of near-seafloor magnetic data with application to the Brothers volcano hydrothermal system, Southern Pacific Ocean, New Zealand, *J. Geophys. Res. Solid Earth*, *117*(B10), B10102, doi:10.1029/2012JB009349.

Carbotte, S. M., J. P. Canales, M. R. Nedimović, H. Carton, and J. C. Mutter (2012), Recent seismic studies at the East Pacific Rise 8°20'–10°10'N and Endeavour Segment: Insights into mid-ocean ridge hydrothermal and magmatic processes., *Oceanography*, *25*((1)), 100–112, doi:org/10.5670/oceanog.2012.08.

Charlou, J. L., J. P. Donval, C. Konn, H. OndréAs, Y. Fouquet, P. Jean-Baptiste, and E. Fourré (2010), High production and fluxes of H2 and CH4 and evidence of abiotic hydrocarbon synthesis by serpentinization in ultramafic-hosted hydrothermal systems on the Mid-Atlantic Ridge, in *Diversity Of Hydrothermal Systems On Slow Spreading Ocean Ridges*, pp. 265–296, American Geophysical Union.

Cherkashov, G., V. Bel'tenev, V. Ivanov, L. Lazareva, M. Samovarov, V. Shilov, T. Stepanova, G. P. Glasby, and V. Kuznetsov (2008), Two New Hydrothermal Fields at the Mid-Atlantic Ridge, *Mar. Georesources Geotechnol.*, *26*(4), 308–316, doi:10.1080/10641190802400708.

Connelly, D. P. et al. (2012), Hydrothermal vent fields and chemosynthetic biota on the world's deepest seafloor spreading centre, *Nat Commun*, *3*, 620.

Corliss, J. B. et al. (1979), Submarine Thermal Springs on the Galápagos Rift, *Science (80-.).*, *203*(4385), 1073–1083, doi:10.1126/science.203.4385.1073.

Von Damm, K. L. (1995), Controls on the chemistry and temporal variability of seafloor hydrothermal fluids, in *Seafloor Hydrothermal Systems: Physical, Chemical, Biological, and Geological Interactions*, vol. 91, pp. 222–247, AGU, Washington, DC.

Davis, E. E., W. D. Goodfellow, B. D. Bornhold, J. Adshead, B. Blaise, H. Villinger, and G. M. Le Cheminant (1987), Massive sulfides in a sedimented rift valley, northern Juan de Fuca Ridge, *Earth Planet. Sci. Lett.*, *82*(1-2), 49–61, doi:10.1016/0012-821X(87)90106-3.

Day, R., M. Fuller, and V. A. Schmidt (1977), Hysteresis properties of titanomagnetites: Grain-size and compositional dependence, *Phys. Earth Planet. Inter.*, *13*(4), 260–267, doi:10.1016/0031-9201(77)90108-X.

Delaney, J. R., V. Robigou, R. E. McDuff, and M. K. Tivey (1992), Geology of a vigorous hydrothermal system on the Endeavour Segment, Juan de Fuca Ridge, *J. Geophys. Res.*, *97*(B13), 19663, doi:10.1029/92JB00174.

deMartin, B. J., R. A. Sohn, J. Pablo Canales, and S. E. Humphris (2007), Kinematics and geometry of active detachment faulting beneath the Trans-Atlantic Geotraverse (TAG) hydrothermal field on the Mid-Atlantic Ridge, *Geol.* , *35* (8), 711–714, doi:10.1130/G23718A.1.

DeMets, C., R. G. Gordon, and D. F. Argus (2010), Geologically current plate motions, *Geophys. J. Int.*, *181*(1), 1–80.

Deschamps, A., and T. Fujiwara (2003), Asymmetric accretion along the slow-spreading Mariana Ridge, *Geochem. Geophys. Geosyst.*, *4*(10), 8622, doi:10.1029/2003GC000537.

Dick, H. J. B. (1989), Abyssal peridotites, very slow spreading ridges and ocean ridge magmatism, *Geol. Soc. London, Spec. Publ.* , *42* (1), 71–105, doi:10.1144/GSL.SP.1989.042.01.06.

Doubrovine, P. V, and J. A. Tarduno (2006), Alteration and self-reversal in oceanic basalts, *J. Geophys. Res.*, *111*(B12), B12S30, doi:10.1029/2006JB004468.

Dunlop, D. J. (2002), Theory and application of the Day plot (Mrs/Ms versus Hcr/Hc) 1. Theoretical curves and tests using titanomagnetite data, *J. Geophys. Res.*, *107*(B3), 2056, doi:10.1029/2001JB000486.

Dunlop, D. J., and O. Ozdemir (1997), *Rock Magnetism - Fundamentals and frontiers*, Cambridge University Press.

Dunlop, D. J., and O. Ozdemir (2007), Magnetizations in Rocks and Minerals, in *Geomagnetism, Treatise on Geophysics*, pp. 277–336.

Dyment, J., J. Arkani-Hamed, and A. Ghods (1997), Contribution of serpentinized ultramafics to marine magnetic anomalies at slow and intermediate spreading centres: insights from the shape of the anomalies, *Geophys. J. Int.*, *129*(3), 691–701, doi:10.1111/j.1365-246X.1997.tb04504.x.

Dyment, J., K. Tamaki, H. Horen, Y. Fouquet, K. Nakase, M. Yamamoto, M. Ravilly, and M. Kitazawa (2005), A Positive Magnetic Anomaly at Rainbow Hydrothermal Site in Ultramafic Environment, in *American Geophysical Union, Fall Meeting 2005, abstract #OS21C-08*.

Dyment, J., Y. Choi, M. Hamoudi, V. Lesur, and E. Thebault (2015), Global equivalent magnetization of the oceanic lithosphere, *Earth Planet. Sci. Lett.*, *430*, 54–65, doi:http://dx.doi.org/10.1016/j.epsl.2015.08.002.

Elderfield, H., and A. Schultz (1996), Mid-ocean ridge hydrothermal fluxes and the chemical composition of the ocean, *Annu. Rev. Earth Planet. Sci.*, *24*(1), 191–224, doi:10.1146/annurev.earth.24.1.191.

Escartin, J., D. K. Smith, J. Cann, H. Schouten, C. H. Langmuir, and S. Escrig (2008), Central role of detachment faults in accretion of slow-spreading oceanic lithosphere, *Nature*, *455*(7214), 790–794, doi:10.1038/nature07333.

Escartín, J., G. Hirth, and B. Evans (1997), Effects of serpentinization on the lithospheric strength and the style of normal faulting at slow-spreading ridges, *Earth Planet. Sci. Lett.*, *151*(3–4), 181–189, doi:http://dx.doi.org/10.1016/S0012-821X(97)81847-X.

Ferré, E. C., S. A. Friedman, F. Martín-Hernández, J. M. Feinberg, J. A. Conder, and D. A. Ionov (2013), The magnetism of mantle xenoliths and potential implications for sub-Moho magnetic sources, *Geophys. Res. Lett.*, *40*(1), 105–110, doi:10.1029/2012GL054100.

Fiske, R. S., J. Naka, K. Iizasa, M. Yuasa, and A. Klaus (2001), Submarine silicic caldera at the front of the Izu-Bonin arc, Japan: Voluminous seafloor eruptions of rhyolite pumice, *Geol. Soc. Am. Bull.* , *113* (7), 813–824, doi:10.1130/0016-7606(2001)113<0813:SSCATF>2.0.CO;2.

Fouquet, Y., U. von Stackelberg, J. L. Charlou, J. Erzinger, P. M. Herzig, R. Muehe, and M. Wiedicke (1993), Metallogenesis in back-arc environments; the Lau Basin example, *Econ. Geol.* , *88* (8), 2154–2181, doi:10.2113/gsecongeo.88.8.2154.

Fouquet, Y., H. Ondreas, J.-L. Charlou, J.-P. Donval, J. Radford-Knoery, I. Costa, N. Lourenco, T. M. K., and M. K. Tivey (1995), Atlantic lava lakes and hot vents, *Nature*, *377*(6546), 201.

Fouquet, Y. et al. (2010), Geodiversity of hydrothermal processes along the Mid-Atlantic Ridge and ultramafic-hosted mineralization: A new type of oceanic Cu-Zn-Co-Au volcanogenic massive sulfide deposit, in *Diversity of Hydrothermal Systems on Slow Spreading Ocean Ridges*, vol. 188, pp. 321–367, AGU, Washington, DC.

Francheteau, J., and R. D. Ballard (1983), The East Pacific Rise near 21°N, 13°N and 20°S: inferences for along-strike variability of axial processes of the Mid-Ocean Ridge, *Earth Planet. Sci. Lett.*, *64*(1), 93–116, doi:10.1016/0012-821X(83)90055-9.

Frost, B. R., K. A. Evans, S. M. Swapp, J. S. Beard, and F. E. Mothersole (2013), The process of serpentinization in dunite from New Caledonia, *Lithos*, *178*(0), 24–39, doi:http://dx.doi.org/10.1016/j.lithos.2013.02.002.

Frost, D. J., and C. A. McCammon (2008), The Redox State of Earth's Mantle, *Annu. Rev. Earth Planet. Sci.*, *36*(1), 389–420, doi:10.1146/annurev.earth.36.031207.124322.

Früh-Green, G. L., D. S. Kelley, S. M. Bernasconi, J. A. Karson, K. A. Ludwig, D. A. Butterfield, C. Boschi, and G. Proskurowski (2003), 30,000 Years of Hydrothermal Activity at the Lost City Vent Field, *Sci.* , *301* (5632), 495–498, doi:10.1126/science.1085582.

Fujiwara, T., and H. Fujimoto (1998), Seafloor geomagnetic vector anomaly of the intersection of the Mid-Atlantic Ridge and the Kane Transform Fault: Implications for magnetization of the oceanic crust, *J. Geophys. Res. Solid Earth*, *103*(B12), 30335–30349, doi:10.1029/1998JB900015.

Fujiwara, T., S. Toyoda, A. Uchida, J. Ishibashi, S. Nakai, and A. Takamasa (2015), ESR Dating of Barite in Sea-Floor Hydrothermal Sulfide Deposits in the Okinawa Trough, in *Subseafloor Biosphere Linked to Hydrothermal Systems SE - 29*, edited by J. Ishibashi, K. Okino, and M. Sunamura, pp. 369–386, Springer Japan.

Gamo, T. et al. (2001), Chemical characteristics of newly discovered black smoker fluids and associated hydrothermal plumes at the Rodriguez Triple Junction, Central Indian Ridge, *Earth Planet. Sci. Lett.*, *193*(3–4), 371–379, doi:http://dx.doi.org/10.1016/S0012-821X(01)00511-8.

Gee, J., and D. V Kent (1994), Variations in layer 2A thickness and the origin of the central anomaly magnetic high, *Geophys. Res. Lett.*, *21*(4), 297–300, doi:10.1029/93GL03422.

Gee, J., and D. V Kent (1997), Magnetization of axial lavas from the southern East Pacific Rise (14°-23°S): Geochemical controls on magnetic properties, *J. Geophys. Res.*, *102*(B11), 24873–24886, doi:10.1029/97JB02544.

Gee, J. S., and D. V Kent (2007), Source of Oceanic Magnetic Anomalies and the Geomagnetic Polarity Timescale, in *Geomagnetism, Treatise on Geophysics*, pp. 455–507.

Gee, J. S., S. C. Cande, J. A. Hildebrand, K. Donnelly, and R. L. Parker (2000), Geomagnetic intensity variations over the past 780 kyr obtained from near-seafloor magnetic anomalies, *Nature*, *408*(6814), 827–832.

Gee, J. S., S. C. Webb, J. Ridgway, H. Staudigel, and M. A. Zumberge (2001), A deep tow magnetic survey of Middle Valley, Juan de Fuca Ridge, *Geochemistry, Geophys. Geosystems*, *2*(11), 1059, doi:10.1029/2001GC000170.

German, C. ., and L. . Parson (1998), Distributions of hydrothermal activity along the Mid-Atlantic Ridge: interplay of magmatic and tectonic controls, *Earth Planet. Sci. Lett.*, *160*(3-4), 327–341, doi:10.1016/S0012-821X(98)00093-4.

German, C. R., and J. Lin (2004), The Thermal Structure of the Oceanic Crust, Ridge-Spreading and Hydrothermal Circulation: How Well do we Understand

their Inter-Connections?, in *Mid-Ocean Ridges*, pp. 1–18, American Geophysical Union.

German, C. R., G. P. Klinkhammer, and M. D. Rudnicki (1996), The Rainbow Hydrothermal Plume, 36°15′N, MAR, *Geophys. Res. Lett.*, *23*(21), 2979–2982, doi:10.1029/96GL02883.

German, C. R. et al. (2008), Hydrothermal activity on the southern Mid-Atlantic Ridge: Tectonically- and volcanically-controlled venting at 4–5°S, *Earth Planet. Sci. Lett.*, *273*(3–4), 332–344, doi:http://dx.doi.org/10.1016/j.epsl.2008.06.048.

Gillis, K. M., and P. T. Robinson (1988), Distribution of alteration zones in the upper oceanic crust, *Geol.* , *16* (3), 262–266, doi:10.1130/0091-7613(1988)016<0262:DOAZIT>2.3.CO;2.

Gillis, K. M., and P. T. Robinson (1990), Patterns and processes of alteration in the lavas and dykes of the Troodos Ophiolite, Cyprus, *J. Geophys. Res. Solid Earth*, *95*(B13), 21523–21548, doi:10.1029/JB095iB13p21523.

Goodfellow, W. D., and J. M. Peter (1994), GEOCHEMISTRY OF HYDROTHERMALLY ALTERED SEDIMENT, MIDDLE VALLEY, *Proc. Ocean Drill. Program, Sci. Results*, *139*, 207–289.

Granot, R., J. Dyment, and Y. Gallet (2012), Geomagnetic field variability during the Cretaceous Normal Superchron, *Nat. Geosci*, *5*(3), 220–223.

Guyodo, Y., and J. P. Valet (1999), Global changes in intensity of the Earth's magnetic field during the past 800 kyr, *Nature*, *399*(6733), 249–252.

Halbach, P. et al. (1989), Probable modern analogue of Kuroko-type massive sulphide deposits in the Okinawa Trough back-arc basin, *Nature*, *338*(6215), 496–499.

Hall, J. M. (1992), Interaction of submarine volcanic and high-temperature hydrothermal activity proposed for the formation of the Agrokipia, volcanic massive sulfide deposits of Cyprus, *Can. J. Earth Sci.*, *29*(9), 1928–1936, doi:10.1139/e92-150.

Hannington, M., J. Jamieson, T. Monecke, S. Petersen, and S. Beaulieu (2011), The abundance of seafloor massive sulfide deposits, *Geol.* , *39* (12), 1155–1158, doi:10.1130/G32468.1.

Hannington, M. D., I. R. Jonasson, P. M. Herzig, and S. Petersen (1995), Physical and chemical processes of seafloor mineralization at mid-ocean ridges, in *Seafloor*

Hydrothermal Systems: Physical, Chemical, Biological, and Geological Interactions, vol. 91, pp. 115–157, AGU, Washington, DC.

Hannington, M. D., C. E. J. de Ronde, and S. Petersen (2005), Sea-Floor Tectonics and Submarine Hydrothermal Systems, *Econ. Geol.*, *100th Anni*, 111–141.

Haymon, R. M., and M. Kastner (1981), Hot spring deposits on the East Pacific Rise at 21°N: preliminary description of mineralogy and genesis, *Earth Planet. Sci. Lett.*, *53*(3), 363–381, doi:10.1016/0012-821X(81)90041-8.

Haymon, R. M., D. J. Fornari, M. H. Edwards, S. Carbotte, D. Wright, and K. C. Macdonald (1991), Hydrothermal vent distribution along the East Pacific Rise crest (9°09′–54′N) and its relationship to magmatic and tectonic processes on fast-spreading mid-ocean ridges, *Earth Planet. Sci. Lett.*, *104*(2-4), 513–534, doi:10.1016/0012-821X(91)90226-8.

Haymon, R. M. et al. (1993), Volcanic eruption of the mid-ocean ridge along the East Pacific Rise crest at 9°45–52′N: Direct submersible observations of seafloor phenomena associated with an eruption event in April, 1991, *Earth Planet. Sci. Lett.*, *119*(1-2), 85–101, doi:10.1016/0012-821X(93)90008-W.

Hearn, C. K., K. L. Homola, and H. P. Johnson (2013), Surficial permeability of the axial valley seafloor: Endeavour Segment, Juan de Fuca Ridge, *Geochemistry, Geophys. Geosystems*, *14*(9), 3409–3424, doi:10.1002/ggge.20209.

Herzig, P. M., S. E. Humphris, D. J. Miller, and R. A. Zierenberg (1998), No Title, *Proc. Ocean Drill. Program, Sci. results*, *158*, doi:10.2973/odp.proc.sr.158.1998.

Hochstein, M. P., and S. Soengkono (1997), Magnetic anomalies associated with high temperature 779 reservoirs in the Taupo volcanic zone (New Zealand), *Geothermics*, *26*(1), 1–24.

Hofmann, A. W. (1988), Chemical differentiation of the Earth: the relationship between mantle, continental crust, and oceanic crust, *Earth Planet. Sci. Lett.*, *90*(3), 297–314, doi:10.1016/0012-821X(88)90132-X.

Honsho, C. (1999), Magnetic structure of the Mid-Atlantic ridge 21°40′N segment: an approach from near-bottom magnetic measurements onboard a submersible.

Honsho, C., K. Tamaki, and H. Fujimoto (1996), Three-dimensional magnetic and gravity studies of the Rodriguez Triple Junction in the Indian Ocean, *J. Geophys. Res.*, *101*(B7), 15837–15848, doi:10.1029/96JB00644.

Honsho, C., J. Dyment, K. Tamaki, M. Ravilly, H. Horen, and P. Gente (2009), Magnetic structure of a slow spreading ridge segment: Insights from near-bottom magnetic measurements on board a submersible, *J. Geophys. Res.*, *114*(B5), B05101, doi:10.1029/2008JB005915.

Honsho, C., T. Ura, and K. Tamaki (2012), The inversion of deep-sea magnetic anomalies using Akaike's Bayesian information criterion, *J. Geophys. Res.*, *117*(B1), B01105, doi:10.1029/2011JB008611.

Honsho, C., T. Ura, and K. Kim (2013), Deep-sea magnetic vector anomalies over the Hakurei hydrothermal field and the Bayonnaise knoll caldera, Izu-Ogasawara arc, Japan, *J. Geophys. Res. Solid Earth*, *118*(10), 5147–5164, doi:10.1002/jgrb.50382.

Hsu, H.-W. et al. (2015), Ongoing hydrothermal activities within Enceladus, *Nature*, *519*(7542), 207–210.

Humphris, S. E., and J. R. Cann (2000), Constraints on the energy and chemical balances of the modern TAG and ancient Cyprus seafloor sulfide deposits, *J. Geophys. Res.*, *105*(B12), 28477, doi:10.1029/2000JB900289.

Humphris, S. E., and T. M. McCollom (1998), The Cauldron Beneath the Seafloor: Percolating Through Volcanic Subsurface Rocks, Seawater is Chemically Transformed into Hydrothermal Fluid, *Oceanus*, *41*(2).

Humphris, S. E., P. M. Herzig, D. J. Miller, and E. Al. (1996), No Title, *Proc. Ocean Drill. Program, Initial reports*, *158*, doi:10.2973/odp.proc.ir.158.1996.

Hunt, C. P., B. M. Moskowitz, and S. K. Banerjee (1995), Magnetic Properties of Rocks and Minerals, in *Rock Physics & Phase Relations*, pp. 189–204, American Geophysical Union.

Hussenoeder, S. A., M. A. Tivey, and H. Schouten (1995), Direct inversion of potential fields from an uneven track with application to the Mid‐Atlantic Ridge, *Geophys. Res. Lett.*, *22*(23), 3131–3134, doi:10.1029/95GL03326.

Hussong, D. M., and S. Uyeda (1982), Tectonic processes and the history of the Mariana Arc: A synthesis of the results of deep-sea drilling project Leg 60, *Initial Rep. Deep Sea Drill. Proj.*, *60*, 909–929.

Iizasa, K. et al. (1999), A Kuroko-Type Polymetallic Sulfide Deposit in a Submarine Silicic Caldera, *Sci.* , *283* (5404), 975–977, doi:10.1126/science.283.5404.975.

International Association of Geomagnetism and Aeronomy, W. G. V.-M. P. members et al. (2010), International Geomagnetic Reference Field: the eleventh generation, *Geophys. J. Int.*, *183*(3), 1216–1230, doi:10.1111/j.1365-246X.2010.04804.x.

Irving, E. (1970), The Mid-Atlantic Ridge at 45° N. XIV. Oxidation and magnetic properties of basalt; review and discussion, *Can. J. Earth Sci.*, *7*(6), 1528–1538, doi:10.1139/e70-144.

Isezaki, N. (1986), A new shipboard three‐component magnetometer, *GEOPHYSICS*, *51*(10), 1992–1998, doi:10.1190/1.1442054.

Ishibashi, J., and T. Urabe (1995), Hydrothermal activity related to arc-backarc magmatism in the western Pacific, in *Backarc Basins: Tectonics and Magmatism*, edited by B.Taylor, pp. 451–495.

Ishibashi, J. et al. (2004), Geochemistry of Hydrothermal Fluids in South Mariana Backarc Spreading Center, in *American Geophysical Union, Fall Meeting 2004, abstract #V44A-05*.

Ishibashi, J. et al. (2015), Dating of hydrothermal mineralizatoin in active hydrothermal fields in the Southern Mariana Trough, in *Subseafloor Biosphere Linked to Global Hydrothermal Systems; TAIGA Concept*, edited by J.-I. Ishibashi, K. Okino, and M. Sunamura.

Jannasch, H. W., and M. J. Mottl (1985), Geomicrobiology of Deep-Sea Hydrothermal Vents, *Sci.* , *229* (4715), 717–725, doi:10.1126/science.229.4715.717.

Johnson, H. P., and T. Atwater (1977), Magnetic study of basalts from the Mid-Atlantic Ridge, lat 37°N, *Geol. Soc. Am. Bull.*, *88*(5), 637–647, doi:10.1130/0016-7606(1977)88<637:MSOBFT>2.0.CO;2.

Johnson, H. P., and R. T. Merrill (1972), Magnetic and Mineralogical Changes Associated with Low-Temperature Oxidation of Magnetite, *J. Geophys. Res.*, *77*(2), 334–341, doi:10.1029/JB077i002p00334.

Johnson, H. P., and R. T. Merrill (1973), Low-Temperature Oxidation of a Titanomagnetite and the Implications for Paleomagnetism, *J. Geophys. Res.*, *78*(23), 4938–4949, doi:10.1029/JB078i023p04938.

Johnson, H. P., and M. A. Tivey (1995), Magnetic properties of zero‐age oceanic crust; A new submarine lava flow on the Juan de Fuca Ridge, *Geophys. Res. Lett.*, *22*(2), 175–178, doi:10.1029/94GL02053.

Johnson, H. P., J. L. Karsten, F. J. Vine, G. C. Smith, and G. Schonharting (1982), Low-level magnetic survey over a massive sulfide ore body in the Troodos ophiolite complex, Cyprus, *Mar. Technol. Soc. J.*, *16*(3), 76–80.

Kadko, D., R. Koski, M. Tatsumoto, and R. Bouse (1985), An estimate of hydrothermal fluid residence times and vent chimney growth rates based on210Pb/Pb ratios and mineralogic studies of sulfides dredged from the Juan de Fuca Ridge, *Earth Planet. Sci. Lett.*, *76*(1-2), 35–44, doi:10.1016/0012-821X(85)90146-3.

Kakegawa, T., M. Utsumi, and K. Marumo (2008), Geochemistry of Sulfide Chimneys and Basement Pillow Lavas at the Southern Mariana Trough (12.55°N–12.58°N), *Resour. Geol.*, *58*(3), 249–266.

Karson, J., and J. Brown (1988), Geologic setting of the Snake Pit hydrothermal site: An active vent field on the Mid-Atlantic Ridge, *Mar. Geophys. Res.*, *10*(1-2), 91–107, doi:10.1007/BF02424662.

Kelley, D. S. et al. (2001), An off-axis hydrothermal vent field near the Mid-Atlantic Ridge at 30[deg] N, *Nature*, *412*(6843), 145–149.

Kelley, D. S. et al. (2005), A Serpentinite-Hosted Ecosystem: The Lost City Hydrothermal Field, *Sci.* , *307* (5714), 1428–1434, doi:10.1126/science.1102556.

Kent, D. V, and J. Gee (1996), Magnetic alteration of zero-age oceanic basalt, *Geology*, *24*(8), 703–706, doi:10.1130/0091-7613(1996)024<0703:MAOZAO>2.3.CO;2.

Kitada, K., N. Seama, T. Yamazaki, Y. Nogi, and K. Suyehiro (2006), Distinct regional differences in crustal thickness along the axis of the Mariana Trough, inferred from gravity anomalies, *Geochemistry, Geophys. Geosystems*, *7*(4), Q04011, doi:10.1029/2005GC001119.

Klein, F., W. Bach, and T. M. McCollom (2013a), Compositional controls on hydrogen generation during serpentinization of ultramafic rocks, *Lithos*, *178*(0), 55–69, doi:10.1016/j.lithos.2013.03.008.

Klein, F., W. Bach, S. E. Humphris, W.-A. Kahl, N. Jöns, B. Moskowitz, and T. S. Berquó (2013b), Magnetite in seafloor serpentinite—Some like it hot, *Geol.* , doi:10.1130/G35068.1.

Kleinrock, M. C., and S. E. Humphris (1996), Structural control on sea-floor hydrothermal activity at the TAG active mound, *Nature*, *382*(6587), 149–153.

Klingelhoefer, F., C.-S. Lee, J.-Y. Lin, and J.-C. Sibuet (2009), Structure of the southernmost Okinawa Trough from reflection and wide-angle seismic data, *Tectonophysics*, *466*(3-4), 281–288, doi:10.1016/j.tecto.2007.11.031.

Korenaga, J. (1995), Comprehensive analysis of marine magnetic vector anomalies, *J. Geophys. Res.*, *100*(B1), 365–378, doi:10.1029/94JB02596.

Korner, U. (1994), Rock magnetic properties of hydrothermally formed iron sulfides from Middle Valley, Juan de Fuca ridge, *Proc. Ocean Drill. Program, Sci. Results*, *139*, 535–542.

Koschinsky, A., D. Garbe-Schönberg, S. Sander, K. Schmidt, H.-H. Gennerich, and H. Strauss (2008), Hydrothermal venting at pressure-temperature conditions above the critical point of seawater, 5°S on the Mid-Atlantic Ridge, *Geol.* , *36* (8), 615–618, doi:10.1130/G24726A.1.

Koski, R. A., I. R. Jonasson, D. C. Kadko, V. K. Smith, and F. L. Wong (1994), Compositions, growth mechanisms, and temporal relations of hydrothermal sulfide-sulfate-silica chimneys at the northern Cleft segment, Juan de Fuca Ridge, *J. Geophys. Res.*, *99*(B3), 4813, doi:10.1029/93JB02871.

Kumagai, H. et al. (2008), Geological background of the Kairei and Edmond hydrothermal fields along the Central Indian Ridge: Implications of their vent fluids' distinct chemistry, *Geofluids*, *8*(4), 239–251, doi:10.1111/j.1468-8123.2008.00223.x.

Kuznetsov, V., G. Cherkashev, A. Lein, V. Sshilov, F. Maksimov, K. Arslanov, T. Stepanova, N. Baranova, S. Chernov, and D. Tarasenko (2006), 230Th/U DATING OF MASSIVE SULFIDES FROM THE LOGATCHEV AND RAINBOW HYDROTHERMAL FIELDS, *J. Methods Appl. Absol. Chronol.*, *25*, 51–55.

Lalou, C., J.-L. Reyss, E. Brichet, P. A. Rona, and G. Thompson (1995), Hydrothermal activity on a 10 5 -year scale at a slow-spreading ridge, TAG hydrothermal field, Mid-Atlantic Ridge 26°N, *J. Geophys. Res.*, *100*(B9), 17855, doi:10.1029/95JB01858.

Lartaud, F. et al. (2010), Fossil clams from a serpentinite-hosted sedimented vent field near the active smoker complex Rainbow, MAR, 36°13′N: Insight into the biogeography of vent fauna, *Geochemistry, Geophys. Geosystems*, *11*(8), n/a–n/a, doi:10.1029/2010GC003079.

Lister, C. R. B. (1970), Measurement of in Situ Sediment Conductivity by means of a Bullard-type Probe, *Geophys. J. Int.* , *19* (5), 521–532, doi:10.1111/j.1365-246X.1970.tb00157.x.

Lister, C. R. B. (1972), On the Thermal Balance of a Mid-Ocean Ridge, *Geophys. J. Int.* , *26* (5), 515–535, doi:10.1111/j.1365-246X.1972.tb05766.x.

Lowell, R. P., and M. DuBose (2005), Hydrothermal systems on Europa, *Geophys. Res. Lett.*, *32*(5), L05202, doi:10.1029/2005GL022375.

Lowell, R. P., P. A. Rona, and R. P. Von Herzen (1995), Seafloor hydrothermal systems, *J. Geophys. Res. Solid Earth*, *100*(B1), 327–352, doi:10.1029/94JB02222.

Ludwig, K. A., C.-C. Shen, D. S. Kelley, H. Cheng, and R. L. Edwards (2011), U–Th systematics and 230Th ages of carbonate chimneys at the Lost City Hydrothermal Field, *Geochim. Cosmochim. Acta*, *75*(7), 1869–1888, doi:http://dx.doi.org/10.1016/j.gca.2011.01.008.

Macdonald, K. C., S. P. Miller, S. P. Huestis, and F. N. Spiess (1980), Three-dimesional modeling of a magnetic reversal boundary from inversion of deep-tow memasurements, *J. Geophys. Res.*, *85*(B7), 3670–3680, doi:10.1029/JB085iB07p03670.

Maffione, M., A. Morris, O. Plümper, and D. J. J. van Hinsbergen (2014), Magnetic properties of variably serpentinized peridotites and their implication for the evolution of oceanic core complexes, *Geochemistry, Geophys. Geosystems*, n/a–n/a, doi:10.1002/2013GC004993.

Malvoisin, B., J. Carlut, and F. Brunet (2012), Serpentinization of oceanic peridotites: 1. A high-sensitivity method to monitor magnetite production in hydrothermal experiments, *J. Geophys. Res. Solid Earth*, *117*(B1), B01104, doi:10.1029/2011JB008612.

Marques, A. F. A., F. Barriga, V. Chavagnac, and Y. Fouquet (2006), Mineralogy, geochemistry, and Nd isotope composition of the Rainbow hydrothermal field, Mid-Atlantic Ridge, *Miner. Depos.*, *41*(1), 52–67, doi:10.1007/s00126-005-0040-8.

Marshall, M., and A. Cox (1971), Magnetism of Pillow Basalts and Their Petrology, *Geol. Soc. Am. Bull.*, *82*(3), 537–552, doi:10.1130/0016-7606(1971)82[537:MOPBAT]2.0.CO;2.

Martínez, F., P. Fryer, and N. Becker (2000), Geophysical characteristics of the southern Mariana Trough, 11°50′N–13°40′N, *J. Geophys. Res. Solid Earth*, *105*(B7), 16591–16607, doi:10.1029/2000JB900117.

McCaig, A. M., R. A. Cliff, J. Escartin, A. E. Fallick, and C. J. MacLeod (2007), Oceanic detachment faults focus very large volumes of black smoker fluids, *Geol.* , *35* (10), 935–938, doi:10.1130/G23657A.1.

McCollom, T. M., and W. Bach (2009), Thermodynamic constraints on hydrogen generation during serpentinization of ultramafic rocks, *Geochim. Cosmochim. Acta*, *73*(3), 856–875, doi:http://dx.doi.org/10.1016/j.gca.2008.10.032.

McKenzie, D., and C. Bowin (1976), The relationship between bathymetry and gravity in the Atlantic Ocean, *J. Geophys. Res.*, *81*(11), 1903–1915, doi:10.1029/JB081i011p01903.

Melchert, B. et al. (2008), First evidence for high-temperature off-axis venting of deep crustal/mantle heat: The Nibelungen hydrothermal field, southern Mid-Atlantic Ridge, *Earth Planet. Sci. Lett.*, *275*(1–2), 61–69, doi:http://dx.doi.org/10.1016/j.epsl.2008.08.010.

Mendel, V., D. Sauter, P. Patriat, and M. Munschy (2000), Relationship of the Central Indian Ridge segmentation with the evolution of the Rodrigues Triple Junction for the past 8 Myr, *J. Geophys. Res. Solid Earth*, *105*(B7), 16563–16575, doi:10.1029/2000JB900098.

Michael, P. J. et al. (2003), Magmatic and amagmatic seafloor generation at the ultraslow-spreading Gakkel ridge, Arctic Ocean, *Nature*, *423*(6943), 956–961.

Miller, D. J., and N. I. Christensen (1997), Seismic velocities of lower crustal and upper mantle rocks from the slow-spreading Mid-Atlantic Ridge, south of the Kane Fracture Transform Zone (MARK)., in *Karson, J.A., Cannat, M., Miller, D.J., and Elthon, D. (Eds.), Proc. ODP, Sci. Results, 153: College Station, TX (Ocean Drilling Program)*, pp. 437–454.

Mitchell, N., J. Escartin, and S. Allerton (1998), Detachmentfaultsatmid- ocean ridges garner interest, *Eos Trans. AGU*, *79*(127).

Miyoshi, A., T. Kogiso, N. Ishikawa, and K. Mibe (2014), Role of silica for the progress of serpentinization reactions: Constraints from successive changes in mineralogical textures of serpentinites from Iwanaidake ultramafic body, Japan, *Am. Mineral.* , *99* (5-6), 1035–1044, doi:10.2138/am.2014.4748.

Mochizuki, N., N. Yoshifumi, M. Asada, S. Yoshikawa, and K. Okino (2012), Decay of natural remanent magnetization of oceanic basalt on the back-arc spreading axis of the southern Mariana, in *American Geophysical Union, Fall Meeting 2012; T43D-2705*.

Morishita, T., K. Hara, K. Nakamura, T. Sawaguchi, A. Tamura, S. Arai, K. Okino, K. Takai, and H. Kumagai (2009), Igneous, Alteration and Exhumation Processes Recorded in Abyssal Peridotites and Related Fault Rocks from an Oceanic Core Complex along the Central Indian Ridge, *J. Petrol.* , doi:10.1093/petrology/egp025.

Morishita, T., K. Nakamura, T. Shibuya, H. Kumagai, T. Sato, K. Okino, H. Sato, R. Nauchi, K. Hara, and R. Takamaru (2015), Petrology of Peridotites and Related Gabbroic Rocks Around the Kairei Hydrothermal Field in the Central Indian Ridge, in *Subseafloor Biosphere Linked to Hydrothermal Systems SE - 14*, edited by J. Ishibashi, K. Okino, and M. Sunamura, pp. 177–193, Springer Japan.

Moss, R., and S. D. Scott (2001), GEOCHEMISTRY AND MINERALOGY OF GOLD-RICH HYDROTHERMAL PRECIPITATES FROM THE EASTERN MANUS BASIN, PAPUA NEW GUINEA, *Can. Mineral.* , *39* (4), 957–978, doi:10.2113/gscanmin.39.4.957.

Mottl, M. J., C. G. Wheat, and J. Boulegue (1994), TIMING OF ORE DEPOSITION AND SILL INTRUSION AT SITE 856: EVIDENCE FROM STRATIGRAPHY, ALTERATION, AND SEDIMENT PORE-WATER COMPOSITION, *Proc. Ocean Drill. Program, Sci. Results*, *139*, 679–693.

Munschy, M., and R. Schlich (1989), The Rodriguez Triple Junction (Indian Ocean): Structure and evolution for the past one million years, *Mar. Geophys. Res.*, *11*(1), 1–14, doi:10.1007/BF00286244.

Nakamura, K., and K. Takai (2014), Theoretical constraints of physical and chemical properties of hydrothermal fluids on variations in chemolithotrophic microbial communities in seafloor hydrothermal systems, *Prog. Earth Planet. Sci.*, *1*(1), 5, doi:10.1186/2197-4284-1-5.

Nakamura, K., and K. Takai (2015), Indian Ocean Hydrothermal Systems: Seafloor Hydrothermal Activities, Physical and Chemical Characteristics of Hydrothermal Fluids, and Vent-Associated Biological Communities, in *Subseafloor Biosphere*

Linked to Hydrothermal Systems SE - 12, edited by J. Ishibashi, K. Okino, and M. Sunamura, pp. 147–161, Springer Japan.

Nakamura, K., T. Morishita, W. Bach, F. Klein, K. Hara, K. Okino, K. Takai, and H. Kumagai (2009), Serpentinized troctolites exposed near the Kairei Hydrothermal Field, Central Indian Ridge: Insights into the origin of the Kairei hydrothermal fluid supporting a unique microbial ecosystem, *Earth Planet. Sci. Lett.*, *280*(1–4), 128–136, doi:http://dx.doi.org/10.1016/j.epsl.2009.01.024.

Nakamura, K., T. Toki, N. Mochizuki, M. Asada, J. Ishibashi, Y. Nogi, S. Yoshikawa, J. Miyazaki, and K. Okino (2013), Discovery of a new hydrothermal vent based on an underwater, high-resolution geophysical survey, *Deep Sea Res. Part I Oceanogr. Res. Pap.*, *74*April, 1–10, doi:10.1016/j.dsr.2012.12.003.

Nakase, K. (2002), Magnetic structure of the Rainbow hydrothermal field at the Mid-Atlantic Ridge 36°14′N obtained from near-bottom geomagnetic measurements, Universtity of Tokyo.

Nazarova, K. (1994), Serpentinized peridotites as a possible source for oceanic magnetic anomalies, *Mar. Geophys. Res.*, *16*(6), 455–462 LA – English, doi:10.1007/BF01270519.

Newsom, H. E. (1980), Hydrothermal alteration of impact melt sheets with implications for Mars, *Icarus*, *44*(1), 207–216, doi:http://dx.doi.org/10.1016/0019-1035(80)90066-4.

Nishimura, S., M. Hashimoto, and M. Ando (2004), A rigid block rotation model for the GPS derived velocity field along the Ryukyu arc, *Phys. Earth Planet. Inter.*, *142*(3–4), 185–203, doi:http://dx.doi.org/10.1016/j.pepi.2003.12.014.

Nogi, Y., N. Mochizuki, K. Okino, and M. Asada (2011), Near-bottom magnetic surveys around hydrothermal sites in the southern Mariana Trough, in *American Geophysical Union, Fall Meeting 2011, abstract #GP41A-0993*.

NT09-10-leg2 cruise report (2009), http://www.godac.jamstec.go.jp/darwin/cruise/natsushima/NT09-10_leg2/j.

NT10-06-leg2 cruise report (2010), http://www.godac.jamstec.go.jp/darwin/cruise/natsushima/NT10-06_leg2/j.

NT11-17 cruise report (2011), http://www.godac.jamstec.go.jp/darwin/cruise/natsushima/NT11-17/j.

NT11-18 cruise report (2011), http://www.godac.jamstec.go.jp/darwin/cruise/natsushima/NT11-18/j.

NT11-20 cruise summary (2011), http://www.godac.jamstec.go.jp/darwin/cruise/natsushima/NT11-20/j.

NT13-25 cruise report (2013), http://www.godac.jamstec.go.jp/darwin/cruise/natsushima/NT13-25/j.

O'Reilly, W., and S. K. Banerjee (1966), Oxidation of Titanomagnetites and Self-Reversal, *Nature*, *211*(5044), 26–28.

Ohara, Y. et al. (2012), A serpentinite-hosted ecosystem in the Southern Mariana Forearc, *Proc. Natl. Acad. Sci.* , doi:10.1073/pnas.1112005109.

Okino, K., Y. Ohara, S. Kasuga, and Y. Kato (1999), The Philippine Sea: New survey results reveal the structure and the history of the marginal basins, *Geophys. Res. Lett.*, *26*(15), 2287–2290, doi:10.1029/1999GL900537.

Okino, K., K. Nakamura, and H. Sato (2015), Tectonic Background of Four Hydrothermal Fields Along the Central Indian Ridge, in *Subseafloor Biosphere Linked to Hydrothermal Systems SE - 11*, edited by J. Ishibashi, K. Okino, and M. Sunamura, pp. 133–146, Springer Japan.

Oufi, O., M. Cannat, and H. Horen (2002), Magnetic properties of variably serpentinized abyssal peridotites, *J. Geophys. Res. Solid Earth*, *107*(B5), EPM 3–1–EPM 3–19, doi:10.1029/2001JB000549.

Özdemir, Ö., D. J. Dunlop, and B. M. Moskowitz (1993), The effect of oxidation on the Verwey transition in magnetite, *Geophys. Res. Lett.*, *20*(16), 1671–1674, doi:10.1029/93GL01483.

Pariso, J. E., and H. P. Johnson (1991), Alteration processes at Deep Sea Drilling Project/Ocean Drilling Program Hole 504B at the Costa Rica Rift: Implications for magnetization of oceanic crust, *J. Geophys. Res. Solid Earth*, *96*(B7), 11703–11722, doi:10.1029/91JB00872.

Parker, R. L., and S. P. Huestis (1974), The Inversion of Magnetic Anomalies in the Presence of Topography, *J. Geophys. Res.*, *79*(11), 1587–1593, doi:10.1029/JB079i011p01587.

Pedersen, R. B., H. T. Rapp, I. H. Thorseth, M. D. Lilley, F. J. A. S. Barriga, T. Baumberger, K. Flesland, R. Fonseca, G. L. Fruh-Green, and S. L. Jorgensen

(2010), Discovery of a black smoker vent field and vent fauna at the Arctic Mid-Ocean Ridge, *Nat Commun*, *1*, 126.

Peter, J. M. (1994), FLUID INCLUSION PETROGRAPHY AND MICROTHERMOMETRY OF THE MIDDLE VALLEY HYDROTHERMAL SYSTEM, NORTHERN JUAN DE FUCA RIDGE, *Proc. Ocean Drill. Program, Sci. Results*, *139*, 411–428.

Pontbriand, C. W., and R. A. Sohn (2014), Microearthquake evidence for reaction-driven cracking within the Trans-Atlantic Geotraverse active hydrothermal deposit, *J. Geophys. Res. Solid Earth*, *119*(2), 822–839, doi:10.1002/2013JB010110.

Pouliquen, G., Y. Gallet, P. Patriat, J. Dyment, and C. Tamura (2001), A geomagnetic record over the last 3.5 million years from deep-tow magnetic anomaly profiles across the Central Indian Ridge, *J. Geophys. Res. Solid Earth*, *106*(B6), 10941–10960, doi:10.1029/2000JB900442.

Ravilly, M., H. Horen, M. Perrin, J. Dyment, P. Gente, and H. Guillou (2001), NRM intensity of altered oceanic basalts across the MAR (21°N, 0–1.5 Ma): a record of geomagnetic palaeointensity variations?, *Geophys. J. Int.*, *145*(2), 401–422.

Richards, H. G., J. R. Cann, and J. Jensenius (1989), Mineralogical zonation and metasomatism of the alteration pipes of Cyprus sulfide deposits, *Econ. Geol.* , *84* (1), 91–115, doi:10.2113/gsecongeo.84.1.91.

Roberts, A. P., C. R. Pike, and K. L. Verosub (2000), First-order reversal curve diagrams: A new tool for characterizing the magnetic properties of natural samples, *J. Geophys. Res. Solid Earth*, *105*(B12), 28461–28475, doi:10.1029/2000JB900326.

Roman, C., and H. Singh (2007), A Self-Consistent Bathymetric Mapping Algorithm, *J. F. Robot.*, *24*(1-2), 23–50, doi:10.1002/rob.20164.

Rona, P. A. (1978), Magnetic signatures of hydrothermal alteration and volcanogenic mineral deposits in oceanic crust, *J. Volcanol. Geotherm. Res.*, *3*(1–2), 219–225, doi:http://dx.doi.org/10.1016/0377-0273(78)90010-0.

Rona, P. A. (2008), The changing vision of marine minerals, *Ore Geol. Rev.*, *33*(3–4), 618–666, doi:http://dx.doi.org/10.1016/j.oregeorev.2007.03.006.

Rona, P. A., G. Klinkhammer, T. A. Nelsen, J. H. Trefry, and H. Elderfield (1986), Black smokers, massive sulphides and vent biota at the Mid-Atlantic Ridge, *Nature*, *321*(6065), 33–37.

De Ronde, C. E. J., E. T. Baker, G. J. Massoth, J. E. Lupton, I. C. Wright, R. A. Feely, and R. R. Greene (2001), Intra-oceanic subduction-related hydrothermal venting, Kermadec volcanic arc, New Zealand, *Earth Planet. Sci. Lett.*, *193*(3-4), 359–369, doi:10.1016/S0012-821X(01)00534-9.

De Ronde, C. E. J. et al. (2005), Evolution of a Submarine Magmatic-Hydrothermal System: Brothers Volcano, Southern Kermadec Arc, New Zealand, *Econ. Geol.* , *100* (6), 1097–1133, doi:10.2113/gsecongeo.100.6.1097.

Ryall, P. J. C., and J. M. Ade-Hall (1975), Radial Variation of Magnetic Properties in Submarine Pillow Basalt, *Can. J. Earth Sci.*, *12*(12), 1959–1969, doi:10.1139/e75-174.

Sager, W. W., C. J. Weiss, M. A. Tivey, and H. P. Johnson (1998), Geomagnetic polarity reversal model of deep‐tow profiles from the Pacific Jurassic Quiet Zone, *J. Geophys. Res.*, *103*(B3), 5269–5286, doi:10.1029/ 97JB03404.

Salmi, M. S., H. P. Johnson, M. A. Tivey, and M. Hutnak (2014), Quantitative estimate of heat flow from a mid-ocean ridge axial valley, Raven field, Juan de Fuca Ridge: Observations and inferences, *J. Geophys. Res. Solid Earth*, *119*(9), 6841–6854, doi:10.1002/2014JB011086.

Sato, H., K. Nakamura, H. Kumagai, R. Senda, T. Morishita, A. Tamura, and S. Arai (2015a), Petrology and Geochemistry of Mid-Ocean Ridge Basalts from the Southern Central Indian Ridge, in *Subseafloor Biosphere Linked to Hydrothermal Systems SE - 13*, edited by J. Ishibashi, K. Okino, and M. Sunamura, pp. 163–175, Springer Japan.

Sato, T., K. Okino, and H. Kumagai (2009), Magnetic structure of an oceanic core complex at the southernmost Central Indian Ridge: Analysis of shipboard and deep-sea three-component magnetometer data, *Geochemistry, Geophys. Geosystems*, *10*(6), Q06003, doi:10.1029/2008GC002267.

Sato, T., M. Mizuno, T. Takata, T. Yamada, T. Isse, K. Mochizuki, M. Shinohara, and N. Seama (2015b), Seismic structure and seismicity in the Southern Mariana Trough and their relation to hydrothermal activity, in *Subseafloor Biosphere*

Linked to Global Hydrothermal Systems; TAIGA Concept, edited by J. Ishibashi, K. Okino, and M. Sunamura.

Sayanagi, K., A. Oshida, M. Watanabe, and K. Tamaki (1994), New Self-Contained Deep-Towed Proton Magnetometer System, *J. Geomagn. Geoelectr.*, *46*(8), 631–642, doi:10.5636/jgg.46.631.

Schouten, H., M. A. Tivey, D. J. Fornari, and J. R. Cochran (1999), Central anomaly magnetization high: constraints on the volcanic construction and architecture of seismic layer 2A at a fast-spreading mid-ocean ridge, the EPR at 9°30′–50′N, *Earth Planet. Sci. Lett.*, *169*(1–2), 37–50, doi:10.1016/S0012-821X(99)00063-1.

Schroeder, T., B. John, and B. R. Frost (2002), Geologic implications of seawater circulation through peridotite exposed at slow-spreading mid-ocean ridges, *Geol.* , *30* (4), 367–370, doi:10.1130/0091-7613(2002)030<0367:GIOSCT>2.0.CO;2.

Scott, R. B., P. A. Rona, B. A. Mcgregor, and M. R. Scott (1974), The TAG hydrothermal field, *Nature*, *251*(5473), 301–302.

Seama, N., Y. Nogi, and N. Isezaki (1993), A New Method For Precise Determination of the Position and Strike of Magnetic Boundaries Using Vector Data of the Geomagnetic Anomaly Field, *Geophys. J. Int.*, *113*(1), 155–164.

Seama, N., H. Sato, Y. Nogi, and K. Okino (2015), The mantle dynamics, the crustal formation, and the hydrothermal activity of the Southern Mariana Trough back-arc Basin, in *Subseafloor Biosphere Linked to Global Hydrothermal Systems; TAIGA Concept*, edited by J.-I. Ishibashi, K. Okino, and M. Sunamura.

Seno, T., and S. Maruyama (1984), Paleogeographic reconstruction and origin of the Philippine Sea, *Tectonophysics*, *102*(1–4), 53–84, doi:http://dx.doi.org/10.1016/0040-1951(84)90008-8.

Seyfried, W. E. (1987), Experimental and Theoretical Constraints on Hydrothermal Alteration Processes at Mid-Ocean Ridges, *Annu. Rev. Earth Planet. Sci.*, *15*(1), 317–335, doi:10.1146/annurev.ea.15.050187.001533.

Seyfried, W. E., M. E. Berndt, and J. S. Seewald (1988), Hydrothermal alteration processes at mid-ocean ridges: constraints from diabase alteration experiments, hot-spring fluids and composition of the oceanic crust, *Can. Mineral.*, *26*(3), 787–804.

Shinjo, R., S.-L. Chung, Y. Kato, and M. Kimura (1999), Geochemical and Sr-Nd isotopic characteristics of volcanic rocks from the Okinawa Trough and Ryukyu Arc: Implications for the evolution of a young, intracontinental back arc basin, *J. Geophys. Res.*, *104*(B5), 10591, doi:10.1029/1999JB900040.

Sibuet, J.-C. et al. (1987), Back Arc Extension in the Okinawa Trough, *J. Geophys. Res. Solid Earth*, *92*(B13), 14041–14063, doi:10.1029/JB092iB13p14041.

Singh, S. C., W. C. Crawford, H. Carton, T. Seher, V. Combier, M. Cannat, J. Pablo Canales, D. Dusunur, J. Escartin, and J. Miguel Miranda (2006), Discovery of a magma chamber and faults beneath a Mid-Atlantic Ridge hydrothermal field, *Nature*, *442*(7106), 1029–1032.

Sinton, J. M., and R. S. Detrick (1992), Mid-ocean ridge magma chambers, *J. Geophys. Res.*, *97*(B1), 197, doi:10.1029/91JB02508.

Sohn, R. A., and K. W. W. Sims (2005), Bending as a mechanism for triggering off-axis volcanism on the East Pacific Rise, *Geol.* , *33* (2), 93–96, doi:10.1130/G21116.1 .

Spiess, F.N., Macdonald, K.C., Atwater, T., Ballard, R., Carranza, A., Cordoba, D., Cox, C., Diaz-Garcia, V., Francheteau, J., Guerrero, J., Hawkins, J., Haymon, R., Hessler, R., Juteau, T., Kastner, M., Larson, R., Luyendyk, B., MacDougall, D., Miller, S, C. (1980), Hot springs and geophysical experiments on the East Pacific Rise., *Science (80-.).*, *207*, 1421–1433.

Stakes, D., and W. S. Moore (1991), Evolution of hydrothermal activity on the Juan de Fuca Ridge: Observations, mineral ages, and Ra isotope ratios, *J. Geophys. Res.*, *96*(B13), 21739, doi:10.1029/91JB02038.

Stein, C. A., and S. Stein (1992), A model for the global variation in oceanic depth and heat flow with lithospheric age, *Nature*, *359*(123-129), doi:10.1038/359123a0.

Stein, C. A., and S. Stein (1994), Constraints on hydrothermal heat flux through the oceanic lithosphere from global heat flow, *J. Geophys. Res.*, *99*(B2), 3081–3095, doi:10.1029/93JB02222.

Stern, R. J., M. J. Fouch, and S. L. Klemperer (2003), An overview of the Izu-Bonin-Mariana subduction factory, in *Inside the Subduction Factory*, vol. 138, pp. 175–222, AGU, Washington, DC.

Szitkar, F., and J. Dyment (2014), Near-seafloor magnetics reveal tectonic rotation and deep structure at the TAG (Trans-Atlantic Geotraverse) hydrothermal site (Mid-Atlantic Ridge, 26°N), *Geol.* , doi:10.1130/G36086.1.

Szitkar, F., J. Dyment, Y. Fouquet, C. Honsho, and H. Horen (2014a), The magnetic signature of ultramafic-hosted hydrothermal sites, *Geology*, *42*(8), 715–718, doi:10.1130/G35729.1.

Szitkar, F., J. Dyment, Y. Choi, and Y. Fouquet (2014b), What causes low magnetization at basalt-hosted hydrothermal sites? Insights from inactive site Krasnov (MAR 16°38′N), *Geochemistry, Geophys. Geosystems*, *15*(4), 1441–1451, doi:10.1002/2014GC005284.

Szitkar, F., S. Petersen, F. Caratori-Tontini, and L. Cocchi (2015), High-resolution magnetics reveal the deep structure of a volcanic-arc-related basalt-hosted hydrothermal site (Palinuro, Tyrrhenian Sea), *Geochemistry, Geophys. Geosystems*, *16*(6), 1950–1961, doi:10.1002/2015GC005769.

Takai, K., T. Gamo, U. Tsunogai, N. Nakayama, H. Hirayama, K. Nealson, and K. Horikoshi (2004), Geochemical and microbiological evidence for a hydrogen-based, hyperthermophilic subsurface lithoautotrophic microbial ecosystem (HyperSLiME) beneath an active deep-sea hydrothermal field, *Extremophiles*, *8*(4), 269–282, doi:10.1007/s00792-004-0386-3.

Takai, K., K. Nakamura, K. Suzuki, F. Inagaki, K. H. Nealson, and H. Kumagai (2006), Ultramafics-Hydrothermalism-Hydrogenesis-HyperSLiME (UltraH3) linkage: a key insight into early microbial ecosystem in the Archean deep-sea hydrothermal systems, *Paleontol. Res.*, *10*(4), 269–282, doi:10.2517/prpsj.10.269.

Takamasa, A., S. Nakai, F. Sato, S. Toyoda, D. Banerjee, and J. Ishibashi (2013), U–Th radioactive disequilibrium and ESR dating of a barite-containing sulfide crust from South Mariana Trough, *Quat. Geochronol.*, *15*, 38–46, doi:10.1016/j.quageo.2012.12.002.

Talwani, M., and J. R. Heirtzler (1964), Computation of magnetic anomalies caused by two-dimensional structures of arbitrary shape, in *Computers in the Mineral Industries*, edited by G. A. Parks, pp. 464– 480.

Tanahashi, M., K. Fujioka, and S. Machida (2008), Myojin Rift, Izu–Bonin Arc as the Modern Analog of Hokuroku Basin, Northeast Japan: Geotectonic Significance of the New Hydrothermal Deposit in the Back-Arc Rift, *Resour. Geol.*, *58*(3), 301–312, doi:10.1111/j.1751-3928.2008.00063.x.

Tivey, M. A. (1994), Fine-scale magnetic anomaly field over the southern Juan de Fuca Ridge: Axial magnetization low and implications for crustal structure, *J. Geophys. Res.*, *99*(B3), 4833–4855, doi:10.1029/93JB02110.

Tivey, M. A. (1996), Vertical magnetic structure of ocean crust determined from near-bottom magnetic field measurements, *J. Geophys. Res.*, *101*(B9), 20275–20296, doi:10.1029/96JB01307.

Tivey, M. A., and J. Dyment (2010), The magnetic signature of hydrothermal systems in slow spreading environments, in *Diversity of Hydrothermal Systems on Slow Spreading Ocean Ridges*, vol. 188, pp. 43–66, AGU, Washington, DC.

Tivey, M. A., and H. P. Johnson (1993), Variations in oceanic crustal structure and implications for the fine-scale magnetic anomaly signal, *Geophys. Res. Lett.*, *20*(17), 1879–1882, doi:10.1029/93GL01485.

Tivey, M. A., and H. P. Johnson (2002), Crustal magnetization reveals subsurface structure of Juan de Fuca Ridge hydrothermal vent fields, *Geology*, *30*(11), 979–982.

Tivey, M. A., P. A. Rona, and H. Schouten (1993), Reduced crustal magnetization beneath the active sulfide mound, TAG hydrothermal field, Mid-Atlantic Ridge at 26°N, *Earth Planet. Sci. Lett.*, *115*(1–4), 101–115, doi:http://dx.doi.org/10.1016/0012-821X(93)90216-V.

Tivey, M. A., P. A. Rona, and M. C. Kleinrock (1996), Reduced crustal magnetization beneath Relict Hydrothermal Mounds: TAG Hydrothermal Field, Mid-Atlantic Ridge, 26°N, *Geophys. Res. Lett.*, *23*(23), 3511–3514, doi:10.1029/96GL02082.

Tivey, M. A., H. P. Johnson, A. Bradley, and D. Yoerger (1998), Thickness of a submarine lava flow determined from near-bottom magnetic field mapping by autonomous underwater vehicle, *Geophys. Res. Lett.*, *25*(6), 805–808, doi:10.1029/98GL00442.

Tivey, M. A., H. Schouten, and M. C. Kleinrock (2003), A near-bottom magnetic survey of the Mid-Atlantic Ridge axis at 26°N: Implications for the tectonic evolution of the TAG segment, *J. Geophys. Res.*, *108*(B5), 2277, doi:10.1029/2002JB001967.

Tivey, M. A., W. W. Sager, S.-M. Lee, and M. Tominaga (2006), Origin of the Pacific Jurassic quiet zone, *Geology*, *34*(9), 789–792, doi:10.1130/G22894.1.

Tivey, M. A., H. P. Johnson, M. S. Salmi, and M. Hutnak (2014), High-resolution near-bottom vector magnetic anomalies over Raven Hydrothermal Field, Endeavour Segment, Juan de Fuca Ridge, *J. Geophys. Res. Solid Earth*, *119*(10), 2014JB011223, doi:10.1002/2014JB011223.

Tivey, M. K. (2007), Generation of Seafloor Hydrothermal Vent Fluids and Associated Mineral Deposits, *Oceanography*, *20*(1), 50–65.

Tivey, M. K., and J. R. Delaney (1986), Growth of large sulfide structures on the endeavour segment of the Juan de Fuca ridge, *Earth Planet. Sci. Lett.*, *77*(3–4), 303–317, doi:http://dx.doi.org/10.1016/0012-821X(86)90142-1.

Toft, P. B., J. Arkani-Hamed, and S. E. Haggerty (1990), The effects of serpentinization on density and magnetic susceptibility: a petrophysical model, *Phys. Earth Planet. Inter.*, *65*(1–2), 137–157, doi:http://dx.doi.org/10.1016/0031-9201(90)90082-9.

Urabe, T., J. Ishibashi, A. Maruyama, K. Marumo, N. Seama, and M. Utsumi (2004), Discovery and drilling of on- and off-axis hydrothermal sites in backarc spreading center of southern Mariana Trough, Western Pacific, in *American Geophysical Union, Fall Meeting 2004, abstract #V44A-03*.

Verhoogen, J. (1956), Ionic ordering and self-reversal of magnetization in impure magnetites, *J. Geophys. Res.*, *61*(2), 201–209, doi:10.1029/JZ061i002p00201.

Walls, C. C., and J. M. Hall (1998), Interpretation of aeromagnetic anomalies in terms of hydrothermal alteration in Cretaceous normal polarity superchron extrusives of the Troodos, Cyprus, ophiolite, *J. Geophys. Res. Solid Earth*, *103*(B12), 30311–30321, doi:10.1029/98JB02846.

Watkins, N. D., and T. P. Paster (1971), The Magnetic Properties of Igneous Rocks from the Ocean Floor, *Philos. Trans. R. Soc. London A Math. Phys. Eng. Sci.*, *268*(1192), 507–550.

Watts, A. B. (1978), An analysis of isostasy in the world's oceans 1. Hawaiian-Emperor Seamount Chain, *J. Geophys. Res. Solid Earth*, *83*(B12), 5989–6004, doi:10.1029/JB083iB12p05989.

Wessel, P., and W. H. F. Smith (1998), New, improved version of generic mapping tools released, *Eos, Trans. Am. Geophys. Union*, *79*(47), 579, doi:10.1029/98EO00426.

Wheat, C. G., and M. J. Mottl (2000), Composition of pore and spring waters from Baby Bare: global implications of geochemical fluxes from a ridge flank

hydrothermal system, *Geochim. Cosmochim. Acta*, *64*(4), 629–642, doi:10.1016/S0016-7037(99)00347-6.

Wheat, C. G., P. Fryer, S. Hulme, N. Becker, A. Curtis, and C. Moyer (2003), Hydrothermal Venting in the Southern Most Portion of the Mariana Backarc Spreading Center at 12.57 Degrees N, in *American Geophysical Union, Fall Meeting 2003, abstract #T32A-0920*.

White, S., S. Humphris, and M. Kleinrock (1998), New Observations on the Distribution of Past and Present Hydrothermal Activity in the TAG Area of the Mid-Atlantic Ridge (26°08′ N), *Mar. Geophys. Res.*, *20*(1), 41–56, doi:10.1023/A:1004376229719.

White, W. M., and E. M. Klein (2014), Composition of the Oceanic Crust, in *The Crust, Treatise on Geochemistry (Second Edition)*, pp. 457–496.

Wolfe, C. J., G. M. Purdy, D. R. Toomey, and S. C. Solomon (1995), Microearthquake characteristics and crustal velocity structure at 29°N on the Mid-Atlantic Ridge: The architecture of a slow spreading segment, *J. Geophys. Res.*, *100*(B12), 24449, doi:10.1029/95JB02399.

Wooldridge, A. L., S. E. Haggerty, P. A. Rona, and C. G. A. Harrison (1990), Magnetic properties and opaque mineralogy of rocks from selected seafloor hydrothermal sites at oceanic ridges, *J. Geophys. Res. Solid Earth*, *95*(B8), 12351–12374, doi:10.1029/JB095iB08p12351.

Wooldridge, A. L., C. G. A. Harrison, M. A. Tivey, P. A. Rona, and H. Schoutens (1992), Magnetic Modeling Near Selected Areas of Hydrothermal Activity on the Mid-Atlantic and Gorda Ridges, *J. Geophys. Res.*, *97*(B7), 10911–10926, doi:10.1029/92JB00605.

Yamanaka, T. et al. (2015), The Tarama Knoll: Geochemical and Biological Profiles of Hydrothermal Activity BT, in *Subseafloor Biosphere Linked to Global Hydrothermal Systems; TAIGA Concept*, edited by J.-I. Ishibashi, K. Okino, and M. Sunamura.

Yamamoto, M., N. Seama, and N. Isezaki (2005), Geomagnetic paleointensity over 1.2 Ma from deep-tow vector magnetic data across the East Pacific Rise, *Earth, Planets Sp.*, *57*(5), 465–470, doi:10.1186/BF03351835.

Yamazaki, T., N. Seama, K. Okino, K. Kitada, M. Joshima, H. Oda, and J. Naka (2003), Spreading process of the northern Mariana Trough: Rifting-spreading transition at 22°N, *Geochemistry, Geophys. Geosystems*, *4*(9), n/a–n/a, doi:10.1029/2002GC000492.

YK05-09-leg2 cruise report (2005), http://www.godac.jamstec.go.jp/darwin/cruise/yokosuka/YK05-09_leg2/j.

YK12-05 cruise report (2012), http://www.godac.jamstec.go.jp/darwin/cruise/yokosuka/YK12-05/j.

Yoshikawa, S., K. Okino, and M. Asada (2012), Geomorphological variations at hydrothermal sites in the southern Mariana Trough: Relationship between hydrothermal activity and topographic characteristics, *Mar. Geol.*, *303–306*(0), 172–182, doi:http://dx.doi.org/10.1016/j.margeo.2012.02.013.

Zhao, X., D. Heslop, and A. P. Roberts (2015), A protocol for variable-resolution first-order reversal curve measurements, *Geochemistry, Geophys. Geosystems*, *16*(5), 1364–1377, doi:10.1002/2014GC005680.

Zhou, W., R. Van der Voo, and D. R. Peacor (1997), Single-domain and superparamagnetic titanomagnetite with variable Ti content in young ocean-floor basalts: No evidence for rapid alteration, *Earth Planet. Sci. Lett.*, *150*(3–4), 353–362, doi:http://dx.doi.org/10.1016/S0012-821X(97)00099-X.

Zhou, W., R. Van der Voo, D. R. Peacor, D. Wang, and Y. Zhang (2001), Low-temperature oxidation in MORB of titanomagnetite to titanomaghemite: A gradual process with implications for marine magnetic anomaly amplitudes, *J. Geophys. Res.*, *106*(B4), 6409–6421, doi:10.1029/2000JB900447.

Zhu, J., J. Lin, Y. J. Chen, C. Tao, C. R. German, D. R. Yoerger, and M. A. Tivey (2010), A reduced crustal magnetization zone near the first observed active hydrothermal vent field on the Southwest Indian Ridge, *Geophys. Res. Lett.*, *37*(18), L18303, doi:10.1029/2010GL043542.